Shedding Light on Electrochemically Doped Semiconductors

Photochemical Stabilization of the Charge Density in Quantum Dots and Organic Semiconductors

Eren, H.

DOI
10.4233/uuid:03e18765-d269-4637-a801-7a79bec023d0

Publication date
2023

Document Version
Final published version

Citation (APA)
Eren, H. (2023). *Shedding Light on Electrochemically Doped Semiconductors: Photochemical Stabilization of the Charge Density in Quantum Dots and Organic Semiconductors*. [Dissertation (TU Delft), Delft University of Technology]. https://doi.org/10.4233/uuid:03e18765-d269-4637-a801-7a79bec023d0

Shedding Light on Electrochemically Doped Semiconductors:

Photochemical Stabilization of the Charge Density in Quantum Dots and Organic Semiconductors

Hamit Eren

Shedding Light on Electrochemically Doped Semiconductors:

Photochemical Stabilization of the Charge Density in Quantum Dots and Organic Semiconductors

Dissertation

for the purpose of obtaining the degree of doctor
at Delft University of Technology
by the authority of the Rector Magnificus Prof. dr. ir. T.H.J.J. van der Hagen
chair of the Board for Doctorates,

to be defended publicly on
Thursday 13th of April 2023 at 15:00 o'clock

by

Hamit EREN

Master of Science in Materials Science and Nanotechnology
Bilkent University, Turkey
born in Istanbul, Turkey

This dissertation has been approved by the promotors.

Prof. dr. A. J. Houtepen	Delft University of Technology, promotor
Dr. R. Eelkema	Delft University of Technology, promotor

Composition of the doctoral committee:

Rector Magnificus,	chairperson
Prof. dr. A. J. Houtepen	Delft University of Technology, promotor
Dr. R. Eelkema	Delft University of Technology, promotor

Independent members:

Prof. dr. B. Dam	Delft University of Technology
Prof. dr. D.A.M. Vanmaekelbergh	Utrecht University
Prof. dr. F.C. Grozema	Delft University of Technology
Prof. dr. L.D.A. Siebbeles	Delft University of Technology

Other members:

Dr. W.F. Jager	Delft University of Technology

This work received financial support from the European Research Council Horizon 2020 ERC Grant Agreement No. 678004 (Doping on Demand).

Table of Contents

Chapter 1

Introduction

"Only a life lived for others is a life worthwhile"

A. Einstein – quote to The New York Times, June 20, 1932.

1.1 Introduction

This thesis deals with electrochemical doping of various semiconductor materials such as quantum dots and conductive polymers to utilize their full potential for use in optoelectronic applications. Due to the difficulties to implement traditional doping methods (thermal diffusion and ion implantation) into those semiconductor materials, it has remained a challenge to introduce extra charges in a reversible, non-destructive and controllable manner. Electrochemical doping is in potential a highly effective method to controllably dope nanoporous semiconductors like quantum dots and conductive polymers. However, the electrochemically injected charges in these materials are typically not stable after disconnecting the external voltage source. Here, throughout this thesis, we use photopolymerization after electrochemical charge injection in an attempt to stabilize and tune the doping density in semiconductor films. These concepts will be elaborated in this introduction.

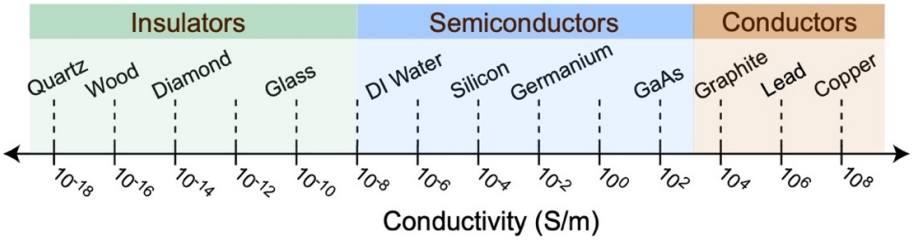

Figure 1.1 Room temperature conductivity of typical insulator, semiconductor, and conductor materials. DI water stands for deionized water.

Solid materials can be classified into three groups as metals, insulators and semiconductors based on their electric conductivity properties as shown in Figure 1.1. A conductor is defined as a type of material having a high number of "free electrons" at room temperature that can move readily in the material and can participate in the flow of electricity in one or more directions, which then give rise to high conductivity of conductors. Many metals such as silver, copper or gold are common electrical conductor materials used in today's world. On the other hand, insulators are materials with very low conductivity of electric or heat. They possess very high resistivity that inhibits the flow of electrical current as a result of tightly bound electrons in their atoms and molecules. Having such high resistivity makes them very suitable for insulating the

current carrying parts of household items and electrical circuits. Some common examples include ceramics, plastic, and glass.

Semiconductors are substances whose electrical properties lie in between insulators and conductors. Interestingly, the conductivity of semiconductors might alter with respect to the conditions they are exposed to; for example, temperature. At low temperatures, the conductivity of semiconductors is very low whereas with increase in temperature the conductivity increases exponentially. In addition to temperature, various factors such as impurity atoms, incident light, magnetic field and voltage could also have enormous effect on the ability of semiconductors to conduct electricity. Gallium arsenide, germanium and silicon are some of the most important commercial semiconductors as well as the most commonly used ones in many device applications.[1]

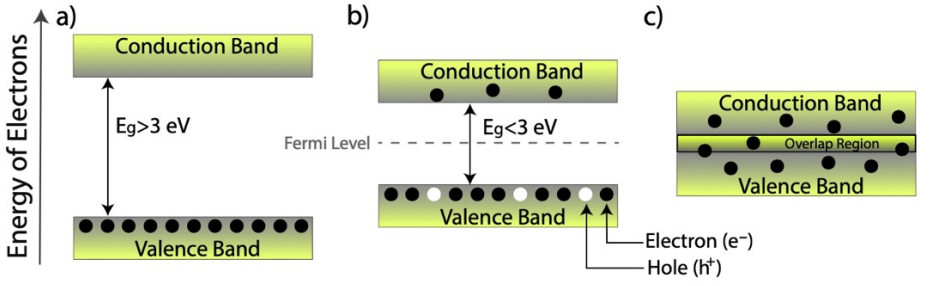

Figure 1.2 Classification of materials based on energy band theory.

A practical and useful way to distinguish conductors, semiconductors and insulators is to plot the energy states for electrons in the materials as schematically shown in Figure 1.2. In insulators, the electrons in the valence band are separated by a large energy gap from the conduction band, meaning that a large amount of energy is required to move up electrons from the valence band into the conduction band. In a conductor, there are no energy band gaps between the valence and conduction bands as they overlap each other. The electrons can move freely between the bands.

In the case of a semiconductor, it has a small energy gap between valence band and conduction band. Some of the electrons in the valence band gain energy by random thermal excitation or by external stimuli such as photoexcitation or electric fields, and cross the energy gap between the bands, which makes the conduction possible. By this movement, it creates a free electron in the conduction band and leaves a positive hole

behind in the valence band. An important parameter in the electronic band structure shown in Figure 1.2 is the Fermi level, which is defined as the highest energy level occupied by an electron in a material at temperature equals to 0 K. The Fermi level is defined in the Fermi-Dirac distribution for electrons:

$$f(E) = \frac{1}{1 + \exp\left(\frac{E - E_f}{kT}\right)}$$

Where $f(E)$ is the probability that the available energy state E will be occupied by an electron, k is the Boltzmann constant, T is the temperature in Kelvin, E_f is the Fermi energy level. If E is equal to E_f, then $f(E) = 1/2$ for any value of temperature, meaning that the Fermi level represents the energy state with a 50% probability of being occupied.

The position of the Fermi level with respect to the conduction band is a critical factor in determining electrical properties. In the purest form of a semiconductor without any added impurities (intrinsic semiconductors) like silicon and germanium, the Fermi level lies nearly midway between the valence and conduction bands. When extra charge carriers (electrons or holes) are introduced into an intrinsic semiconductor the position of the Fermi level changes. One can expect a greater number of electrons to be present in n-type semiconductors in comparison to the number of holes. Therefore, n-type semiconductor materials have their Fermi level located nearer to the conduction band. Conversely, one can expect a greater number of holes to be present in p-type semiconductors in comparison the number of electrons. This means the Fermi level in the case of p-type semiconductors will be located near the valence band. Both p- and n-type concepts in semiconductor materials are discussed in detail in the following section.

1.2 Doping semiconductors

Thanks to semiconductors, I was able to write this thesis and you are able to read it online. From smartphones to planes, it comes down to the fact that semiconductors power almost everything in our daily lives.[2] One of the main reasons why semiconductors are being used in so many applications is that we can control their electrical conductivity readily in contrast to changing the conductivity of an insulator or a conductor. Changing the electron and hole concentrations in semiconductors is called

electronic doping. The most common way to achieve this is by introducing controlled quantity of aliovalent impurity atoms into the crystal structure of semiconductor material.[3] By doing so, the electrical conductivity may be varied by factors of thousands or millions.

This dramatic change in their electrical properties can be attained by adding a small percentage of impurity atoms in crystal lattice of semiconductors, which provides free charge carriers (electrons or holes) to carry electric current through the crystal. For example; a pure germanium semiconductor at 20 °C contains approximately $2.5x10^{13}$ free electrons and $2.5x10^{13}$ holes per cm^3. The addition of 0.001% arsenic (dopant) increases the number of free electrons to 10^{17} in the same volume and the electrical conductivity is enhanced by a factor of 10,000.

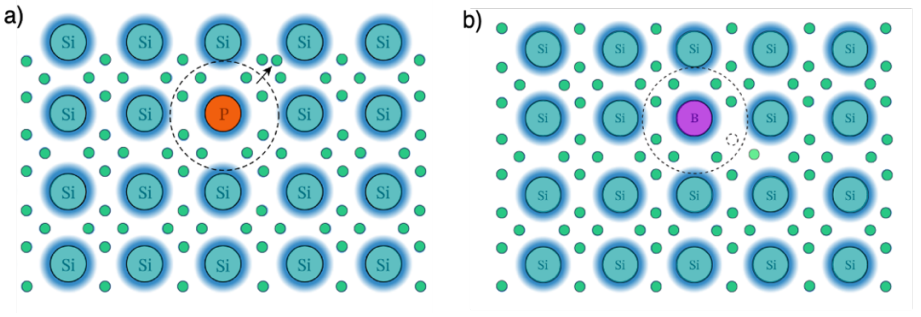

Figure 1.3 Schematic of a silicon crystal lattice doped with impurities like phosphorus (a) and boron (b) to create n-type and p-type semiconductor materials, respectively. Figure adapted from Ref [4].

Introducing impurity atoms to the semiconductors makes them no longer "pure (intrinsic)" or composed of one single element. The impurity atoms function as either electron donors or acceptors and the corresponding doped semiconductors are known as n-type semiconductors and p-type semiconductors, respectively.[5] N-type semiconductors can be created by doping impurity atoms like arsenic, phosphorus in an intrinsic semiconductor crystal. For example; silicon is a tetravalent element and doping it with phosphorus, a pentavalent element, will yield an extra unpaired electron in the semiconductor crystal as illustrated in Figure 1.3a. This extra electron will increase the concentration of electron in crystal and thus greatly increasing the conductivity of the intrinsic semiconductor at room temperature.

On the other hand, p-type semiconductors can be formed by doping aliovalent impurity atoms in semiconductor crystals. For instance; doping tetravalent silicon with boron, a trivalent atom, will create holes in the valence band. These positively charged holes are able to delocalize in the material and are responsible (together with free electrons) for creating electric current in semiconductor materials as shown in Figure 1.3b. Unlike in an intrinsic semiconductor, the number of free electrons and holes are not the same. In a p-type semiconductor, the number of free holes greatly outnumbers free electrons, meaning that holes are the majority carriers and while electrons become minority carriers in p-type semiconductor materials.

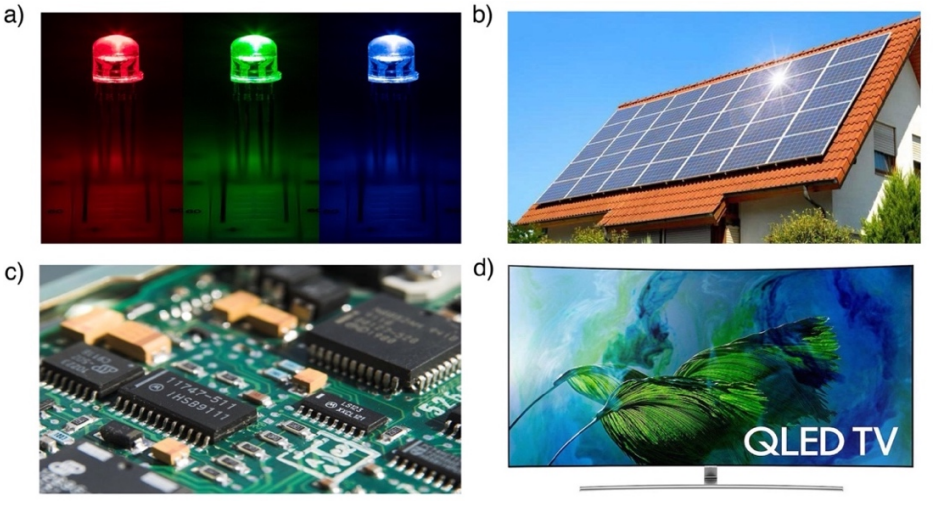

Figure 1.4 Various semiconductor devices. (a) Light-emitting diodes, LEDs, (b) Solar panels (c) Circuit board, (d) Television display made out of semiconductor quantum dots.

These p- and n-type semiconductors have more interesting properties when joined them together in a suitable manner, which results in the formation of a p-n junction.[6] There is a difference in concentration of electrons and holes at the two sides of the junction. Due to the concentration gradient, holes start to diffuse from the p-side to the n-side and electrons from the n-side to the p-side. At the interface electron and holes recombine, leaving behind a region with charged donor and acceptor ions. This is called the space-charge region or the depletion region. In a p-n junction structure, electrons are only able to flow in one direction, which is a very useful and important property for

creating basic semiconductor devices. By itself, a p-n junction functions as a diode, which is one of the simplest and most commonly used electronic components.[7] As it forms a highly critical and elementary building block of almost all semiconductor electronic devices, it is found in wide range of applications such as in solar cells, LEDs, integrated circuits, displays as shown in Figure 1.4.

1.3 Doping methods

In general, there are two different routes to dope semiconductor materials: internal doping and external doping (or remote doping). In both methods, the goal is to introduce free charge carriers (electron or holes) into a semiconductor material for the purpose of tuning its electrical, optical and structural properties in a controllable manner.

1.3.1 Internal (impurity) doping

Internal doping of semiconductors can be achieved by addition of dopants either during crystal growth or in post-growth of the crystal.[8] For example, in the former case, n-type gas doping of gallium arsenide is carried out with hydrogen sulfide, in which sulfur is incorporated into the crystal structure.[9] The deliberate introduction of dopant atoms can also be realized in post-growth of the semiconductor crystal by such processes called as thermal diffusion[10] and ion implantation.[11] These two techniques are the most prevalent ways for internal doping of semiconductors, although the latter technique is being more popular in large production runs due to increased controllability and lower temperature processability.

Thermal diffusion is carried out in two steps. First, the dopant molecules react with oxygen on the wafer surface resulting in a dopant oxide. Next, the dopants diffuse into the wafer, forming a uniform dopant concentration across the surface. A concentration gradient is obtained as a result of motion of dopants at atomic scale from a higher concentration region to lower region during the diffusion process. There are three main sources of dopants: solids, liquid and gaseous. Since the diffusion of dopants increases exponentially with temperature, the diffusion process takes place at elevated temperatures.

Ion implantation is another technique for introducing dopants to semiconductor materials. In this process of doping, a beam of highly energetic ions, which are accelerated by an electric field, strike onto the wafer. Physical and chemical changes on the target are expected as a result of the collision between high-energy ions and lattice atoms in the crystal structure. To rectify this distortion problem in the structure, an extra annealing step is performed at high temperature (800 – 1000 °C). Compared to thermal diffusion, ion implantation is more expensive and may damage the surface of the target material. Yet, ion implantation method offers higher control for dopant concentration and the junction depth in the process and it is a low-temperature method in contrast to thermal diffusion.

Although both methods are being used effectively for creating doped structures in semiconductor industry, not all semiconductor materials can survive at such elevated temperature and bombardment of high-energy ions. With this protocol, the impurity doping of organic semiconductors (e.g. conductive polymers) or other inorganic semiconductor materials (e.g. quantum dots) does not give satisfactory results that are obtained with silicon and germanium semiconductors, for example.

This approach of impurity doping in quantum dots has been challenging due to the nanometer size of the material which introduces new difficulties not seen in bulk materials.[12] Incorporating, for example, even a single dopant atom into a typical 5 nm diameter quantum dot results in a doping concentration of 10^{19} cm^{-3}. Introducing such a high concentration of impurity atoms into quantum dots causes significant distortions in the crystal lattice. Additionally, it has been proposed that dopant ions are readily expelled out of quantum dot crystals in a process called self-purification.[13, 14] In that regard, a wide variety of successful strategies have been developed and implemented for doping of such semiconductor materials, which will be discussed in more details in the following sections.

1.3.2 External (remote) doping

External doping is an attractive approach for doping semiconductor materials as it does not suffer from many of the drawbacks associated with impurity doping above-mentioned, for instance the structural distortion of crystal lattice upon dopant implantation. In the case of external doping, dopants or extra charge carriers are

introduced from a material located in close vicinity to the semiconductor.[15-17] Therefore, no structural disruption in crystal lattice should occur. Besides, it does not insert any additional defect states in the band gap of the material, that might serve as recombination centers for electrons and holes, as is the case in substitutional impurity doping. There are two primary methods for external doping of semiconductor materials: chemical doping and electrochemical doping.

1.3.2.1 Chemical doping

Chemical doping is based on redox reactions between a semiconductor material and dopant molecules.[18-21] As in the case of impurity doping, the dopant can be either an electron donor or electron acceptor. With this approach, molecular electron donors (reducing agent) are used for n-type doping and, conversely molecular electron acceptors (oxidizing agent) are employed for p-type doping in semiconductors. Standard reduction potential of the dopant should be above the LUMO level of the semiconductor for n-type doping and should be below the HOMO level for p-type doping.

Chemical doping is commonly used in doping of organic semiconductors, which dates back to the 1970s.[22] Today almost all commercially available OLED displays contain molecularly doped organic semiconductors. Various molecules have been studied as n-type and p-type dopants since the discovery of the method. Nevertheless, using molecular dopants for organic semiconductors can necessitate some practical issues which can severely limit chemical doping method in applications. For example, the solubility and air stability of the dopant molecules (especially for n-dopants) are among the issues to overcome. Additionally, possible electronic interactions taking place between dopant ion and organic semiconductors makes complicated the doping process as such interactions result in formation of locally bound charge transfer complex particularly with small conjugated molecules and oligomers as well as formation of new local HOMO and LUMO levels.[23, 24]

In spite of many complications and drawbacks, the conductivity of organic semiconductors can be enhanced by several orders of magnitude through chemical doping method. For example, in a ground-breaking study in the late 1970s, the conductivity of polyacetylene was increased by ten million times via chemical doping

using volatile halogens. However, it is not easy to attain intermediate state of doping, and the semiconductor polymer is usually fully doped. This doping approach has also been used in inorganic semiconductors, e.g. quantum dots.[25-27] In order for using less harsh oxidants and reductants, photochemical doping method can also be preferred.[28-30] With this method, electrons are excited from the valence band to the conduction band by light in the presence of a sacrificial reductant, or hole quencher. This will leave a free electron in the conduction band as the photogenerated hole in the valence band might be irreversibly reduced by hole quencher. Unfortunately, upon exposure to air, photodoped electrons usually disappear and the semiconductor goes back to its original state.

1.3.2.2 Electrochemical doping

In electrochemical doping, charge carriers (electrons or holes) are injected into the semiconductor material by using a potentiostat.[31-35] As a result of regulating externally applied potential, the charge carrier concentration can be tuned very precisely and controllably in a reversible and non-destructive manner. This way of doping does not lead to a structural distortion in crystal lattice, nor bring in any defect states in the band gap, nor interfere with the surface chemistry of semiconductor material, in general.

1.4 Electrochemical cell and doping process

Electrochemical doping is conducted in an electrochemical cell, which typically contains an electrolyte solution with three different electrodes, namely the working electrode (WE), the counter electrode (CE), and the reference electrode (RE). The doping process under study takes place on the WE. The semiconductor material of interest is placed on the WE and the potentiostat applies and controls a potential between the WE and the RE. The RE's role is to act as a reference during electrochemical measurements and to control the potential of the WE precisely without passing any current. Therefore, the RE should be stable for reproducible potential values, to which other potential differences can be related. The role of the CE is to act as an electron sink and pass all the current needed to balance the current observed at the WE. The CEs are usually made from electrochemically inert materials such as gold, platinum, or carbon.

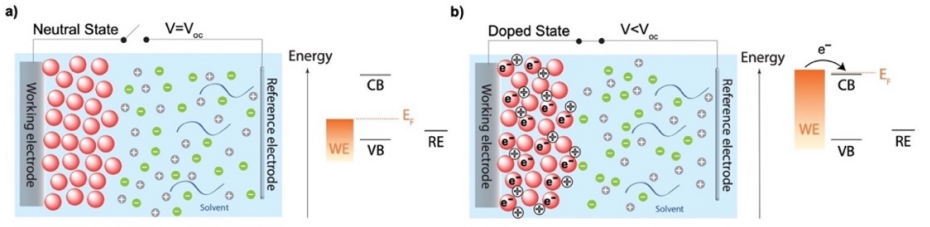

Figure 1.5 Schematic of electrochemical charge injection into semiconductor film. (a) shows a situation where the Fermi level is inside the band gap of the semiconductor when there is no applied potential to the WE, (b) shows a situation where the Fermi level in this case is below the valence band of the semiconductor as a function of applied negative potential with respect to RE. To neutralize the injected electrons electrostatically, electrolyte cations diffuse into the voids of the film.

In addition to the three electrodes, the electrolyte solution, which is capable of conducting an electric current during electrochemical measurement and completing the circuit between the WE and the CE, is of equal importance. It most often contains anions and cations of a salt dissolved in a suitable solvent, usually at concentrations ranging from 0.01 to 1 M. One of the main criteria for the electrolyte solution is its electrochemical stability within the potential range that is needed for the study of the materials of interest. Therefore, an electrolyte solution is preferred to have a wide potential window, that indicates at what potentials the solvent itself gets oxidized or reduced.

A schematic of electrochemical doping of a semiconductor film can be seen in Figure 1.5. Here the semiconductor film is deposited on the WE and placed into the electrochemical cell containing electrolyte anions and cations. After the deposition of semiconductor film on the WE, the Fermi level in the semiconductor film and in the WE will equilibrate and be in the band gap of the semiconductor, as depicted in Figure 1.5a, when there is no external potential applied. Practically, there are no charges in the semiconductor film. As shown Figure 1.5b, when a negative potential is applied with respect to a RE, then the Fermi level of the system will raise near the conduction band of the semiconductor to inject electrons from the WE into the semiconductor film. As a result of this electron injection into the film, the positive ions from the electrolyte solution diffuse into the voids of semiconductor film. These electrolyte ions, which act

as external dopants, will lower the electrostatic potential for electrons in the conduction band of the semiconductor. In the end, the overall film remains neutral. In a similar manner, a positive potential can also be applied in order to lower the Fermi level near the valance band of the semiconductor so that the hole injection into the film can take place. This will then attract the negative ions from the electrolyte solution into the voids of the film for charge neutrality.

Figure 1.6 Photograph of CdSe quantum dots of different sizes under UV illumination, demonstrating the size tunable emission wavelength. This figure is taken from the ERC starting grant proposal "Doping on Demand", 2015.[66]

For an effective electrochemical doping in semiconductor films, there are at least three basic requirements that need to be taking into consideration beforehand. First of all, the semiconductor film deposited on the WE should not be soluble or dispersible in the chosen electrolyte solution. Such a delamination issue in semiconductor films can make the electrochemical doping measurements complicated and unreliable. Secondly, it is possible that the surface of semiconductor material itself can either oxidize or reduce instead of being charged during electrochemical doping process.[36, 37] Therefore, it is highly important that the material of interest should withstand to the applied potential. Last but not least, as explained before, in order to keep the charge neutrality after electrochemical charge injection into the semiconductor film, relevant ions in the electrolyte solution should be able to diffuse into the voids of semiconductor film. This is, of course, realized by the porous nature of the semiconductor film, which results in

uniform doping throughout the entire volume of the film. This case is in contrast to non-porous semiconductor films, in which a space charge region forms and changes in the charge carrier density only take place near the surface in the space charge region.[38, 39] Thanks to the porosity, high level of doping densities in semiconductor films can be achieved as a result of this nanoscale charge compensation. Some of the examples of porous semiconductor films that can be used for electrochemical doping are conductive polymers,[40] fullerenes,[41] metal-organic frameworks,[42] and quantum dots (QDs).[43]

As the two-third of this thesis involves electrochemical doping of QDs, it is worth mentioning a bit why this class of semiconductor material is unique enough to be used in a variety of applications.[44-47] QDs are tiny semiconductor nanocrystals with diameters in the range of 2-10 nanometers typically. QDs are mostly used for their unique optical properties, as they can absorb or emit light of specific wavelengths, merely by controlling their size as shown in Figure 1.6.

The optical properties of the QDs are not only determined by their size, but also by their shape and material composition. As a result of their accurately tunable optical and electronic properties in conjunction with their facile and cheap solution-based synthesis, QDs have attracted considerable attention to be exploited as a novel class of building blocks in a wide range of applications including solar cells,[48-50] light-emitting diodes,[51-53] lasers,[54-56] displays,[57, 58] biological imaging,[59-61] catalysis,[62, 63] sensing.[64, 65]

1.5 (Spectro)electrochemical measurements

Electrochemistry is a powerful tool to investigate the reactions involving electron transfers.[67] And one of the most commonly used electrochemical technique in that manner is the cyclic voltammetry (CV), in which the potential of the WE is scanned while the positive and negative currents are measured. If electrons are injected from WE into the semiconductor material (reduction), a negative current is measured according to IUPAC convention. Conversely, if the injection of electrons takes place from semiconductor to the WE (oxidation), then a positive current is measured in the CV. If these injected charges are equal in number to those extracted charges, as shown in Figure 1.7a, the process or the reaction is called chemically reversible. This injected/extracted charge ratio can be determined from the area under the measured current. CVs with slightly asymmetric features after a forward and reverse scan cycle can also be observed. This asymmetric behaviour on CVs generally indicates diffusion

limitation of electrolyte ions during charging and discharging of the WE over the course of CV scan.

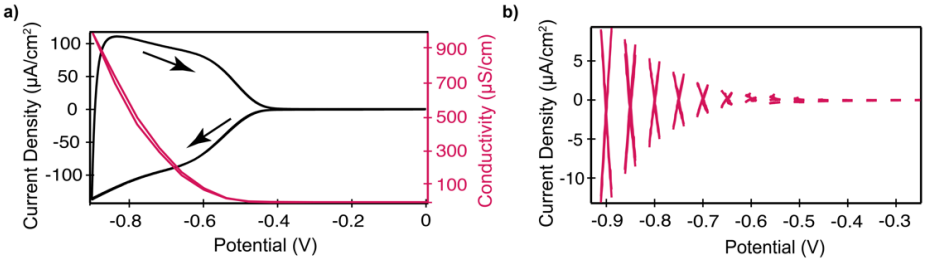

Figure 1.7 (a) The CV of ZnO QD film with a scan rate of 50 mV/s (black line) and the conductivity of the same film as a function of applied potential (red line), (b) the conductivity measurements of a ZnO QD film with a source-drain bias of ±10 mV. All measurements are performed in an electrolyte solution containing 0.1 M $LiClO_4$ in ACN.

With an additional WE to the three-electrode configuration system, the conductivity of an electrochemically doped semiconductor film can also be measured. This can be carried out by applying a potential difference between two working electrodes while measuring the current. The slope of the current *vs.* potential gives the conductance of the film deposited on the working electrodes and from the conductance, one can derive the electrical conductivity of the doped semiconductor film as shown in Figure 1.7a (red line) and 1.7b.

Additionally, by combining electrochemistry and spectroscopy, known as spectroelectrochemistry, a more comprehensive picture of the doped semiconductor films can be acquired. As a function of applied potential, changes in absorption or in photoluminescence of the semiconductor film can be recorded simultaneously with such combined powerful characterization method. Furthermore, by performing *in situ* spectroelectrochemical measurements, a large amount of information can be gained about the surface of the electrochemically charged semiconductors; for instance, the trap state distribution on the surface of quantum dots.[68-70]

1.6 Stability of electrochemically doped semiconductor films

The ability to achieve stable doped semiconductor materials is crucial for advanced semiconductor devices. Ideally, the semiconductor film is electrochemically doped to

the desired charge carrier density by using external voltage source. After disconnecting the cell from potentiostat, the doping density or the Fermi level of the system is expected to remain stable so that the stable doped film can be implemented in a device of choice. Unfortunately, this is generally not the case. Electrochemically injected charges leave the semiconductor film quickly when disconnected from the potentiostat, thus making their integration into optoelectronic devices delayed.[31, 71, 72]

There are at least two major reasons for the disappearance of the injected charges in electrochemically doped semiconductor films: (1) electrochemical side reactions with impurity molecules such as dissolved O_2 or H_2O present in the cell environment,[73, 74] (2) intrinsic side reactions taking place on the surface of the semiconductor material.[28, 68, 75] It is equally important that when these electrochemically doped semiconductor films are incorporated into devices, they should withstand to external electric field.[76] If the external dopant ions in the voids of semiconductor film are able to diffuse out when an electric field is applied, this will cause the loss of injected charges, hence unstable doping densities in semiconductor films. In that regard, it is highly essential that the immobilization of those chemically unbound external dopant ions after electrochemical doping. Overall, this situation clearly emphasizes that it would not be practical to attach the doped semiconductor film in an electrochemical cell connected to an external voltage source forever.

In order to achieve stable electrochemically doped semiconductors, certain strategies have been proposed and demonstrated to circumvent abovementioned issues. These strategies can be mainly categorized into two groups: physical treatments and (photo)chemical treatments. The former method usually involves the stabilization of doped semiconductor films at low temperatures while the latter one is mostly engaged with (photo)chemical reactions of electrolyte solution for stabilization of doping density in semiconductor films.

Most of the studies on the stability of electrochemical doping can be found in the field of polymer light-emitting electrochemical cells (LECs).[77-80] Gao and co-workers demonstrated LEC devices with stable doping structures by freezing the ion-transport polymer at low temperatures (100 K).[81, 82] At such low operation temperatures, electrochemical side reactions can be slowed down and both dopant ions and impurities present in the cell can be immobilized. Gudjonsdottir et al. reported that

highly stable doping densities in QDs and CPs can be achieved by employing electrolyte solvents which are in solid state at room temperature.[31, 32] By completely melting the electrolyte solvent above the room temperature, electrochemical charge injection can be carried out. After charge injection is complete by reaching desired doping density, the cell is cooled down to the room temperature resulting in solidification of the electrolyte solvent and hence stable electrochemical doping. From a practical point of view, this way of stabilizing of electrochemically injected charges and immobilizing dopant ions might not be applicable to be exploited in many applications in which such low and high temperature of operation is required.

A more elegant and practical route to achieve stable doping structures at room temperature is shown by Leger and co-workers by immobilizing of dopant ions chemically in LEC and photovoltaic devices.[83-85] The dopant ions effectively have been locked in place via polymerization in which they employ polymerizable electrolyte ions. Similarly, Tang et al. demonstrated stable junction doping structures by means of photochemical fixation of dopant ions in LEC device at room temperature.[86, 87]

1.6 Thesis outline

This thesis stems from an attempt to stabilize the doping densities in electrochemically doped semiconductor films (quantum dots and conductive polymers) and to increase the understanding of the underlying mechanisms of electrochemical doping process itself as well as to gain further insight into the possible causes for charge instabilities in doped films and how to fix them with photopolymerization treatment.

In **Chapter 2**, we apply photopolymerization treatments to chemically fixate polymerizable electrolyte solutions after electrochemical electron injection in n-doped QD films. We show the significance of employing polymerizable dopant ions in comparison to non-polymerizable electrolyte ions, for example, $LiClO_4$ in electrochemical doping process. The results demonstrate that the stability of injected charge carriers in QD films can be improved by many orders of magnitude, from minutes to several weeks, after photochemical fixation of ions.

In **Chapter 3**, we systematically study the effect of the photopolymerization parameters on charge stability and dopant ion diffusion in electrochemically p-doped P3DT film at room temperature. Specifically, the effect of monomer/cross-linking agents,

photoinitiator type, and impurities in electrolyte solvent were researched. With the help of electrical conductivity and Fermi-level stability measurements, we report that by combining electrochemical doping and photopolymerization treatment, the stability of injected holes in P3DT film can be increased greatly. By measuring CVs, we investigated the mobility of dopant ions before and after photopolymerization treatment.

In **Chapter 4**, we systematically examine the effect of employing two types of photoinitiator molecules (type I and type II initiators) and UV light exposure time on dopant ion immobilization and injected charge stability in electrochemically n-doped ZnO QD films. By systematically decreasing the irradiation time, we compare the degree of photochemical fixation of dopant ions and how it pertains to the stability of injected charges when both types of photoinitiator systems are used. By performing Fermi-level stability measurements, we show that the photopolymerization treatment employing Type I initiator greatly outperforms the treatment with Type II initiator with reducing irradiation time. With the analyses from CV and FT-IR, we demonstrate that a much higher degree of photochemical immobilization of dopant ions can be achieved using Type I photoinitiators.

References

1. Neamen, D. A., Semiconductor physics and devices: Basic principles. 4th ed., McGraw-Hill Education: New York, United States, 2012.

2. https://pnpntransistor.com/applications-of-semiconductor-in-daily-life/(accessed December 22).

3. https://www.pveducation.org/pvcdrom/pn-junctions/doping (accessed December 22).

4. https://www.nagwa.com/en/explainers/128152463062/ (accessed December 22).

5. https://www.nuclear-power.com/nuclear-engineering/radiation-detection/semiconductor-detectors/types-of-semiconductors/n-type-and-p-type-semiconductor/ (accessed December 22).

6. https://en.wikipedia.org/wiki/P%E2%80%93n_junction (accessed December 22).

7. https://www.rfwireless-world.com/ApplicationNotes/PN-junction-diode-applications.html (accessed December 22).

8. Schubert, E. F., Doping in III-V semiconductors. E. Fred Schubert: 2015.

9. Field, R. J.; Ghandhi, S. K., Doping of gallium arsenide in a low pressure organometallic CVD system: II. Hydrogen sulfide. Journal of Crystal Growth 1986, 74 (3), 551-558.

10. Satpathy, R.; Pamuru, V., Chapter 4 - Making of crystalline silicon solar cells. In Solar PV Power, Satpathy, R.; Pamuru, V., Eds. Academic Press: 2021; pp 71-134.

11. Large, L. N.; Bicknell, R. W., Ion-implantation doping of semiconductors. Journal of Materials Science 1967, 2 (6), 589-609.

12. Makkar, M.; Viswanatha, R., Frontier challenges in doping quantum dots: synthesis and characterization. RSC Advances 2018, 8 (39), 22103-22112.

13. Chikan, V., Challenges and Prospects of Electronic Doping of Colloidal Quantum Dots: Case Study of CdSe. The Journal of Physical Chemistry Letters 2011, 2 (21), 2783-2789.

14. Dalpian, G. M.; Chelikowsky, J. R., Self-Purification in Semiconductor Nanocrystals. Physical Review Letters 2006, 96 (22), 226802.

15. Shin, J.; Kim, Y. M.; Park, C.; Char, K., Remote Doping of the Two-Dimensional-Electron-Gas State at the Polar Interface. Physical Review Applied 2020, 13 (6), 064066.

16. Friedl, M.; Cerveny, K.; Huang, C.; Dede, D.; Samani, M.; Hill, M. O.; Morgan, N.; Kim, W.; Güniat, L.; Segura-Ruiz, J.; Lauhon, L. J.; Zumbühl, D. M.; Fontcuberta i Morral, A., Remote Doping of Scalable Nanowire Branches. Nano Letters 2020, 20 (5), 3577-3584.

17. Lee, D.; Lee, J. J.; Kim, Y. S.; Kim, Y. H.; Kim, J. C.; Huh, W.; Lee, J.; Park, S.; Jeong, H. Y.; Kim, Y. D.; Lee, C.-H., Remote modulation doping in van der Waals heterostructure transistors. Nature Electronics 2021, 4 (9), 664-670.

18. Zhao, W.; Ding, J.; Zou, Y.; Di, C.-a.; Zhu, D., Chemical doping of organic semiconductors for thermoelectric applications. Chemical Society Reviews 2020, 49 (20), 7210-7228.

19. Scaccabarozzi, A. D.; Basu, A.; Aniés, F.; Liu, J.; Zapata-Arteaga, O.; Warren, R.; Firdaus, Y.; Nugraha, M. I.; Lin, Y.; Campoy-Quiles, M.; Koch, N.; Müller, C.; Tsetseris, L.; Heeney, M.; Anthopoulos, T. D., Doping Approaches for Organic Semiconductors. Chemical Reviews 2022, 122 (4), 4420-4492.

20. Salzmann, I.; Heimel, G.; Oehzelt, M.; Winkler, S.; Koch, N., Molecular Electrical Doping of Organic Semiconductors: Fundamental Mechanisms and Emerging Dopant Design Rules. Accounts of Chemical Research 2016, 49 (3), 370-378.

21. Liu, H.; Liu, Y.; Zhu, D., Chemical doping of graphene. Journal of Materials Chemistry 2011, 21 (10), 3335-3345.

22. Chiang, C. K.; Heeger, A. J.; Macdiarmid, A. G., Synthesis, Structure, and Electrical Properties of Doped Polyacetylene. Berichte der Bunsengesellschaft für physikalische Chemie 1979, 83 (4), 407-417.

23. Stanfield, D. A.; Wu, Y.; Tolbert, S. H.; Schwartz, B. J., Controlling the Formation of Charge Transfer Complexes in Chemically Doped Semiconducting Polymers. Chemistry of Materials 2021, 33 (7), 2343-2356.

24. Lüssem, B.; Riede, M.; Leo, K., Doping of organic semiconductors. physica status solidi (a) 2013, 210 (1), 9-43.

25. Yu, D.; Wang, C.; Guyot-Sionnest, P., n-Type Conducting CdSe Nanocrystal Solids. Science 2003, 300 (5623), 1277-1280.

26. Shim, M.; Wang, C.; Guyot-Sionnest, P., Charge-Tunable Optical Properties in Colloidal Semiconductor Nanocrystals. The Journal of Physical Chemistry B 2001, 105 (12), 2369-2373.

27. Palomaki, P. K. B.; Miller, E. M.; Neale, N. R., Control of Plasmonic and Interband Transitions in Colloidal Indium Nitride Nanocrystals. Journal of the American Chemical Society 2013, 135 (38), 14142-14150.

28. Schimpf, A. M.; Gunthardt, C. E.; Rinehart, J. D.; Mayer, J. M.; Gamelin, D. R., Controlling Carrier Densities in Photochemically Reduced Colloidal ZnO Nanocrystals: Size Dependence and Role of the Hole Quencher. Journal of the American Chemical Society 2013, 135 (44), 16569-16577.

29. Rinehart, J. D.; Schimpf, A. M.; Weaver, A. L.; Cohn, A. W.; Gamelin, D. R., Photochemical Electronic Doping of Colloidal CdSe Nanocrystals. Journal of the American Chemical Society 2013, 135 (50), 18782-18785.

30. Baltazar, J.; Sojoudi, H.; Paniagua, S. A.; Zhang, S.; Lawson, R. A.; Marder, S. R.; Graham, S.; Tolbert, L. M.; Henderson, C. L., Photochemical Doping and Tuning of the Work Function and Dirac Point in Graphene Using Photoacid and Photobase Generators. Advanced Functional Materials 2014, 24 (32), 5147-5156.

31. Gudjonsdottir, S.; van der Stam, W.; Koopman, C.; Kwakkenbos, B.; Evers, W. H.; Houtepen, A. J., On the Stability of Permanent Electrochemical Doping of

Quantum Dot, Fullerene, and Conductive Polymer Films in Frozen Electrolytes for Use in Semiconductor Devices. ACS Applied Nano Materials 2019, 2 (8), 4900-4909.

32. Gudjonsdottir, S.; Houtepen, A. J., Permanent Electrochemical Doping of Quantum Dots and Semiconductor Polymers. Advanced Functional Materials 2020, 30 (49), 2004789.

33. Gozzi, G.; Cagnani, L. D.; Faria, R. M.; Santos, L. F., Electrical properties of electrochemically doped organic semiconductors using light-emitting electrochemical cells. Journal of Solid State Electrochemistry 2016, 20 (8), 2127-2133.

34. Yuen, J. D.; Dhoot, A. S.; Namdas, E. B.; Coates, N. E.; Heeney, M.; McCulloch, I.; Moses, D.; Heeger, A. J., Electrochemical Doping in Electrolyte-Gated Polymer Transistors. Journal of the American Chemical Society 2007, 129 (46), 14367-14371.

35. Shimotani, H.; Diguet, G.; Iwasa, Y., Direct comparison of field-effect and electrochemical doping in regioregular poly(3-hexylthiophene). Applied Physics Letters 2005, 86 (2), 022104.

36. du Fossé, I.; ten Brinck, S.; Infante, I.; Houtepen, A. J., Role of Surface Reduction in the Formation of Traps in n-Doped II–VI Semiconductor Nanocrystals: How to Charge without Reducing the Surface. Chemistry of Materials 2019, 31 (12), 4575-4583.

37. Guyot-Sionnest, P., Charging colloidal quantum dots by electrochemistry. Microchimica Acta 2008, 160 (3), 309-314.

38. Vanmaekelbergh, D.; Houtepen, A. J.; Kelly, J. J., Electrochemical gating: A method to tune and monitor the (opto)electronic properties of functional materials. Electrochimica Acta 2007, 53 (3), 1140-1149.

39. Krishnan, R., Fundamentals of Semiconductor Electrochemistry and Photoelectrochemistry. In Encyclopedia of Electrochemistry, 2007.

40. Le, T.-H.; Kim, Y.; Yoon, H. Electrical and Electrochemical Properties of Conducting Polymers Polymers [Online], 2017.

41. Kavan, L.; Kalbáč, M.; Zukalová, M.; Dunsch, L., Electrochemical and chemical redox doping of fullerene (C60) peapods. Carbon 2006, 44 (1), 99-106.

42. Wang, C.; Xie, Z.; deKrafft, K. E.; Lin, W., Doping Metal–Organic Frameworks for Water Oxidation, Carbon Dioxide Reduction, and Organic Photocatalysis. Journal of the American Chemical Society 2011, 133 (34), 13445-13454.

43. Stavrinadis, A.; Konstantatos, G., Strategies for the Controlled Electronic Doping of Colloidal Quantum Dot Solids. ChemPhysChem 2016, 17 (5), 632-644.

44. Ulrike Woggon, Optical Properties of Semiconductor Quantum Dots, 1st ed., Springer Berlin, Heidelberg.

45. Murphy, C. J.; Coffer, J. L., Quantum Dots: A Primer. Appl. Spectrosc. 2002, 56 (1), 16A-27A.

46. Reimann, S. M.; Manninen, M., Electronic structure of quantum dots. Reviews of Modern Physics 2002, 74 (4), 1283-1342.

47. Kouwenhoven, L.; Marcus, C., Quantum dots. Physics World 1998, 11 (6), 35.

48. Raffaelle, R. P.; Castro, S. L.; Hepp, A. F.; Bailey, S. G., Quantum dot solar cells. Progress in Photovoltaics: Research and Applications 2002, 10 (6), 433-439.

49. Nozik, A. J., Quantum dot solar cells. Physica E: Low-dimensional Systems and Nanostructures 2002, 14 (1), 115-120.

50. Carey, G. H.; Abdelhady, A. L.; Ning, Z.; Thon, S. M.; Bakr, O. M.; Sargent, E. H., Colloidal Quantum Dot Solar Cells. Chemical Reviews 2015, 115 (23), 12732-12763.

51. Sun, Q.; Wang, Y. A.; Li, L. S.; Wang, D.; Zhu, T.; Xu, J.; Yang, C.; Li, Y., Bright, multicoloured light-emitting diodes based on quantum dots. Nature Photonics 2007, 1 (12), 717-722.

52. Dai, X.; Zhang, Z.; Jin, Y.; Niu, Y.; Cao, H.; Liang, X.; Chen, L.; Wang, J.; Peng, X., Solution-processed, high-performance light-emitting diodes based on quantum dots. Nature 2014, 515 (7525), 96-99.

53. Bozyigit, D.; Yarema, O.; Wood, V., Origins of Low Quantum Efficiencies in Quantum Dot LEDs. Advanced Functional Materials 2013, 23 (24), 3024-3029.

54. Dieter, B.; Nikolai, L., Quantum dots: lasers and amplifiers. Journal of Physics: Condensed Matter 2003, 15 (24), R1063.

55. Grundmann, M., The present status of quantum dot lasers. Physica E: Low-dimensional Systems and Nanostructures 1999, 5 (3), 167-184.

56. Park, Y.-S.; Roh, J.; Diroll, B. T.; Schaller, R. D.; Klimov, V. I., Colloidal quantum dot lasers. Nature Reviews Materials 2021, 6 (5), 382-401.

57. Bourzac, K., Quantum dots go on display. Nature 2013, 493 (7432), 283-283.

58. Shu, Y.; Lin, X.; Qin, H.; Hu, Z.; Jin, Y.; Peng, X., Quantum Dots for Display Applications. Angewandte Chemie International Edition 2020, 59 (50), 22312-22323.

59. Byers, R. J.; Hitchman, E. R., Quantum Dots Brighten Biological Imaging. Progress in Histochemistry and Cytochemistry 2011, 45 (4), 201-237.

60. Green, M., Semiconductor Quantum Dots as Biological Imaging Agents. Angewandte Chemie International Edition 2004, 43 (32), 4129-4131.

61. Arya, H.; Kaul, Z.; Wadhwa, R.; Taira, K.; Hirano, T.; Kaul, S. C., Quantum dots in bio-imaging: Revolution by the small. Biochemical and Biophysical Research Communications 2005, 329 (4), 1173-1177.

62. Du, Z.; Shen, S.-l.; Tang, Z.-h.; Yang, J.-h., Graphene quantum dots-based heterogeneous catalysts. New Carbon Materials 2021, 36 (3), 449-467.

63. Wang, X.; Sun, G.; Li, N.; Chen, P., Quantum dots derived from two-dimensional materials and their applications for catalysis and energy. Chemical Society Reviews 2016, 45 (8), 2239-2262.

64. Li, M.; Chen, T.; Gooding, J. J.; Liu, J., Review of Carbon and Graphene Quantum Dots for Sensing. ACS Sensors 2019, 4 (7), 1732-1748.

65. Foerster, A.; Besley, N. A., Quantum Chemical Characterization and Design of Quantum Dots for Sensing Applications. The Journal of Physical Chemistry A 2022, 126 (19), 2899-2908.

66. Houtepen, A. J., ERC Starting Grant, 2015: Doping on Demand: precise and permanent control of the Fermi level in nanocrystal assemblies.

67. Faulkner, A. J. B. a. L. R., Electrochemical Methods: Fundamentals and Applications, 2nd edition.

68. van der Stam, W.; du Fossé, I.; Grimaldi, G.; Monchen, J. O. V.; Kirkwood, N.; Houtepen, A. J., Spectroelectrochemical Signatures of Surface Trap Passivation on CdTe Nanocrystals. Chemistry of Materials 2018, 30 (21), 8052-8061.

69. van der Stam, W.; de Graaf, M.; Gudjonsdottir, S.; Geuchies, J. J.; Dijkema, J. J.; Kirkwood, N.; Evers, W. H.; Longo, A.; Houtepen, A. J., Tuning and Probing the Distribution of Cu+ and Cu2+ Trap States Responsible for Broad-Band Photoluminescence in CuInS2 Nanocrystals. ACS Nano 2018, 12 (11), 11244-11253.

70. Boehme, S. C.; Azpiroz, J. M.; Aulin, Y. V.; Grozema, F. C.; Vanmaekelbergh, D.; Siebbeles, L. D. A.; Infante, I.; Houtepen, A. J., Density of Trap States and Auger-

mediated Electron Trapping in CdTe Quantum-Dot Solids. Nano Letters 2015, 15 (5), 3056-3066.

71. Gudjonsdottir, S.; Koopman, C.; Houtepen, A. J., Enhancing the stability of the electron density in electrochemically doped ZnO quantum dots. The Journal of Chemical Physics 2019, 151 (14), 144708.

72. Eren, H.; Bednarz, R. J.-R.; Alimoradi Jazi, M.; Donk, L.; Gudjonsdottir, S.; Bohländer, P.; Eelkema, R.; Houtepen, A. J., Permanent Electrochemical Doping of Quantum Dot Films through Photopolymerization of Electrolyte Ions. Chemistry of Materials 2022, 34 (9), 4019-4028.

73. Lakhwani, G.; Roijmans, R. F. H.; Kronemeijer, A. J.; Gilot, J.; Janssen, R. A. J.; Meskers, S. C. J., Probing Charge Carrier Density in a Layer of Photodoped ZnO Nanoparticles by Spectroscopic Ellipsometry. The Journal of Physical Chemistry C 2010, 114 (35), 14804-14810.

74. Gooding, A. K.; Gómez, D. E.; Mulvaney, P., The Effects of Electron and Hole Injection on the Photoluminescence of CdSe/CdS/ZnS Nanocrystal Monolayers. ACS Nano 2008, 2 (4), 669-676.

75. du Fossé, I.; Boehme, S. C.; Infante, I.; Houtepen, A. J., Dynamic Formation of Metal-Based Traps in Photoexcited Colloidal Quantum Dots and Their Relevance for Photoluminescence. Chemistry of Materials 2021, 33 (9), 3349-3358.

76. Matyba, P.; Maturova, K.; Kemerink, M.; Robinson, N. D.; Edman, L., The dynamic organic p–n junction. Nature Materials 2009, 8 (8), 672-676.

77. Bolink, H. J.; Coronado, E.; Costa, R. D.; Ortí, E.; Sessolo, M.; Graber, S.; Doyle, K.; Neuburger, M.; Housecroft, C. E.; Constable, E. C., Long-Living Light-Emitting Electrochemical Cells – Control through Supramolecular Interactions. Advanced Materials 2008, 20 (20), 3910-3913.

78. Tang, S.; Edman, L., Light-Emitting Electrochemical Cells: A Review on Recent Progress. Topics in Current Chemistry 2016, 374 (4), 40.

79. Pei, Q.; Yu, G.; Zhang, C.; Yang, Y.; Heeger, A. J., Polymer Light-Emitting Electrochemical Cells. Science 1995, 269 (5227), 1086-1088.

80. Pei, Q.; Yang, Y.; Yu, G.; Zhang, C.; Heeger, A. J., Polymer Light-Emitting Electrochemical Cells: In Situ Formation of a Light-Emitting p−n Junction. Journal of the American Chemical Society 1996, 118 (16), 3922-3929.

81. Gao, J.; Yu, G.; Heeger, A. J., Polymer light-emitting electrochemical cells with frozen p-i-n junction. Applied Physics Letters 1997, 71 (10), 1293-1295.

82. Gao, J.; Li, Y.; Yu, G.; Heeger, A. J., Polymer light-emitting electrochemical cells with frozen junctions. Journal of Applied Physics 1999, 86 (8), 4594-4599.

83. Leger, J. M.; Rodovsky, D. B.; Bartholomew, G. P., Self-Assembled, Chemically Fixed Homojunctions in Semiconducting Polymers. Advanced Materials 2006, 18 (23), 3130-3134.

84. Leger, J. M.; Patel, D. G.; Rodovsky, D. B.; Bartholomew, G. P., Polymer Photovoltaic Devices Employing a Chemically Fixed p–i–n Junction. Advanced Functional Materials 2008, 18 (8), 1212-1219.

85. Kosilkin, I. V.; Martens, M. S.; Murphy, M. P.; Leger, J. M., Polymerizable Ionic Liquids for Fixed-Junction Polymer Light-Emitting Electrochemical Cells. Chemistry of Materials 2010, 22 (17), 4838-4840.

86. Tang, S.; Edman, L., On-demand photochemical stabilization of doping in light-emitting electrochemical cells. Electrochimica Acta 2011, 56 (28), 10473-10478.

87. Tang, S.; Irgum, K.; Edman, L., Chemical stabilization of doping in conjugated polymers. Organic Electronics 2010, 11 (6), 1079-1087.

Chapter 2

Permanent Electrochemical Doping of Quantum Dot Films through Photopolymerization of Electrolyte Ions

Abstract

Quantum dots (QDs) are considered for devices like LEDs and photodetectors as a result of their tunable optoelectronic properties. To utilize the full potential of QDs for optoelectronic applications control over the charge carrier density is vital. However, controlled electronic doping of these materials has remained a long-standing challenge, thus slowing their integration into optoelectronic devices. Electrochemical doping offers a way to precisely and controllably tune the charge carrier concentration as a function of applied potential and thus the doping levels in QDs. However, the injected charges are typically not stable after disconnecting the external voltage source, because of electrochemical side reactions with impurities or with the surfaces of the QDs. Here, we use photopolymerization to covalently bind polymerizable electrolyte ions to polymerizable solvent molecules after electrochemical charge injection. We discuss the importance of using polymerizable dopant ions as compared to non-polymerizable conventional electrolyte ions such as $LiClO_4$ when used in electrochemical doping. The results show that the stability of charge carriers in QD films can be enhanced by many orders of magnitude, from minutes to several weeks, after photochemical ion fixation. We anticipate that this novel way of stable doping of QDs will pave the way for new opportunities and potential uses in future QD electronic devices.

This chapter is based on: Hamit Eren, Roland Jan-Reiner Bednarz, Maryam Alimoradi Jazi, Laura Donk, Solrun Gudjonsdottir, Peggy Bohländer, Rienk Eelkema and Arjan J. Houtepen. Chemistry of Materials, 2022, 34, 9, 4019–4028.

2.1 Introduction

Electronic doping, the deliberate introduction of impurity atoms to tune the electronic properties of bulk semiconductors, has played a central role in modern semiconductor technologies.[1-3] The development of semiconductor nanomaterials offers new and improved applications. Colloidal semiconductor nanocrystals, also known as quantum dots (QDs) are one such semiconductor nanomaterial that can be implemented as a building block in many device applications.[4, 5] QDs have attracted considerable attention over the past decades as a result of their tunable optoelectronic properties and their facile and cheap solution-based synthesis, which makes them interesting for a wide range of applications including solar cells,[6, 7] light-emitting diodes,[8, 9] photodetectors,[10, 11] lasers[12, 13] and thermoelectrics.[14, 15]

To utilize the full potential of QDs in such optoelectronic applications, control over the charge carrier density is vital.[16-19] Despite the maturity of electronic doping in bulk semiconductors, it has remained a long-standing challenge to reliably incorporate and manipulate electronic impurities into QDs, thus slowing their integration into optoelectronic devices.[20-22] Some progress has been made in synthesizing n-type CdSe QDs with tin and indium precursors as impurity ions[23, 24] and p-type InP QDs with Cu impurities.[25] Mocatta et al. have demonstrated doped InAs QDs with Cu and Ag impurities via diffusion of the metal ions into the nanocrystals resulting in cation exchange.[26] Impurity doping of CdSe and PbSe QDs via cation exchange with Ag ions as a p-type dopant has also been reported by Norris et al.[27, 28] and n-doping of CdSe QD thin films via thermal annealing of indium contacts deposited onto QDs has been demonstrated.[29]

In spite of these great efforts the concept of impurity doping in QDs has proven challenging because of the nanometer size of QDs which leads to new difficulties not experienced in bulk materials. Introducing even a single impurity atom into a typical 5 nm diameter QD, which consists of a few thousand atoms, yields a doping concentration of 10^{19} cm^{-3}, which is already within the heavily doped limit in a bulk semiconductor; adding such a high concentration of substitutional or interstitial impurity atoms into QDs leads to significant distortions in the crystal structure. Further, it has been suggested that impurity ions are easily expelled out of nanocrystals in a

process termed “self-purification”,[30] although it remains to be proven if this really plays a role below the impurity solubility limit of the bulk materials.

Doping QDs has also been demonstrated by means of chemical doping;[31, 32] through the use of electron or hole donating molecules in the vicinity of the QD surface, and photodoping;[33, 34] in these cases the donor/acceptor atoms remain outside the QD crystal lattice, preventing the problems mentioned above for impurity doping. Although these external doping strategies are attractive, there remains a lack of control over the charge density and stability of the doped QDs.

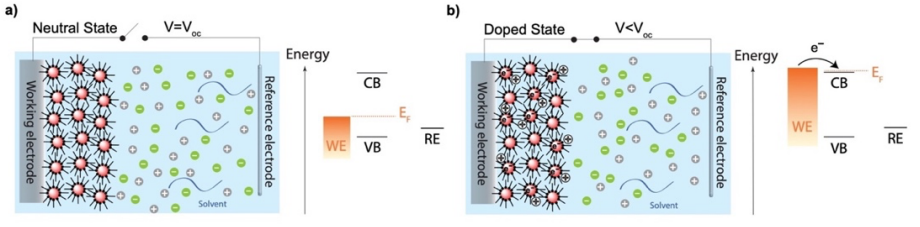

Figure 2.1. Schematic of electrochemical charge injection into QD film. (a) shows a situation where the Fermi level is inside the band gap of the QD when there is no applied potential to the WE, (b) shows a situation where the Fermi level in this case is above the conduction band of the QD as a function of applied negative potential with respect to RE. To neutralize the injected electrons electrostatically, electrolyte cations diffuse into the voids of QD film.

Arguably, the most versatile method for doping QDs is to inject extra carriers by using electrochemistry.[35-38] Electrochemical doping is an effective method which does not interfere with QD surface chemistry, nor lead to a disruption of crystal lattice, nor introduce defect states in the band gap, as is the case for impurity doping. It allows to adjust the charge carrier concentration precisely and controllably as a function of applied potential. Electrons or holes are injected into the QDs by externally changing the Fermi level of the sample through a potentiostat. As a result of this charge injection, electrolyte ions of opposite charge are drawn into the voids of QD film, which act as external dopants and prevent the macroscopic charging of the film, as depicted schematically in Figure 2.1. Efficient charge compensation by diffusing ions is allowed due to the porous nature of QD films, resulting in uniform doping of the full volume of the QD film. This contrasts with non-porous films where charge compensation is only

maintained in a planar manner, causing a change of charge carrier density only near the surface in the space charge region that forms there.

While electrochemical doping offers a high level of control over the charge density, the stability of the injected charges is usually limited. When the electrochemical cell is disconnected from the potentiostat, the injected charges leave the QD film spontaneously in a matter of seconds to minutes.[39] The disappearance of the injected charges could stem from the electrochemical side reactions with solvent impurities present in the cell environment[40, 41] or intrinsic side reactions taking place on the surface of the QDs.[42-45] Additionally, the unbound ions in the void between the QDs will quickly migrate in an electric field, causing unwanted changes to the charge density in operating devices.[46]

Despite the versatility of electrochemical doping, little attention has been paid to the instability of injected charges. An important exception is in the field of light-emitting electrochemical cells [47-51] (LECs), which possess the closest similarity to the electrochemically doped QD films discussed here. Several strategies have been researched to improve the doping stability in LECs. Gao et al. showed that freezing the electrolyte solvent at 100 K stabilizes the doping density in polymer LECs.[52, 53] We have recently extended this approach by using electrolyte solvents that are solid at room temperature; QD films and conducting polymers can be charged at elevated temperature and subsequently cooled down. We showed that this results in electrochemically doped QD films and conducting polymers that have a stable doping density at room temperature.[39, 54] While this shows that immobilizing the electrolyte ions stabilizes electrochemically doped systems, this stability is limited at (slightly) elevated temperatures.

A more practical way of stabilizing electrochemically injected charges is by chemically fixating the electrolyte ions after doping. For LECs this has been investigated by using polymerizable electrolyte ions and/or molecules.[55-61] Polymerization is induced either electrochemically or optically after charge injection. The polymerization of the solvent and electrolyte ions immobilizes the ions and probably also prevents diffusion of redox active impurities, resulting in strongly improved stability of the injected charge density. While these approaches have been investigated in the context of LECs they have not been studied for the stabilization of electrochemically doped QD films.

In this work, we demonstrate the realization of a fixed and stable doping density in electrochemically doped ZnO and PbS QD films at room temperature via photopolymerization. By employing a dedicated polymerizable ion and electrolyte solvent system, we aim to immobilize the dopant ions photochemically after electrochemical charge injection into the QDs, which fixes the electrostatic potential caused by these ions, thus fixing the Fermi level of the system at exactly the potential determined. We monitor the change in stability for doped films by measuring the electrochemical potential and electrical conductivity over time before and after photopolymerization treatment. We show that with this approach the stability of charge carriers can be enhanced by many orders of magnitude, from minutes to weeks at room temperature. By performing cyclic voltammetry (CV), we demonstrate that the ionic mobility of the dopants after photochemical fixation can be lowered by many orders of magnitude. As a comparison study, we report the results from non-polymerizable conventional electrolyte ions used in electrochemistry, such as $LiClO_4$ to emphasize the greater effect of polymerizable dopant ions in both charge stability and ion immobilization. We anticipate that this novel way of stable doping of QDs could pave the way for new opportunities and potential uses in future electronic devices.

2.2 Results and Discussion

Electrochemical charge injection into the QD films was monitored by in-situ absorption spectroscopy in a three-electrode electrochemical cell set-up as shown schematically in Figure 2.2a. As a function of applied potential, changes in the absorption of the QD film were studied. The 2D color map in Figure 2.2b demonstrates the differential absorbance, bleach (ΔA) from ZnO QD film in electrolyte solution of 0.1 M $LiClO_4$ in ACN during three cycles of charging/discharging, with an absorption spectrum of ZnO QDs on top of it (black line). The blue color on the 2D map indicates the bleach of the interband optical transitions as a result of electron injection into the conduction band of the QD film. The reproducibility absorption changes upon charging/discharging reflects the high stability of the ZnO QD film as well as the easiness and controllability in tuning the Fermi level of the system with this method.

Figure 2.2c shows Cyclic Voltammograms (CVs) of the ZnO QD film in the same electrolyte solution where the potential was scanned three times from 0 V to -0.9 V vs Ag PRE with a scan rate of 50 mV/s. At more negative potentials (starting from nearly

-0.45 V), the current density increases, corresponding to electron injection into the QD film. Reversing the scan direction results in an extraction of electrons from QD film.

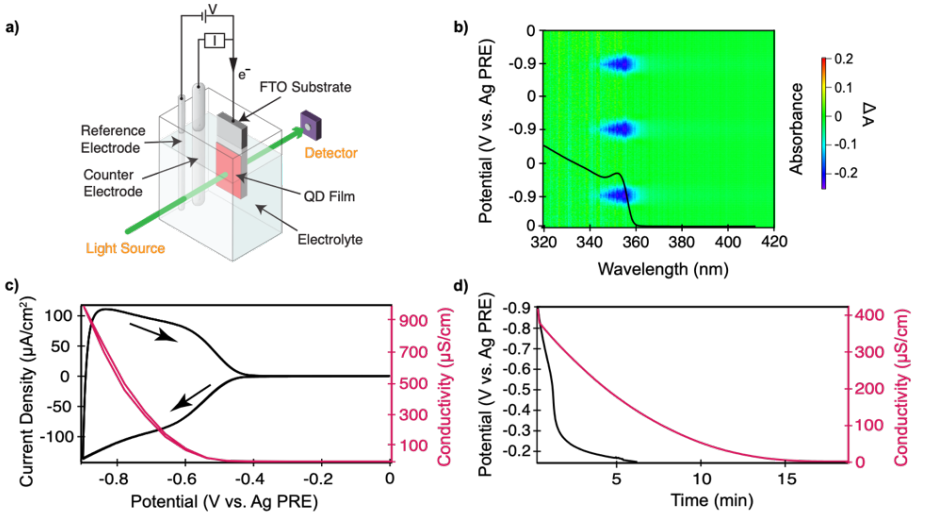

Figure 2.2. (a) The schematic of spectro-electrochemistry cell set-up with three-electrode configuration for in-situ optical absorbance measurement, (b) the 2D color map showing the differential absorbance, bleach (ΔA) from ZnO QD film during electrochemical charging and discharging (with a scan rate of 50 mV/s), with an absorption spectrum (black line) of the film on top of it, (c) the CV of the ZnO QD film scanned starting around 0 V to -0.9 V vs Ag PRE with a scan rate of 50 mV/s (black line) and the conductivity of the same film as a function of applied potential (red line), (d) both conductivity (red line) and Fermi-level stability (black line) measurements over time after disconnecting the cell from the potentiostat. All measurements are performed in an electrolyte solution containing 0.1 M $LiClO_4$ in ACN.

The symmetry in the CV scans indicates the absence of a significant diffusion overpotential: the charge compensating Li^+ ions move through the voids of QD film with very little resistance during electrochemical charging and discharging. Furthermore, the high reversibility in the CV plots indicates that the large majority of the injected electrons can be extracted when the applied potential scanned back to V_{oc}. This is not trivial since in experiments that investigate doping of QDs it is often found that more electrons are injected than that are present in the conduction band.[33, 62] The ZnO QD films have very symmetric CVs with charge extraction ratios of typically ~90%,

see Figure 2.2c. These can be improved to ~99% by very carefully drying the electrolyte, as we showed in our previous study.[42] However, most other QD materials show much less symmetric charging and discharging curves.[39] This is true for instance for CdSe QDs, but also for the PbS QDs shown in the current study.

The electrical conductivity of the ZnO QD film was measured in a source-drain configuration (see Methods) as a function of applied potential plotted and is shown in the same figure as the red line. Like the CV and the absorption bleach, the conductivity is highly reversible. The onset potential of all three measurements correlates (a ΔA vs. Voltage graph can be seen in Appendix, Figure A2.1). All these effects clearly demonstrate that electron injection into the conduction band levels and dopant ion diffusion into the voids of ZnO QD film take place successfully and starts around -0.5V *vs.* Ag PRE.

To measure how stable the injected electrons are we performed both Fermi level stability and conductivity measurements *vs.* time after breaking the connection between the WE and CE. The results are shown in figure 2.2d. In the Fermi-level stability measurement, a rapid potential drop from -0.9 V to Voc is observed within roughly 5 mins upon disconnecting the cell. Likewise, the conductivity measurement shows a similar trend with a fast decay in approximately 20 mins. Hence, in spite of the high control and reversibility of the electron injection shown in Figures 2.2b and 2.2c, the stability measurements in Figure 2.2d clearly show that the injected electrons disappear from the conduction band on the timescale of 5-10 mins. Furthermore, we have previously shown that the potential decay is indeed due to the loss of conduction band electrons as it correlates exactly with a loss of the band-edge bleach. This is carried out by monitoring the differential absorbance of the QD film during Fermi level stability measurement.[39]

We note here that a drop in charge density should not occur spontaneously. After injecting electrons, these become electrostatically bound to the electrolyte cations in the voids of the QD film. While the cations can in principle diffuse back to the bulk electrolyte solution, the electrons cannot move back to the CE if the latter is physically disconnected from the WE. This situation differs from a charged light emitting electrochemical cell mentioned in the introduction, where electrons and holes can move from one electrode to another through the semiconducting material. Rather the

electrochemical cell configuration should be compared to a battery that discharges spontaneously.

The fact that the electrons do not remain in the CB shows that there is another process that removes them. This could be due to impurity molecules such as dissolved O_2 or H_2O in the electrolyte solution that might react with the injected electrons thus lowering the charge density in QD film. O_2 molecules could react with electrons in the conduction band of the QD material, forming oxygen radical anions (superoxide), which may further react with water or surfactants, making the process irreversible. We previously investigated the effect of O_2 and H_2O on the stability of charge density in QD films and found that intentionally exposing doped QD films to oxygen causes a much quicker loss of injected electrons.[42, 54] Another possible explanation for the loss of potential and conductivity could be that conduction band electrons get trapped into states inside the bandgap. However, since the Fermi level lies inside the conduction band, all trap states should already be full. There is ample time for electrons to already fill such trap states during the electrochemical charging that precedes the stability measurements. Unless electron trapping requires a very high activation energy, and happens on a timescale of minutes, we do not expect this to be an important contribution.

Indeed, the CVs of ZnO QD film measured in air differ greatly from CVs taken in the nitrogen-filled glove box environment (see Appendix, Figure A2.2). The electrochemical irreversibility in the CVs of ZnO QD film measured in air clearly demonstrates that injected electrons react with oxygen even during the timescale of the CV measurement (approximately a minute). Removing all trace amounts of oxygen is thus essential for reversible electrochemical measurements and enhancing the stability of the injected electrons.[45] However, for doped QD films that are truly stable on long timescales this becomes impractical.

Even in an ideal scenario where there are no redox active impurities at all in the system, the dynamic nature of ions could cause problems for electrochemically doped system that are used in devices. If we take the example of a pn junction diode used as photodiode, this would involve the application of a reverse bias for efficient charge extraction. However, that bias would also cause the electrolyte ions to migrate and would hence strongly change the doping density.

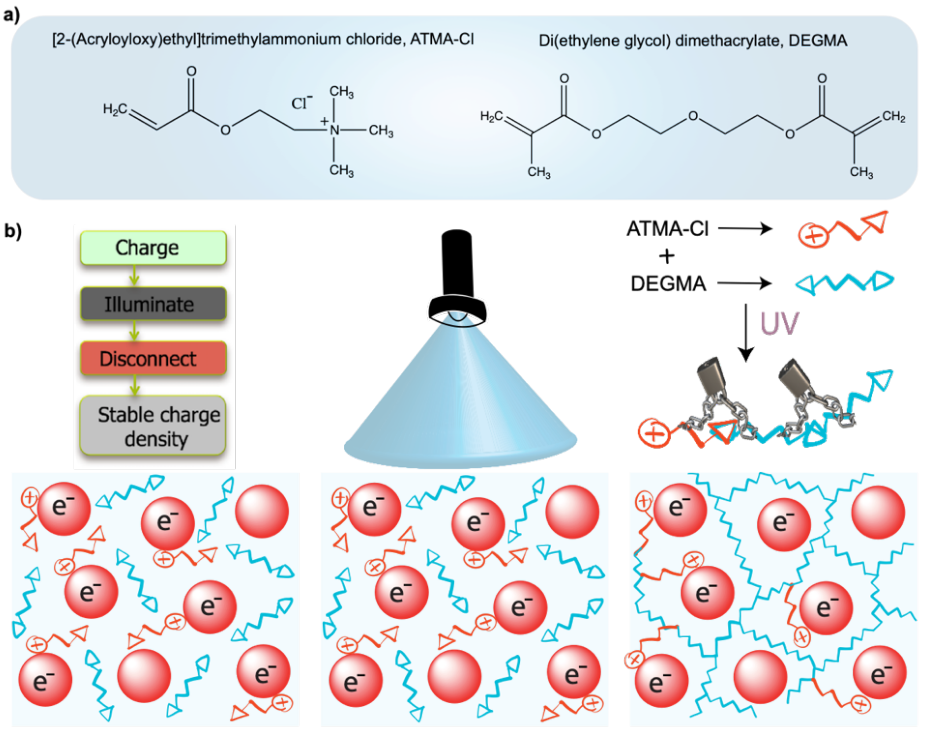

Figure 2.3. (a) The chemical structures of both compounds used for photopolymerization experiment, (b) the schematic of photopolymerization treatment with a UV-LED light source (600 mW/cm^2) with an emission wavelength of 395 nm for chemical immobilization the electrolyte ions after the electrochemical charge injection into the QDs.

With this in mind, we attempt to mitigate both problems (i.e., impurity diffusion and ion diffusion) by photopolymerizing the solvent and electrolyte ions in films of electrochemically doped ZnO and PbS QDs. This should bind the electrolyte ions covalently after the electrochemical charge injection into the QDs, fixing the electrostatic potential caused by these ions and consequently the Fermi level at the potential used during the polymerization, as shown schematically in Figure 2.3. The diffusion of impurities, which causes instability by scavenging the injected charges, will also be substantially hindered due to the formation of a dense polymer matrix, thus enhancing the stability of electrochemically injected charges inside the QD film at room temperature.

The details of the photopolymerization procedure are discussed in the methods section. We chose to employ acrylate photopolymerization because it is simple and reliable. The formation of a densely packed polymer network is crucial for mitigating the diffusion of both electrolyte ions and impurity molecules. To this end we tested a range of cross-linking molecules with different lengths to observe the effect on charge stability in electrochemically doped QD films. Namely, di(ethylene glycol) dimethacrylate (DEGMA), tetra(ethylene glycol) diacrylate (TEGA) and poly(ethylene glycol) dimethacrylate (PEGMA-550). As the length of the cross-linking molecule increases, it is expected to result in a less dense polymer matrix. We found the cross-linking molecule that gave the best stability was DEGMA (see Appendix, Figure A2.3), therefore we focus on this solvent for the remainder of this work. As polymerizable electrolyte ions we used ATMA-Cl. Since we are focusing on n-doping in this work, it is sufficient if the charge compensating cation is polymerizable, although a salt that consists of both polymerizable cations and anions would be ideal, for example, in an electrochemically doped pn junction used in light-emitting electrochemical cell. To mix DEGMA and ATMA-Cl, a small amount of formamide is added. Finally, we employ 4,4'-bis(diethylamino)benzophenone as photoinitiator.

ZnO or PbS QD films are charged negatively in this electrolyte solution. Figure 2.4a, b shows the CVs of ZnO and PbS QD films respectively, before and after the photopolymerization treatment. The CVs before photopolymerization show clear signs of electron injection into the QD films. If we compare the charging of the ZnO QD film in this electrolyte solution (Figure 2.4a) with the charging in acetonitrile (Figure 2.2c), we notice that the former is less symmetric, and the current density is much lower. This is a result of the much higher viscosity of DEGMA than of acetonitrile and the use of much bulkier cations (ATMA *vs*. Li). This strongly slows down the transport of the cations through the film which limits the current and causes a diffusion overpotential. More symmetric CVs obtained at slower scan rates support this argument. However, although charge injection is slower, it is still possible to dope the ZnO QD film *n* type using this electrolyte solution, as verified with the increase in the conductivity (see Figures 2.4e and 2.4f) and the appearance of a band edge absorption bleach (see Appendix, Figure A2.4).

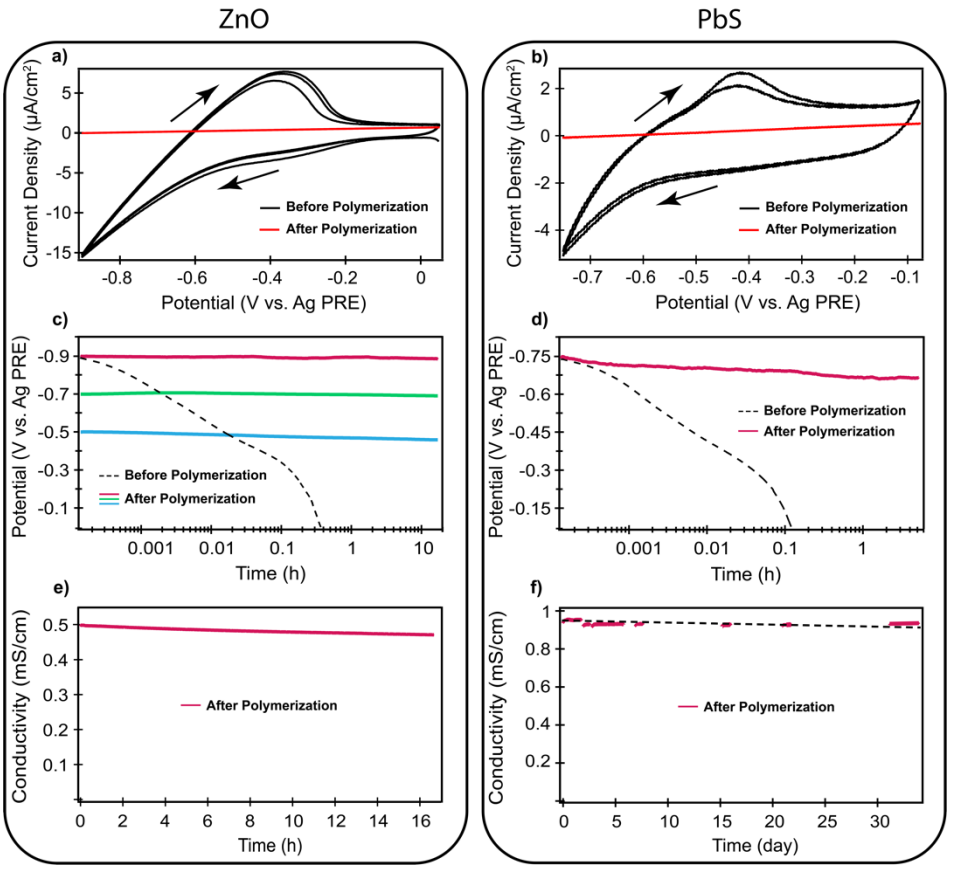

Figure 2.4. (a, b) CVs of the ZnO and PbS QD films with a scan rate of 50 mV/s before and after photopolymerization, (c, d) shows Fermi-level stability measurements before and after photopolymerization when disconnecting the cell from the potentiostat, (e, f) the conductivity measurements of both doped films after photopolymerization upon disconnecting the cell from the potentiostat. The dashed line in f is only to guide the eye.

The QD films were photopolymerized while a negative potential was applied (-0.9 V for the ZnO QD film, -0.75V for the PbS QD film). The CVs after photopolymerization are shown as the red lines in Figure 2.4a and 2.4b. Clearly the polymerization has a dramatic effect on the CV. The current density drops dramatically, and what remains is a straight Ohmic response that is 0 at the applied potential during photopolymerization (see Appendix, Figure A2.5 for a zoom in of the CVs after polymerization). We attribute this

to the immobilization of the ions. Their diffusion coefficient becomes so low after polymerization that charging and discharging is no longer possible.

The results shown so far could potentially be explained by the polymerization of the DEGMA solvent alone. It is conceivable that this also reduces the diffusion coefficient of the ATMA ions. To investigate the relevance of using photopolymerizable ions instead of non-polymerizable conventional electrolyte ions, we performed the same experiment on a film of ZnO QDs, but with 0.1 M $LiClO_4$ as electrolyte, instead of ATMA-Cl. The CVs before and after photopolymerization and Fermi level stability measurement are shown as Figure A2.6 in the Appendix. In this case there is only a four-fold reduction in the current density observed in the CV. This points out that the polymerization of the solvent reduces the diffusion coefficient of the Li^+ ions, but there still able to move through the film and cause charging and discharging of the ZnO QDs. In line with this observation the potential decay over a timescale of 20 hours (Figure A2.6, bottom) is much more significant than when ATMA-Cl is used as supporting electrolyte (Figure 2.4c). This shows that the polymerization of the charge compensating ATMA ions together with the DEGMA matrix has a strong positive effect on the stability of the doping density.

Figures 2.4c and d show the Fermi-level stability measurements for both ZnO and PbS QD films before (dashed lines) and after (solid lines) photopolymerization treatment. For the ZnO film without before photopolymerization (dashed line in Figure 2.4c) the result is very similar to what was shown in Figure 2.2 for charging in acetonitrile. The potential drops from the charging potential of -0.9 V to V_{oc} in approximately 20 minutes. For the PbS QD film, it takes a bit shorter (around 7 mins) for the potential to decay to V_{oc}. After the photopolymerization treatment, the charge stability for both ZnO and PbS QD films is substantially improved as shown by the red lines in Figures 2.4c, d. The Fermi level in the ZnO QD film stays constant over roughly 17 hours of measurement after disconnecting the cell. For the PbS QD film there is a minor decrease in potential, from -0.75V to -0.66V over 5 hours.

The ability to precisely adjust the charge carrier concentration in QDs as a function of applied potential will pave the way for practical implementation of QDs into optoelectronic devices, in particular for situations where moderate doping levels are desired. To demonstrate the ability to control and fix the Fermi level at any desired

potential we used various potentials during the photopolymerization of ZnO QD films. The results are shown as red (-0.9V during polymerization), green (-0.7V) and blue (-0.5V) lines in Figure 2.4c. The results show that the Fermi level can indeed be stabilized at any desired potential, or equivalently, at any desired charge density. As shown in Appendix, Figure A2.7, the three potentials used correspond to electron densities of $3.6x10^{16}$ cm^{-3}, $1.8x10^{17}$ cm^{-3} and $3.1x10^{18}$ cm^{-3}.

As a final test of the long-term stability of the injected electrons after the photopolymerization treatment we measured the electronic conductivity of the doped and photopolymerized films. The results are shown in Figures 2.4e and 2.4f. The conductivity measurement in Figure 2.4e demonstrates that the charge density in the ZnO QD film after photopolymerization is stable over 17 hours of measurement. During this time there is a drop in conductivity of only 4%. The conductivity of a film of PbS QDs was measured for 33 days. The results, shown in Figure 2.4f show that the drop in conductivity during this period is less than 2%, indicating that the stability of the injected electrons has increased from minutes to weeks due to the photopolymerization of the solvent and charge compensating cations.

In the studies described above, we have focused on the stability of electrochemically doped QD films. In principle, the same approach could also be applied to QDs that are doped in solution, either via electrochemistry, chemical doping or photodoping. Photopolymerization of the solvent and counter ions after doping the QD in solution could prepare a system of doped, but isolated QDs. Further, the experiments above describe the stability of doped QD films inside an electrolyte solution. These results can be extended to stable doped films outside of the electrolyte solution, which may be more useful for most applications. Initial proof-of-principle experiments have shown that taking out a doped film from the electrolyte solution followed by immediate photopolymerization results a similar increase in the stability of the conductivity.

2.3 Conclusion

In summary, we showed that electrochemical doping of QD films is reversible, and controllable, but usually not stable. The injected charges leave the QD films spontaneously in minutes when the electrochemical cell is disconnected from the potentiostat. This instability is likely due to reactions with trace amounts of O_2 in the

electrolyte solution. The stability of the injected charge carrier can however be strongly enhanced using photopolymerization after electrochemical charge injection. By employing a dedicated polymerizable ion and electrolyte solvent system, we demonstrated that the stability of electron in electrochemically doped ZnO and PbS QDs is increased from minutes to weeks. The photopolymerization covalently links the electrolyte ions to the polymer matrix and fixes the electrostatic potential. Further it likely also results in the reduced diffusion of impurity ions. We showed that the ionic mobility of the dopant ions after photochemical fixation can be significantly lowered, preventing and further charging or discharging of the QD films. Results with non-polymerizable conventional electrolyte ions show only a marginal improvement of the stability after photochemical ion fixation. An additional advantage of using photopolymerization to stabilize the injected charges is that it may provide a path toward patterning the doping density and forming junctions on demand in the QD films. We anticipate that this novel way of doping QDs will pave the way for new opportunities and potential uses in future QD electronic devices.

2.4 Methods

Materials. Zinc acetate dihydrate ($Zn(CH_3COO)_2{\cdot}2H_2O$ ACS reagent, ≥ 99.8 %), potassium hydroxide (KOH, pellets EMPLURA®), methanol (anhydrous ≥ 99.8 %), ethanol (anhydrous ≥ 99.9 %), acetonitrile (ACN, anhydrous ≥ 99.99 %), hexane (anhydrous ≥ 99.8 %), formamide (FA, ≥ 99 %), lithium perchlorate ($LiClO_4$, 99.99 %), cadmium oxide (CdO, 99.999 %), oleic acid (OA, 90 %), 1-octadecene (ODE, 90 %), sulfur powder (S, 99.99 %), oleylamine (OLA, 70 %), lead chloride ($PbCl_2$, 99.99 %), tetrabutylammonium iodide (TBAI, ≥ 99 %), [2-(Acryloyloxy)ethyl]trimethylammonium chloride (ATMA-Cl, 80 wt. % in H_2O, contains 600 ppm monomethyl ether hydroquinone as inhibitor), tetra(ethylene glycol) diacrylate (TEGA, technical grade, contains 150-200 ppm MEHQ and 100-150 ppm HQ as inhibitors), poly(ethylene glycol) dimethacrylate (PEGMA-550, contains 80-120 ppm MEHQ and 270-330 ppm BHT as inhibitors), di(ethylene glycol) dimethacrylate (DEGMA, 95 %, contains 300 ppm monomethyl ether hydroquinone as inhibitor) and 4,4'-bis(diethylamino)benzophenone (Photoinitiator, ≥ 99 %) were all purchased from Sigma Aldrich. ACN was dried in an Innovative Technology PureSolv Micro column before use. ATMA-Cl salt was further treated to decrease the water content by carefully heating up the salt solution to 85 °C for 30 mins until white salt crystals are observed. Afterwards, it was attached to a vacuum line

overnight at room temperature to obtain dry powder of ATMA-Cl salt, which was then transferred to a nitrogen-filled glove box for storage. ^{1}H-NMR analysis of dried ATMA-Cl salt confirmed that even after the treatment it still retains its chemical structure without being polymerized. (See Appendix, Figure A2.8). NMP, FA and DEGMA were vacuum degassed for 3h under rigorous stirring before use and were stored in a nitrogen-filled glove box. All other chemicals were used as received.

Synthesis & characterization of ZnO and PbS QDs. The synthesis of ZnO QDs was carried out under air by slight modification of two known procedures in the literature.[63, 64] Zinc acetate dihydrate (3.43 mmol) was added to 50 mL of ethanol in an erlenmeyer flask equipped with a magnetic stirbar and heated up to 60 °C. In a separate vial, potassium hydroxide (KOH) pellets (6.25 mmol) and 5 mL of methanol were combined and sonicated for 3 mins at room temperature. When both reagents were dissolved completely, under constant stirring, KOH solution was added dropwise to zinc acetate solution over 10 mins. The solution was then allowed to stir for one additional minute before removing the heat source. The ZnO QDs were purified by adding hexane until the solution became turbid. The flocculates were isolated by centrifugation at 2000 rpm for 1 minute and the colorless supernatant decanted.

The ZnO QDs were then redispersed in ethanol and filtered through a syringe filter (0.2 μm). The dispersion was stored at -20 °C to avoid further growth of nanocrystals. An image of a pale blue-green emission from ZnO QDs was shown in Appendix, Figure A2.9a. Transmission electron microscopy (TEM) characterization further confirmed the successful synthesis of ZnO QDs with an average diameter size of 3.5±0.2 nm as shown in Appendix, Figure A2.9b.

PbS QDs were synthesized via a controlled cation exchange reaction from CdS QDs, where the Cd^{2+} cation is exchanged for the Pb^{2+} cation following the procedure of Zhang et al.[65] The synthesis was started with the preparation of CdS QDs by heating up a mixture of 1 mmol (0.128 g) CdO, 3 mmol (0.942 g) OA and 15 g of ODE for 20 mins at 260 °C, then the temperature was set to 250 °C. The S precursor was made by dissolving S powder in ODE (0.5 M) at 130 °C. The S precursor (1 mL) was injected into Cd precursor at 250 °C, and the solution was maintained at 240 °C. About 13 mins later, additional S precursor was added to the solution dropwise until the desired size was achieved. The CdS QDs were washed twice with hexane and ethanol and centrifuged at 7500 rpm for

5 mins. The CdS QDs were dispersed in ODE. For PbS QDs, OLA (5mL) and $PbCl_2$ (1.5 mmol) were heated at 140 °C for 30 mins until a white and turbid solution was formed. Then, the solution is heated to 190 °C and 1 mL of the CdS QDs was injected swiftly. The reaction was quenched with a water bath 20 seconds later and 5 mL of hexane and 4 mL of OA were added and at 70 °C and 40 °C, respectively. The PbS QDs were washed 3 times using hexane and ethanol and centrifuged at 7500 rpm for 5 mins. The resulting PbS QDs were dispersed in hexane. The absorption spectrum of PbS QDs is shown in Appendix, Figure A2.10.

Preparation of ZnO and PbS QD films. All films were deposited on two different substrates: fluorine-doped tin oxide (FTO) and home-built interdigitated gold electrodes (IDE), which both served as working electrodes (WEs) in our electrochemical cell experiments. The IDE was a glass substrate coated with three individual gold WEs with an interdigitate approach which have source-drain gaps of different sensitivities. An image of the IDE is shown in Appendix, Figure A2.11. The ZnO QDs films were prepared by drop-casting of ZnO dispersion on top of the substrate followed by annealing treatment at 60 °C for one hour in air. The PbS QDs films were prepared by dip-coating. Initially, the substrate is dipped into the QD solution followed by dipping into the ligand solution, which in this case is TBAI (11 mg/mL) in methanol for around 30 seconds. After removal from the TBAI solution, the QD-coated substrate was rinsed in neat methanol for about 10 seconds. This process was repeated several times to build up PbS QD layers on the substrate. A Dektak profilometer was used to determine the film thicknesses which were approximately 4 μm and 90 nm for ZnO and PbS QD films, respectively.

(Spectro)electrochemical measurements. All (spectro)electrochemical measurements were performed in a nitrogen-filled glove box to ensure oxygen- and water-free conditions (≤0.1 ppm O_2 and ≤0.5 ppm H_2O) unless stated otherwise. An Autolab PGSTAT128N potentiostat including an additional dual-mode bi-potentiostat BA module was used to control the potential difference between the WE and the reference electrode (RE) by adjusting the current at the counter electrode (CE). The QD film was immersed in an electrochemical cell containing an electrolyte solution together with an Ag wire as pseudoreference electrode (PRE) and Pt wire as CE. CVs were recorded starting near open circuit potential (Voc), with a scan rate of 50 mV/s in the negative direction until the electron injection into the conduction band of the QD film takes place

followed by electrolyte ions diffusion into the voids of porous QD film for electrostatic charge compensation. As a function of applied potential, changes in absorption of the QD film were recorded concurrently with a fiber-based UV-Vis spectrometer, Ocean Optics USB2000. The spectroelectrochemical measurements of QD films were performed only on FTO substrates.

Fermi-level stability measurements. The stability of electrochemically injected charges was measured by performing the so-called potential *vs.* time measurements, also known as Fermi-level stability measurements. This involves measuring the potential of the working electrode *vs.* the reference electrode after removing the electrical connection between WE and CE. Any change in the potential of the system after doping will result in a change in the Fermi level of the system or vice versa. During photopolymerization of electrolyte solution, a very high electrolyte resistance between WE and RE is built up as the ionic conductivity drops resulting in significant noise in the measured potential. Therefore, smoothing (Savitzky-Golay) was applied to the raw data in the Fermi-level stability measurements. The raw data set for both ZnO and PbS QD films can be seen in Appendix, Figure A2.12.

Conductivity measurements. A second method to measure the stability of injected charges is to monitor the change in the conductivity of the doped QD film after removing the cell connection from the potentiostat. If injected electrons leave the conduction band of the QD film, the conductivity of the film is expected to drop as it is directly proportional to the charge density in the film. Samples of QD film deposited on IDE substrates with source-drain geometry (WE1 and WE2) were used, which enables the measurement of the electronic conductivity laterally through the film by using a Keithley 2400 SourceMeter. The width of the source-drain gap was 50 μm and the length of the gap was 74 cm for QD films. The current was recorded over a constant 10 mV of potential difference applied through Keithley between the source and drain. The slope of the current *vs.* potential gives the conductance, G, of the QD film. From the conductance, one can calculate the source-drain electronic conductivity σ according to:

$$\sigma = \frac{G \times w}{l \times h}$$

where *w* is the source-drain gap width, *l* is the gap length and *h* is the height of the QD film. For measurements of the long-term stability of the conductivity (Figures 4e and

4f) a constant 10 mV source-drain bias (V_{sd}) was applied, and the current was measured. The conductivity was obtained as $G = I/V_{sd}$, assuming that background currents are negligible compared to the source-drain current.

Photopolymerization experiments. All photopolymerization experiments were carried out in a nitrogen-filled glove box. A UV-LED light source (600 mW/cm^2) with an emission wavelength of 395 nm was used to initiate the free radical chain polymerization reaction after electrochemical doping. 0.1 M of polymerizable electrolyte solution was prepared by dissolving ATMA-Cl salt in 10 mL of FA:DEGMA (2:3 v/v) solvent mixture. FA was used to dissolve ATMA-Cl, which is an ammonium salt with a functional acrylate group at one end and DEGMA was employed as a cross-linking agent in the photopolymerization reaction, which has bifunctional methacrylate groups on each side. The chemical structures of both monomers can be seen in Figure 3a. For experiments with non-polymerizable electrolyte ions, solutions of 0.1 M were separately prepared by dissolving $LiClO_4$ salt in 10 mL of ACN and in 10 mL of FA:DEGMA (2:3 v/v) solvent mixture. A photoinitiator molecule (~1 mg) was added in all experiments. A three-electrode electrochemical cell is immersed in electrolyte solution and the electrochemical potential of the WE was set and kept exactly at -0.9 V and -0.75 V *vs.* Ag PRE for ZnO and PbS QD films, respectively during the entire photopolymerization experiment. This is to assure that the QD film is in doped state while the photochemical fixation of the electrolyte solution is in progress, which then fixes the Fermi level of the system at exactly the potential specified. After 90 mins of UV-light irradiation time, the electrochemical cell was disconnected from the potentiostat so that no further electron injection or extraction could occur through the external circuit. The charge stability measurements were then performed as mentioned above in the conductivity and Fermi-level stability measurement sections.

References

1. Abram, R. A.; Rees, G. J.; Wilson, B. L. H., Heavily doped semiconductors and devices. Advances in Physics 1978, 27 (6), 799-892.

2. Schubert, E. F., Doping in III-V Semiconductors. Cambridge University Press: Cambridge, 1993.

3. Electronic properties of doped semiconductors by B. I. Shklovskii and A. L. Efros. Acta Crystallographica Section A 1985, 41 (2), 208-208.

4. Alivisatos, A. P., Semiconductor Clusters, Nanocrystals, and Quantum Dots. Science 1996, 271 (5251), 933.

5. Kagan Cherie, R.; Lifshitz, E.; Sargent Edward, H.; Talapin Dmitri, V., Building devices from colloidal quantum dots. Science 2016, 353 (6302), aac5523.

6. Gur, I.; Fromer, N. A.; Geier, M. L.; Alivisatos, A. P., Air-Stable All-Inorganic Nanocrystal Solar Cells Processed from Solution. Science 2005, 310 (5747), 462.

7. Kamat, P. V., Quantum Dot Solar Cells. The Next Big Thing in Photovoltaics. The Journal of Physical Chemistry Letters 2013, 4 (6), 908-918.

8. Shirasaki, Y.; Supran, G. J.; Bawendi, M. G.; Bulović, V., Emergence of colloidal quantum-dot light-emitting technologies. Nature Photonics 2012, 7, 13.

9. Wood, V.; Bulović, V., Colloidal quantum dot light-emitting devices. Nano Reviews 2010, 1 (1), 5202.

10. Konstantatos, G.; Howard, I.; Fischer, A.; Hoogland, S.; Clifford, J.; Klem, E.; Levina, L.; Sargent, E. H., Ultrasensitive solution-cast quantum dot photodetectors. Nature 2006, 442 (7099), 180-183.

11. McDonald, S. A.; Konstantatos, G.; Zhang, S.; Cyr, P. W.; Klem, E. J. D.; Levina, L.; Sargent, E. H., Solution-processed PbS quantum dot infrared photodetectors and photovoltaics. Nature Materials 2005, 4 (2), 138-142.

12. Klimov, V. I.; Ivanov, S. A.; Nanda, J.; Achermann, M.; Bezel, I.; McGuire, J. A.; Piryatinski, A., Single-exciton optical gain in semiconductor nanocrystals. Nature 2007, 447 (7143), 441-446.

13. Geiregat, P.; Van Thourhout, D.; Hens, Z., A bright future for colloidal quantum dot lasers. NPG Asia Materials 2019, 11 (1), 41.

14. Forster, J. D.; Lynch, J. J.; Coates, N. E.; Liu, J.; Jang, H.; Zaia, E.; Gordon, M. P.; Szybowski, M.; Sahu, A.; Cahill, D. G.; Urban, J. J., Solution-Processed Cu2Se Nanocrystal Films with Bulk-Like Thermoelectric Performance. Scientific Reports 2017, 7 (1), 2765.

15. Harman, T. C.; Taylor, P. J.; Walsh, M. P.; LaForge, B. E., Quantum Dot Superlattice Thermoelectric Materials and Devices. Science 2002, 297 (5590), 2229.

16. Tsu, R.; Babić, D., Doping of a quantum dot. Applied Physics Letters 1994, 64 (14), 1806-1808.

17. Erwin, S. C.; Zu, L.; Haftel, M. I.; Efros, A. L.; Kennedy, T. A.; Norris, D. J., Doping semiconductor nanocrystals. Nature 2005, 436 (7047), 91-94.

18. Shim, M.; Guyot-Sionnest, P., n-type colloidal semiconductor nanocrystals. Nature 2000, 407, 981.

19. Kamat, P. V., Semiconductor Nanocrystals: To Dope or Not to Dope. The Journal of Physical Chemistry Letters 2011, 2 (21), 2832-2833.

20. Norris, D. J.; Efros, A. L.; Erwin, S. C., Doped Nanocrystals. Science 2008, 319 (5871), 1776.

21. Desnica, U. V., Doping limits in II–VI compounds — Challenges, problems and solutions. Progress in Crystal Growth and Characterization of Materials 1998, 36 (4), 291-357.

22. Stavrinadis, A.; Konstantatos, G., Strategies for the Controlled Electronic Doping of Colloidal Quantum Dot Solids. ChemPhysChem 2016, 17 (5), 632-644.

23. Tuinenga, C.; Jasinski, J.; Iwamoto, T.; Chikan, V., In Situ Observation of Heterogeneous Growth of CdSe Quantum Dots: Effect of Indium Doping on the Growth Kinetics. ACS Nano 2008, 2 (7), 1411-1421.

24. Roy, S.; Tuinenga, C.; Fungura, F.; Dagtepe, P.; Chikan, V.; Jasinski, J., Progress toward Producing n-Type CdSe Quantum Dots: Tin and Indium Doped CdSe Quantum Dots. The Journal of Physical Chemistry C 2009, 113 (30), 13008-13015.

25. Xie, R.; Peng, X., Synthesis of Cu-Doped InP Nanocrystals (d-dots) with ZnSe Diffusion Barrier as Efficient and Color-Tunable NIR Emitters. Journal of the American Chemical Society 2009, 131 (30), 10645-10651.

26. Mocatta, D.; Cohen, G.; Schattner, J.; Millo, O.; Rabani, E.; Banin, U., Heavily Doped Semiconductor Nanocrystal Quantum Dots. Science 2011, 332 (6025), 77-81.

27. Sahu, A.; Kang, M. S.; Kompch, A.; Notthoff, C.; Wills, A. W.; Deng, D.; Winterer, M.; Frisbie, C. D.; Norris, D. J., Electronic Impurity Doping in CdSe Nanocrystals. Nano Letters 2012, 12 (5), 2587-2594.

28. Kang, M. S.; Sahu, A.; Frisbie, C. D.; Norris, D. J., Influence of Silver Doping on Electron Transport in Thin Films of PbSe Nanocrystals. Advanced Materials 2013, 25 (5), 725-731.

29. Choi, J.-H.; Fafarman, A. T.; Oh, S. J.; Ko, D.-K.; Kim, D. K.; Diroll, B. T.; Muramoto, S.; Gillen, J. G.; Murray, C. B.; Kagan, C. R., Bandlike Transport in Strongly Coupled and Doped Quantum Dot Solids: A Route to High-Performance Thin-Film Electronics. Nano Letters 2012, 12 (5), 2631-2638.

30. Erwin, S. C.; Zu, L. J.; Haftel, M. I.; Efros, A. L.; Kennedy, T. A.; Norris, D. J., Doping semiconductor nanocrystals. Nature 2005, 436 (7047), 91-94.

31. Koh, W.-k.; Koposov, A. Y.; Stewart, J. T.; Pal, B. N.; Robel, I.; Pietryga, J. M.; Klimov, V. I., Heavily doped n-type PbSe and PbS nanocrystals using ground-state charge transfer from cobaltocene. Scientific Reports 2013, 3 (1), 2004.

32. Engel, J. H.; Surendranath, Y.; Alivisatos, A. P., Controlled Chemical Doping of Semiconductor Nanocrystals Using Redox Buffers. Journal of the American Chemical Society 2012, 134 (32), 13200-13203.

33. Rinehart, J. D.; Schimpf, A. M.; Weaver, A. L.; Cohn, A. W.; Gamelin, D. R., Photochemical Electronic Doping of Colloidal CdSe Nanocrystals. Journal of the American Chemical Society 2013, 135 (50), 18782-18785.

34. Araujo, J. J.; Brozek, C. K.; Kroupa, D. M.; Gamelin, D. R., Degenerately n-Doped Colloidal PbSe Quantum Dots: Band Assignments and Electrostatic Effects. Nano Letters 2018, 18 (6), 3893-3900.

35. Puntambekar, A.; Wang, Q.; Miller, L.; Smieszek, N.; Chakrapani, V., Electrochemical Charging of CdSe Quantum Dots: Effects of Adsorption versus Intercalation. ACS Nano 2016, 10 (12), 10988-10999.

36. Houtepen, A. J.; Vanmaekelbergh, D., Orbital Occupation in Electron-Charged CdSe Quantum-Dot Solids. The Journal of Physical Chemistry B 2005, 109 (42), 19634-19642.

37. Vanmaekelbergh, D.; Houtepen, A. J.; Kelly, J. J., Electrochemical gating: A method to tune and monitor the (opto)electronic properties of functional materials. Electrochimica Acta 2007, 53 (3), 1140-1149.

38. Wehrenberg, B. L.; Guyot-Sionnest, P., Electron and Hole Injection in PbSe Quantum Dot Films. Journal of the American Chemical Society 2003, 125 (26), 7806-7807.

39. Gudjonsdottir, S.; Kwakkenbos, B.; Koopman, C.; Stam, W. v. d.; Evers, W. H.; Houtepen, A. J., On the Stability of Permanent Electrochemical Doping of Quantum Dot, Fullerene, and Conductive Polymer in Frozen Electrolytes for Use in Semiconductor Devices. ACS Appl. Nano. Mater. 2019, 2 (8), 4900-4909.

40. Gooding, A. K.; Gómez, D. E.; Mulvaney, P., The Effects of Electron and Hole Injection on the Photoluminescence of CdSe/CdS/ZnS Nanocrystal Monolayers. ACS Nano 2008, 2 (4), 669-676.

41. Lakhwani, G.; Roijmans, R. F. H.; Kronemeijer, A. J.; Gilot, J.; Janssen, R. A. J.; Meskers, S. C. J., Probing Charge Carrier Density in a Layer of Photodoped ZnO Nanoparticles by Spectroscopic Ellipsometry. J. Phys. Chem. C 2010, 114 (35), 14804-14810.

42. Gudjonsdottir, S.; Koopman, C.; Houtepen, A. J., Enhancing the stability of the electron density in electrochemically doped ZnO quantum dots. The Journal of Chemical Physics 2019, 151 (14), 144708.

43. Schimpf, A. M.; Gunthardt, C. E.; Rinehart, J. D.; Mayer, J. M.; Gamelin, D. R., Controlling Carrier Densities in Photochemically Reduced Colloidal ZnO Nanocrystals: Size Dependence and Role of the Hole Quencher. Journal of the American Chemical Society 2013, 135 (44), 16569-16577.

44. van der Stam, W.; du Fossé, I.; Grimaldi, G.; Monchen, J. O. V.; Kirkwood, N.; Houtepen, A. J., Spectroelectrochemical Signatures of Surface Trap Passivation on CdTe Nanocrystals. Chemistry of Materials 2018, 30 (21), 8052-8061.

45. du Fossé, I.; Boehme, S. C.; Infante, I.; Houtepen, A. J., Dynamic Formation of Metal-Based Traps in Photoexcited Colloidal Quantum Dots and Their Relevance for Photoluminescence. Chemistry of Materials 2021, 33 (9), 3349-3358.

46. Matyba, P.; Maturova, K.; Kemerink, M.; Robinson, N. D.; Edman, L., The dynamic organic p–n junction. Nature Materials 2009, 8 (8), 672-676.

47. Pei, Q.; Yu, G.; Zhang, C.; Yang, Y.; Heeger, A. J., Polymer Light-Emitting Electrochemical Cells. Science 1995, 269 (5227), 1086.

48. Tang, S.; Edman, L., Light-Emitting Electrochemical Cells: A Review on Recent Progress. Topics in Current Chemistry 2016, 374 (4), 40.

49. Bolink, H. J.; Coronado, E.; Costa, R. D.; Ortí, E.; Sessolo, M.; Graber, S.; Doyle, K.; Neuburger, M.; Housecroft, C. E.; Constable, E. C., Long-Living Light-Emitting Electrochemical Cells – Control through Supramolecular Interactions. Advanced Materials 2008, 20 (20), 3910-3913.

50. Pei, Q.; Yang, Y.; Yu, G.; Zhang, C.; Heeger, A. J., Polymer Light-Emitting Electrochemical Cells: In Situ Formation of a Light-Emitting p−n Junction. Journal of the American Chemical Society 1996, 118 (16), 3922-3929.

51. Guyot-Sionnest, P., Charging colloidal quantum dots by electrochemistry. Microchimica Acta 2008, 160 (3), 309-314.

52. Gao, J.; Yu, G.; Heeger, A. J., Polymer light-emitting electrochemical cells with frozen p-i-n junction. Applied Physics Letters 1997, 71 (10), 1293-1295.

53. Gao, J.; Li, Y.; Yu, G.; Heeger, A. J., Polymer light-emitting electrochemical cells with frozen junctions. Journal of Applied Physics 1999, 86 (8), 4594-4599.

54. Gudjonsdottir, S.; Houtepen, A. J., Permanent Electrochemical Doping of Quantum Dots and Semiconductor Polymers. Advanced Functional Materials 2020, 30 (49), 2004789.

55. Yu, Z.; Wang, M.; Lei, G.; Liu, J.; Li, L.; Pei, Q., Stabilizing the Dynamic p−i−n Junction in Polymer Light-Emitting Electrochemical Cells. The Journal of Physical Chemistry Letters 2011, 2 (5), 367-372.

56. Yu, Z.; Sun, M.; Pei, Q., Electrochemical Formation of Stable p-i-n Junction in Conjugated Polymer Thin Films. The Journal of Physical Chemistry B 2009, 113 (25), 8481-8486.

57. Kosilkin, I. V.; Martens, M. S.; Murphy, M. P.; Leger, J. M., Polymerizable Ionic Liquids for Fixed-Junction Polymer Light-Emitting Electrochemical Cells. Chemistry of Materials 2010, 22 (17), 4838-4840.

58. Leger, J. M.; Rodovsky, D. B.; Bartholomew, G. P., Self-Assembled, Chemically Fixed Homojunctions in Semiconducting Polymers. Advanced Materials 2006, 18 (23), 3130-3134.

59. Leger, J. M.; Patel, D. G.; Rodovsky, D. B.; Bartholomew, G. P., Polymer Photovoltaic Devices Employing a Chemically Fixed p–i–n Junction. Advanced Functional Materials 2008, 18 (8), 1212-1219.

60. Tang, S.; Edman, L., On-demand photochemical stabilization of doping in light-emitting electrochemical cells. Electrochimica Acta 2011, 56 (28), 10473-10478.

61. Tang, S.; Irgum, K.; Edman, L., Chemical stabilization of doping in conjugated polymers. Organic Electronics 2010, 11 (6), 1079-1087.

62. Ashokan, A.; Mulvaney, P., Spectroelectrochemistry of Colloidal CdSe Quantum Dots. Chemistry of Materials 2021, 33 (4), 1353-1362.

63. Wood, A.; Giersig, M.; Hilgendorff, M.; Vilas-Campos, A.; Liz-Marzán, L. M.; Mulvaney, P., Size Effects in ZnO: The Cluster to Quantum Dot Transition. Australian Journal of Chemistry 2003, 56 (10), 1051-1057.

64. Mashford, B. S.; Stevenson, M.; Popovic, Z.; Hamilton, C.; Zhou, Z.; Breen, C.; Steckel, J.; Bulovic, V.; Bawendi, M.; Coe-Sullivan, S.; Kazlas, P. T., High-efficiency quantum-dot light-emitting devices with enhanced charge injection. Nature Photonics 2013, 7 (5), 407-412.

65. Zhang, J.; Chernomordik, B. D.; Crisp, R. W.; Kroupa, D. M.; Luther, J. M.; Miller, E. M.; Gao, J.; Beard, M. C., Preparation of Cd/Pb Chalcogenide Heterostructured Janus Particles via Controllable Cation Exchange. ACS Nano 2015, 9 (7), 7151-7163.

Appendix

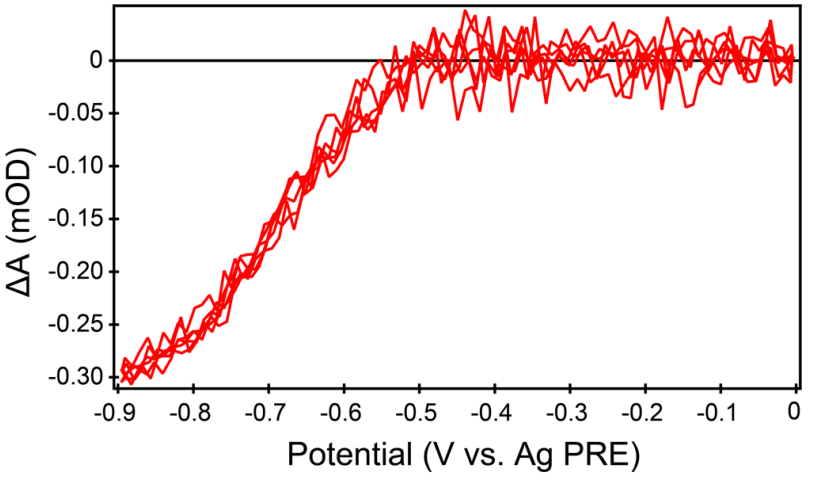

Figure A2.1 Differential absorbance (ΔA) vs voltage graph of the ZnO QD film in an electrolyte solution of 0.1 M $LiClO_4$ in ACN. Simultaneously monitoring the changes in absorption as a function of applied potential gives bleach features.

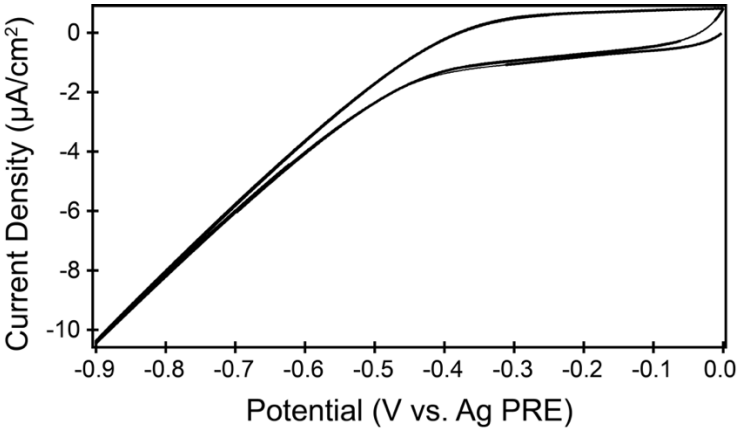

Figure A2.2 CV of ZnO QD film scanned outside of the glove box in an electrochemical cell containing 0.1 M $LiClO_4$ in ACN.

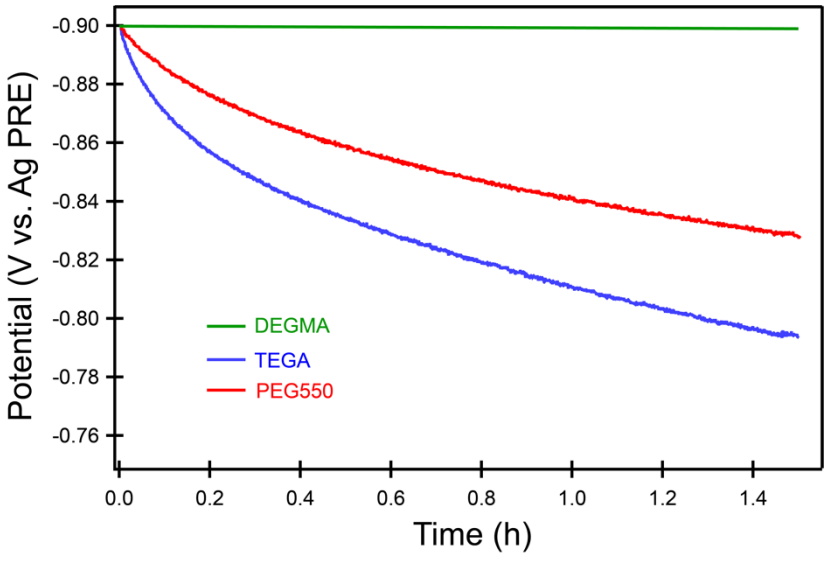

Figure A2.3 Fermi level stability measurements of the ZnO QD film in an electrochemical cell containing 0.1 M ATMA-Cl in different length of cross-linking molecules namely, DEGMA, TEGA and PEG550 all together with FA solvent.

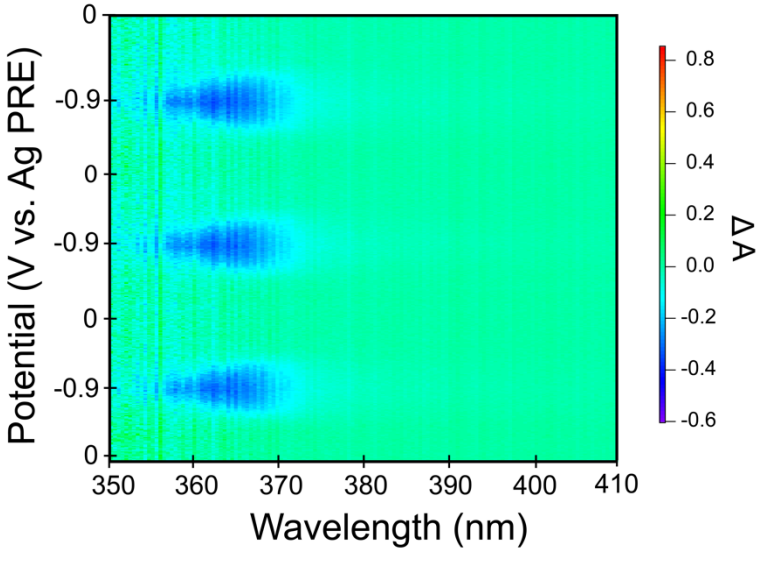

Figure A2.4 The 2D color map showing the differential absorbance, bleach (ΔA) from ZnO QD film during electrochemical charging and discharging in an electrochemical cell containing 0.1 M ATMA-Cl in FA.

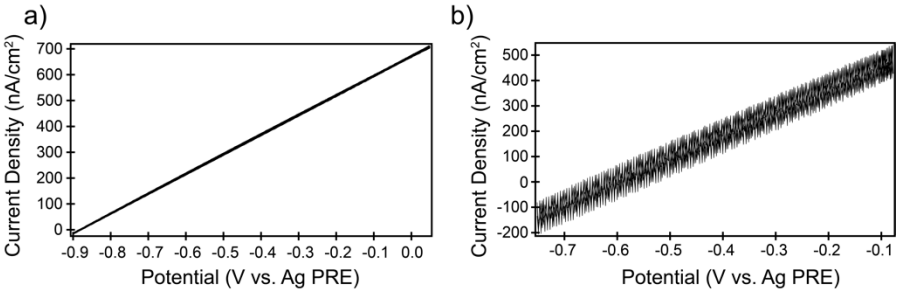

Figure A2.5 CVs of the ZnO (a) and PbS QD films (b) after photopolymerization treatment. As shown in the CVs, only negligible amount of current (nanoampere) is observed during the CV scans after polymerization.

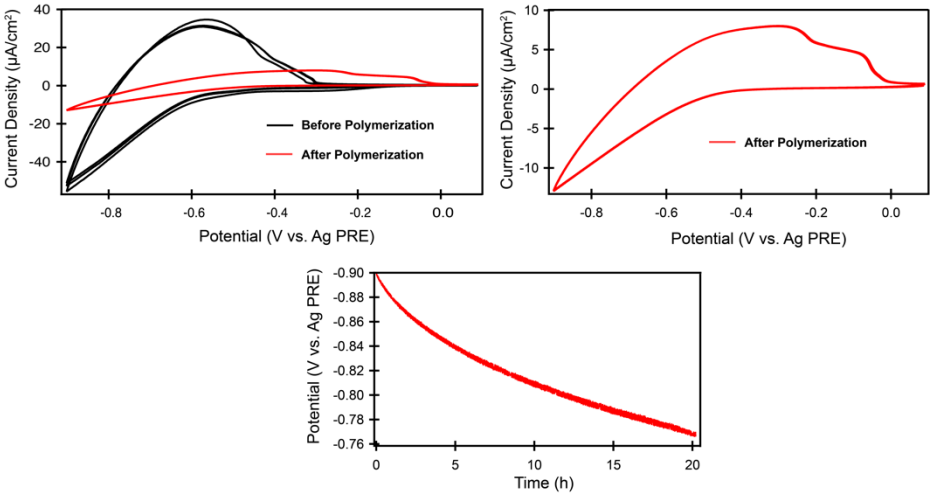

Figure A2.6 CVs of the ZnO QD film before (top right) and after photopolymerization treatment (top left) and Fermi level stability measurement after polymerization (bottom) in an electrochemical cell containing 0.1 M $LiClO_4$ in FA:DEGMA solvent mixture.

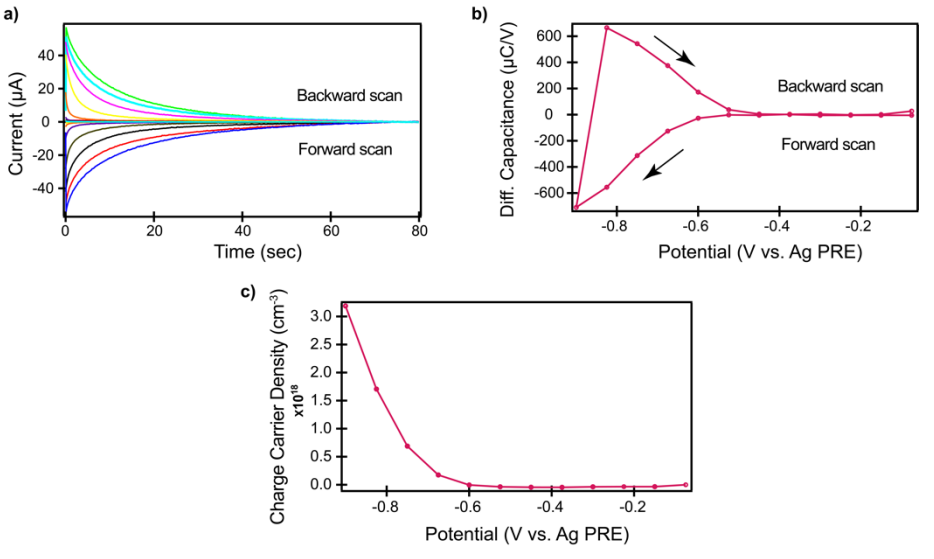

Figure A2.7 Differential capacitance measurements performed on ZnO QD film deposited on IDE substrate in an electrochemical cell containing 0.1 M ATMA-Cl in FA:DEGMA solvent mixture. Potential steps of 75 mV were applied and after each potential step the charging current was recorded for 80 seconds. In all cases, the initial peak currents decayed in an exponential manner to a constant current which can be assigned to background current of the electrolyte which then subtracted to obtain the electrochemical charging of the QD film (a), the integration of this charging current followed by a division of each potential step gives the differential capacitance of the ZnO QD film with a unit of coulomb per volt (b), the total injected charge was calculated by multiplying the differential capacitance with the potential applied which then divided into the film volume in order to derive the charge carrier density of the ZnO QD film as a function of applied potential (c). For example; the charge carrier density of the ZnO QD film at the potential of -0.9 V is ~10^{18} per cm^3.

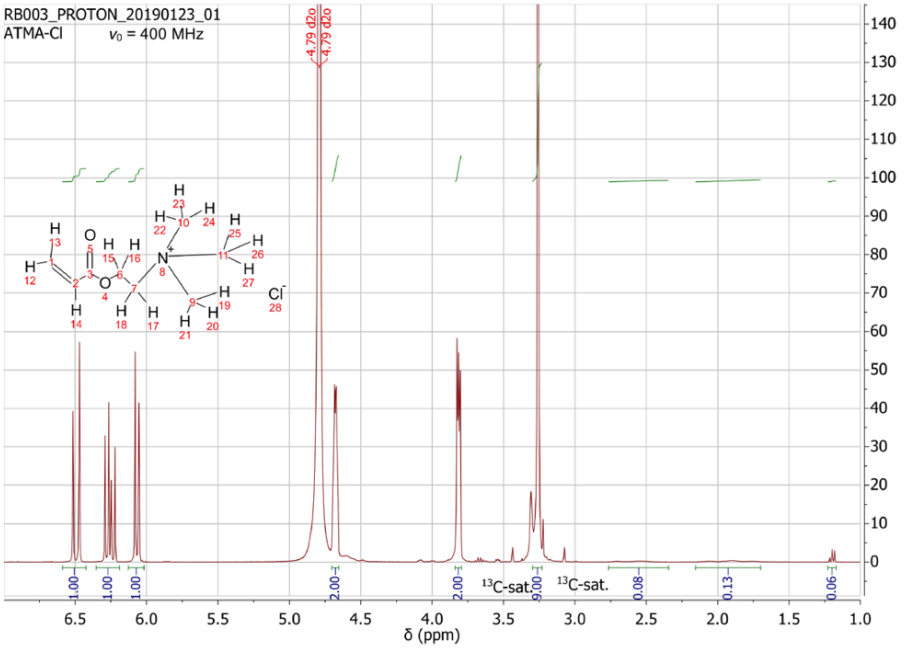

Figure A2.8 ^{1}H-NMR spectrum of dried ATMA-Cl salt in D_2O. In the present ^{1}H-NMR, the ATMA-Cl signals are analysed. ^{1}H-NMR (400 MHz, D_2O, 20 °C): δ= 6.49 (dd, 1H, $^{3}J_{trans}$(^{1}H; ^{1}H) = 17:3 Hz, ^{2}J(^{1}H; ^{1}H) = 1:0 Hz; Vinyl-CH position 1), 6.26 (dd, ^{1}H, $^{3}J_{trans}$ (^{1}H; ^{1}H) = 17:3 Hz, $^{3}J_{cis}$(^{1}H; ^{1}H) = 10.6 Hz; Vinyl-CH, position 2), 6.07 (dd, 1H, $^{3}J_{cis}$(^{1}H; ^{1}H) = 10.6 Hz, ^{2}J(^{1}H; ^{1}H) = 1:0 Hz; Vinyl-CH, position 1), 4.68 (m, 2H; CH_2, position 6), 3.81 (m, 2H; CH_2, position 7) and 3.26 ppm (s, 9H; 3 CH_3, positions 9 - 11).

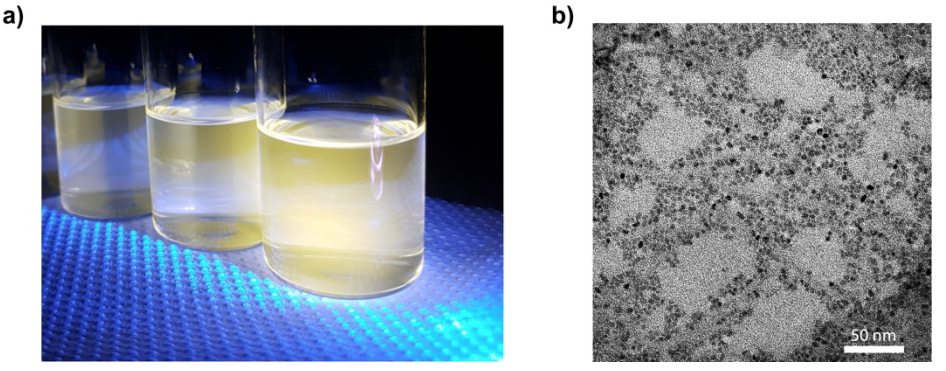

Figure A2.9 An image of a pale blue-green emission from ZnO QDs in ethanol (a), Transmission electron microscopy (TEM) image of synthesized ZnO QDs with an average diameter size of 3.5±0.2 nm.

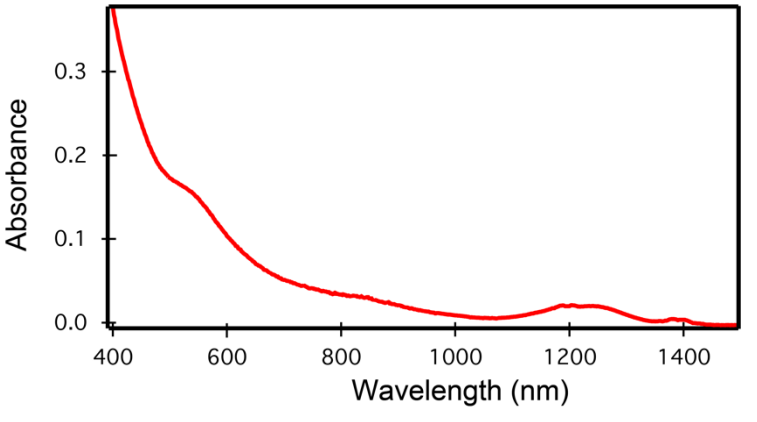

Figure A2.10 The absorption spectrum of PbS QDs dispersed in hexane.

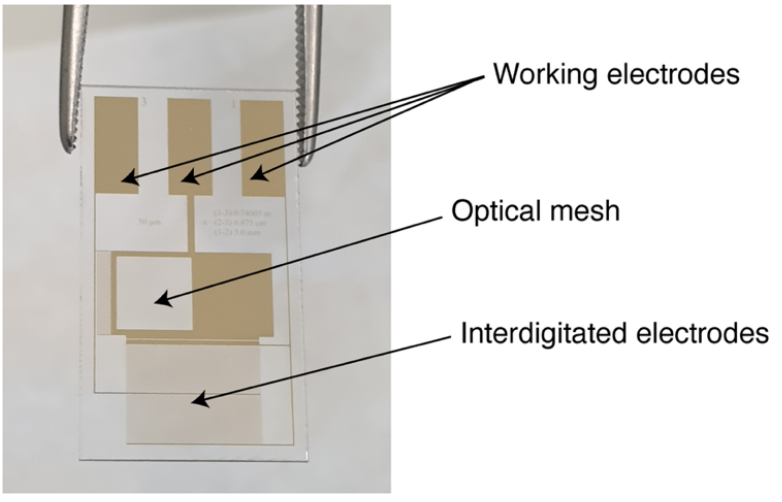

Figure A2.11 Home-built interdigitated gold electrode (IDE). The electrode is a glass substrate coated with three separate gold WEs which provide three source-drain gaps of different sensitivities.

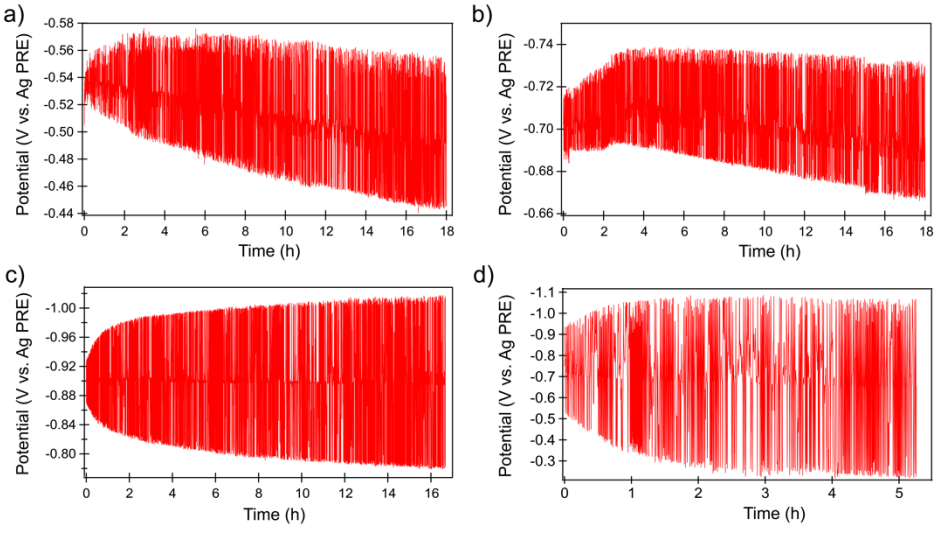

Figure A2.12 The raw data set obtained from voltage vs time experiments (Fermi-level stability measurements) for different potential values, namely: -0.5 V (a), -0.7 V (b), -0.9 V (c) vs Ag PRE for ZnO and -0.75 V vs Ag PRE (d) for PbS QD films.

Chapter 3

Enhancing the Charge Stability in Electrochemically p-Doped Conducting Polymers

Abstract

The ability to precisely and controllably dope conducting polymers (CPs) is indispensable for their use in semiconductor devices. Electrochemical doping allows to adjust the charge carrier concentration precisely and controllably as a function of applied potential through a potentiostat and thus the doping levels in CP films. However, the stability of electrochemically injected charges remains a challenge. Electrochemically injected charges quickly disappear when the doped film is disconnected from the potentiostat due to (electro)chemical side reactions with impurities present in the cell causing the dopant ions to diffuse out and resulting a drop in charge density. Here we substantially improved the stability of electrochemically injected holes in P3DT films using a photopolymerization treatment at room temperature. We photochemically fixate the dopant ions by polymerizing the electrolyte solution and meanwhile hinder the diffusion of impurities into the P3DT film and therefore, enhancing the stability of the electrochemically injected holes inside the film. We systematically studied how the stability of injected charges and diffusion of the dopant ions are related to the impurity concentration in the solvents, the choice of monomer/cross-linking agent and the type of photoinitiator molecules. The results emphasize the promise of photopolymerization after electrochemical doping and suggest that there is still considerable room for improvement of charge stability in doped CP films to be used in future electronic devices.

This chapter is based on: Hamit Eren, Wolter F. Jager and Arjan J. Houtepen. In Preparation.

3.1 Introduction

In the previous chapter we have shown that electrochemical n-doping of ZnO and PbS nanocrystals, followed by cross-linking of the electrolyte solvent and ions through photopolymerization, results in n-doped materials with a tunable electron density that is stable for at least several weeks[1]. This establishes electrochemical doping as viable alternative doping technique for the preparation of semiconductor devices made of nanocrystals. Here we show that this approach is not limited to n-doping of semiconductor nanocrystals, but also applies to p-doping of conducting polymers (CPs).

CPs have received considerable attention over the past several decades.[2-5] Having a unique set of properties such as low-cost, mechanical flexibility, light weight, ease of synthesis and low-temperature processing makes them promising as alternatives to their inorganic semiconductor counterparts for use in semiconductor devices including organic light emitting diodes (OLEDs),[6, 7] field effect transistors (OFETs),[8, 9] light emitting electrochemical cells (LECs),[10, 11] and organic solar cells (OSCs).[12, 13]

In the neutral state, CPs exhibit electronic properties of an insulator. The conductivity of such neutral CPs was enhanced by several orders of magnitude by means of doping in a ground-breaking study in the late 1970s, showing that the electrical conductivity of polyacetylene can be increased by ten million times through vapour doping using volatile halogens.[14]

The ability to precisely and controllably dope CPs is indispensable for advanced semiconductor devices. So far, CPs have been doped by different methods such as chemical doping,[15-17] electrochemical doping,[18-20] and photodoping.[21, 22] Among them, the first two methods are widely used due to their low-cost and convenience. Chemical doping has two forms: solution doping and vapor-phase doping. The former technique simply includes co-blending of the CP and dopants in solution and then directly casting a doped film or immersing the CP film into the solutions of dopant molecules dissolved in proper solvents. In the latter method, the pre-cast film of the CP is exposed to the evaporating dopant molecules such as iodine, bromine and the level of doping with this technique is adjusted by the vapor pressure and exposure time of dopant molecules. Electrochemical doping allows to precisely and controllably adjust the charge carrier concentration as a function of applied potential through a potentiostat and hence the

doping levels in the CP films.[23] Electrochemical doping measurements are typically performed in a three-electrode electrochemical cell containing an electrolyte solution. Here, the electrochemical charge injection (electron or hole) into the CP film deposited on a conductive electrode takes place as a function of applied potential by using a potentiostat. Together with the injected charge carriers, electrolyte ions of opposite charge, which act as external dopants, migrate into the CP film to maintain electroneutrality as depicted schematically in Figure 3.1. With this effective nanoscale charge compensation, high doping densities can be achieved. Compared to chemical doping, electrochemical doping offers an easier way to control the doping level. Variability in choosing the dopant species within the CP films, high reversibility of doping and de-doping, and minimized structural distortion in film morphology upon doping are some of the main advantages over chemical doping.

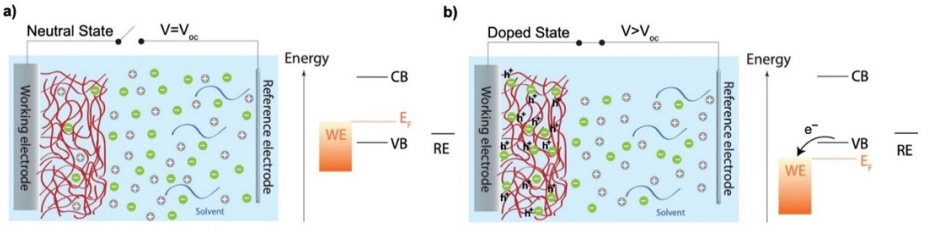

Figure 3.1 Schematic of electrochemical charge injection into CP film. (a) shows a situation where the Fermi level is inside the band gap of the CP when there is no applied potential to the WE, (b) shows a situation where the Fermi level in this case is below the valence band of the CP as a function of applied positive potential with respect to RE. To neutralize the injected holes electrostatically, electrolyte anions diffuse into the voids of the film.

However, the stability of electrochemically injected charges still remains a challenge. Although considerable research has been devoted to the electrochemical doping of CPs, rather less attention has been paid to the stability of injected charges. Several studies on the stability of charges can however be found in the field of polymer LECs,[24, 25] which show close resemblance to the system investigated here. LECs have an active medium of electroluminescent CP sandwiched between two metal electrodes with electrolyte ions and some solvent (typically polyethylene glycol) included for electrochemical doping. When a sufficiently high voltage is applied, charges are injected from the electrodes into the CP layer, resulting in a p-type layer on one side and an n-type layer

on the opposite side. These doped layers grow in size and eventually form a p-n junction at the interface between the two, where light emission takes place.[11] When the voltage source is removed, the device discharges and dopant ions redistribute.[26]

The diffusion of dopant ions in an electrochemically doped system, which affords the easy charging, is problematic for the stability of the doped films. In comparison to, for instance, the highly stable p-n junction structure of doped crystalline silicon, in which the dopant atoms (e.g., boron or phosphorus) are introduced into the material at high temperatures,[27] the p-n junction structure in LECs is quite dynamic.[28] Because of this dynamic nature of the p-n junction, the stability of charges is limited and the fixation of the dopant ions after electrochemical doping is required for achieving stable electrochemical doping of CPs in general and LECs in particular.

Certain strategies have been proposed and demonstrated to overcome this challenge. Gao and co-workers were the first to report LEC devices with stable p-i-n junction doping structures by freezing the ion-transport polymer at very low temperatures.[29, 30] By doing so, electrochemical side reactions can be retarded and both dopant ions and impurities can be immobilized. Similarly, Gudjonsdottir et al. showed that highly stable doping densities in different quantum dots and CPs can be achieved by using electrolyte solvents that are solid at room temperature.[31, 32] The electrochemical charge injection takes place at elevated temperatures above the melting point of the electrolyte solution. After successful charge injection at higher temperature, the system cools down to room temperature causing the electrolyte solvent to solidify, yielding stable electrochemical doping. Despite the success of stable doping in these studies, from a practical point of view, this way of stabilizing of charges and fixing dopant ions may not be applicable to be used in certain applications where such low and high temperature of operation is involved.

An elegant alternative way to achieve stable p-n junction doping structures at room temperature is demonstrated by Leger and co-workers via chemical fixation of dopant ions in polymer LEC and photovoltaic devices.[33-35] They effectively locked in place the dopant ions by means of polymerization where they use polymerizable electrolyte ions. In a similar study, Tang et al. showed stable p-n junction doping structures via photochemical immobilization of dopant ions in LEC device at room temperature.[36, 37] Recently, we extended this method and showed that photopolymerization of the

solvent and dopant ions can drastically enhance the stability of electrochemically n-doped ZnO and PbS quantum dot films.[1]

Here we show that the same methods we applied to stabilize n-doped ZnO and PbS quantum dot films can also be used to stabilize p-doped P3DT films. In addition, we expand on the work of Leger et al.[33-35] and Tang et al.[36, 37] by systematically investigating the effect of photopolymerization parameters on the stability of injected charges and diffusion of the dopant ions in electrochemically p-doped P3DT film at room temperature. In particular, the influence of monomer/cross-linking agents, type of photoinitiators, and impurities in solvents were investigated as will be discussed below in detail. By measuring the electrical conductivity and the stability of the Fermi-level, we show that through the combination of electrochemical doping and photopolymerization, the stability of injected holes can be enhanced substantially. By performing cyclic voltammetry (CV), we examined the mobility of dopant ions before and after photopolymerization treatment.

3.2 Results and Discussion

Electrochemical hole injection into P3DT films was measured by in-situ absorption spectroscopy in a three-electrode electrochemical cell set-up as shown in Figure 3.2a. A change in the optical absorption of the film was monitored as a function of applied potential. The 2D color map in Figure 3.2b shows the differential absorbance (ΔA) of three cycles of charging/discharging a P3DT film. The black line shows the absorption spectrum of the neutral polymer film. On the 2D map, the blue color in the visible region indicates a bleaching of the ground state absorption as a result of hole injection into the valance band, while the red signal in the red and near infrared region is due to induced absorption of (bi)polarons that form upon hole injection.[38]

The reproducibility of the bleach features in Figure 3.2b demonstrates the reversible tuning of the Fermi level of the system as a function of applied potential. Figure 3.2c shows the CV of the P3DT film where the potential was scanned from -0.03 V (the open circuit potential, V_{oc}) to 0.45 V *vs.* Ag PRE with a scan rate of 10 mV/s (black line). It is clear from the CV that the majority of the injected holes can be extracted when the applied potential is scanned back to V_{oc}. However, the CV is not fully symmetric because of the slow diffusion of electrolyte ions inside the P3DT film during electrochemical

charging and discharging. This limitation originates from the relatively large size of the counter ions ($AMPS^-$) moving in a relatively viscous medium. This observation is confirmed by the fact that more symmetrical CVs were obtained with slower scan rates. The conductivity of the P3DT film as a function of applied potential is shown as the red line in the same figure. The increase in conductivity correlates with the appearance of the absorption bleach. For a clearer demonstration, the ΔA *vs.* potential graph can be seen in Appendix, Figure A3.1. All these effects clearly show that both electrochemical hole injection into the valance band and dopant ion diffusion into the P3DT film occur successfully.

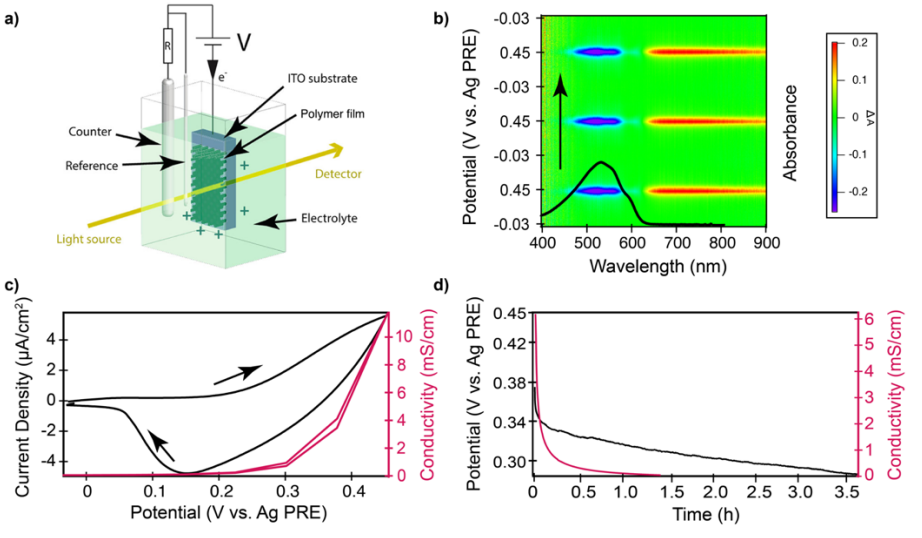

Figure 3.2 (a) Schematic of the three-electrode spectro-electrochemistry set-up for in-situ optical absorbance measurements, reprinted with permission from ref.[39] Copyright (2013) American Chemical Society. (b) the 2D color map shows the differential absorbance (ΔA) of the P3DT film during electrochemical charging and discharging, with an absorption spectrum (black line) of the film on top of it, (c) the CV of the P3DT film scanned starting at -0.03 V to 0.45 V *vs.* Ag PRE with a scan rate of 10 mV/s (black line) and the conductivity of the P3DT film as a function of applied potential (red line), (d) both conductivity (red line) and Fermi-level stability (black line) measurements over time after disconnecting the cell from the potentiostat without any treatment. All measurements are performed in an electrolyte solution containing 0.05 M AMPSH in DMF:MMA:PEGMA-550 (1:7:2 v/v/v).

While similar electrochemical studies on such conducting polymer films can be found broadly in literature, the investigation on the stability of the electrochemically introduced charges is relatively scarce. Here, to determine the stability of electrochemically injected holes, we carried out Fermi-level stability and conductivity measurements after disconnecting working electrode from the counter electrode as shown in Figure 3.2d. What we initially observed after disconnecting the cell is a fast, sub-second decay in electrochemical potential from the pre-set value of 0.45 V to around 0.37 V followed by a slower potential decay over the course of several hours. We attribute the initial sharp decay to electrochemical side reactions between injected holes and impurities that were in close proximity with the injected holes inside the P3DT film. The later slower decay in potential can be assigned to further electrochemical side reactions of remaining holes with impurity molecules from the electrolyte solution that diffuse into the film over the course of the measurement. The conductivity follows a similar trend in charge stability at the beginning of the measurement. While Figure 3.2c tells us that in a steady-state conductivity measurement, a conductivity value of roughly 12 mS/cm can be reached, the highest conductivity measured in Figure 3.2d is approximately 6 mS/cm. This is due to a fast drop in conductivity during the time (~10 seconds) that the electrode is removed from the electrochemical cell and connected to a Keithley source meter for the conductivity measurement.

One can readily notice that the conductivity drops more quickly than the potential. That is expected, since the electrochemical potential is proportional to the logarithm of the hole density, p, as defined by the Nernst equation, whereas the conductivity scales linearly with p: $\sigma = pe\mu$, where μ is the hole mobility and e is the elementary charge. In other words, conductivity measurements are more sensitive to electrochemical charge stability measurements. Both graphs in Figure 3.2d evidently indicate that the injected holes are not stable after disconnecting the cell from the potentiostat. This shows that, while electrochemical doping is useful to tune the Fermi level, it cannot be used to prepare semiconductor films with a stable charge density in absence of an applied potential, such as would be needed for e.g., the formation of *pn* junctions.

Let us consider the nature of the electrochemical side reactions that might scavenge the injected holes. To begin with, even a trace amount of water present in the electrochemical cell can act as reductant. In addition, there could be other redox active impurities in the electrolyte solution that we employ. For example, the solvent DEGMA

itself, which was used as-purchased throughout the electrochemical experiments, contains 5% of impurities.

To investigate the effect of water on the stability of injected holes, we conducted a set of experiments using three different solvents including FA, DMF and water itself. These solvents are mixed with DEGMA in our experiments to solubilize AMPSH that provides the polymerizable electrolyte ions, which are not soluble in DEGMA directly. The water content in each solvent was determined by Karl Fischer titration without exposing the samples to air, resulting in 495 ppm water on average in FA and 4.5 ppm water in DMF, which was treated to lower the water content (see Methods section). Attempts to dry FA to such low level of water content (<10 ppm) failed because of the much higher hygroscopicity of FA.

A CV of a P3DT film outside of the glove box in an electrochemical cell containing 0.05 M AMPSH dissolved in a water/DEGMA mixture is shown in Figure A3.2 in Appendix. There is no sign of hole extraction in the reverse scan, demonstrating that water reacts with the injected holes on the timescale of the scan. In contrast, both CVs of P3DT films in a mixture of FA/DEGMA and DMF/DEGMA exhibit reversible features, with clear signs of hole extraction in the reverse scan, as shown in Figure 3.3 (a), (d). The charging/discharging ratio is higher for the DMF/DEGMA mixture (Figure 3.3d, black line; 94% of holes extracted on the reverse scan than for the FA/DEGMA mixture (Figure 3.3a, black line; 46% of holes extracted on the reverse scan, in line with the lower water content).

As will be shown below, the stability of the Fermi level and conductivity after photopolymerization is also much better when DMF is used than when FA is used. This confirms that water is a key problem for the stability of electrochemically injected holes in P3DT, although we cannot rule out that other redox active impurities can play a similar role. Additionally, we observed a distinct color change in the electrolyte solution after the photopolymerization treatment as shown in the pictures of the beakers in Figure 3.3 (c), (f). The intense blue color when using FA becomes lighter when using DMF under the same experimental conditions. This blue coloring is only observed when using 4,4’-bis(diethylamino)benzophenone photoinitiator (the Type II PI) and appears to correlate to the amount of water in the electrolyte, which is circa 100-fold higher in FA than DMF.

We now turn to the photopolymerization experiments that aim to improve the stability of the injected holes. The general approach to photopolymerization is that we use an electrolyte solution that consists of a polymerizable solvent, polymerizable electrolyte ions and a photoinitiator. We immerse the electrode with the P3DT film on it into such an electrolyte, charge the film with holes by applying a positive potential, and irradiate the system with 395 nm light, while maintaining that potential. The irradiation of the photoinitiator molecules with UV-light leads to generation of reactive radical species which then initiate the polymerization. Free radical photoinitiators can react differently under the UV-light irradiation and depending on their decomposition mechanism, they are classified as Type I and Type II photoinitiators. Briefly, two reactive radical species are generated from one single Type I photoinitiator molecule whereas only one reactive radical species is produced from one single Type II photoinitiator molecule, therefore making the latter less efficient in polymerization reactions. Particularly, Type II photoinitiators, when irradiated with UV-light, abstract a hydrogen atom from a donor molecule in the environment. It is that reactive donor molecule which subsequently initiates the polymerization. Here, we employed both types photoinitiator molecules in polymerization experiments to see the influence on charge stability and dopant ion fixation in electrochemically doped film.

Electrochemical charge injection into the P3DT film would not be possible, if there is no diffusion of mobile counter ions in the film to maintain electroneutrality. Thus, if photopolymerization of the anions is complete, no charging or discharging of the P3DT film is expected. However, the CVs taken after the polymerization with Type II photoinitiators in Figure 3.3 (b), (e) evidently show that electrochemical hole injection and extraction is still possible. The current in these CVs is reduced after polymerization, but recognizable charging and discharging still occurs. On the other hand, in the case of polymerization with Type I photoinitiator, the shape of the CV and the measured current in Figure 3.3 (h), (k) clearly demonstrate that the electrochemical charging and discharging is no longer possible after photopolymerizations. Thus, these results show that the chemical fixation of the electrolyte ions via photopolymerization is more efficient when using the type I PI. Indeed, the less efficient radical generation mechanism with Type II photoinitiators is expected to cause a smaller degree of polymerization than when using Type I photoinitiators, which will result in incomplete fixation of some dopant ions which are able to move around when an electric field is applied.

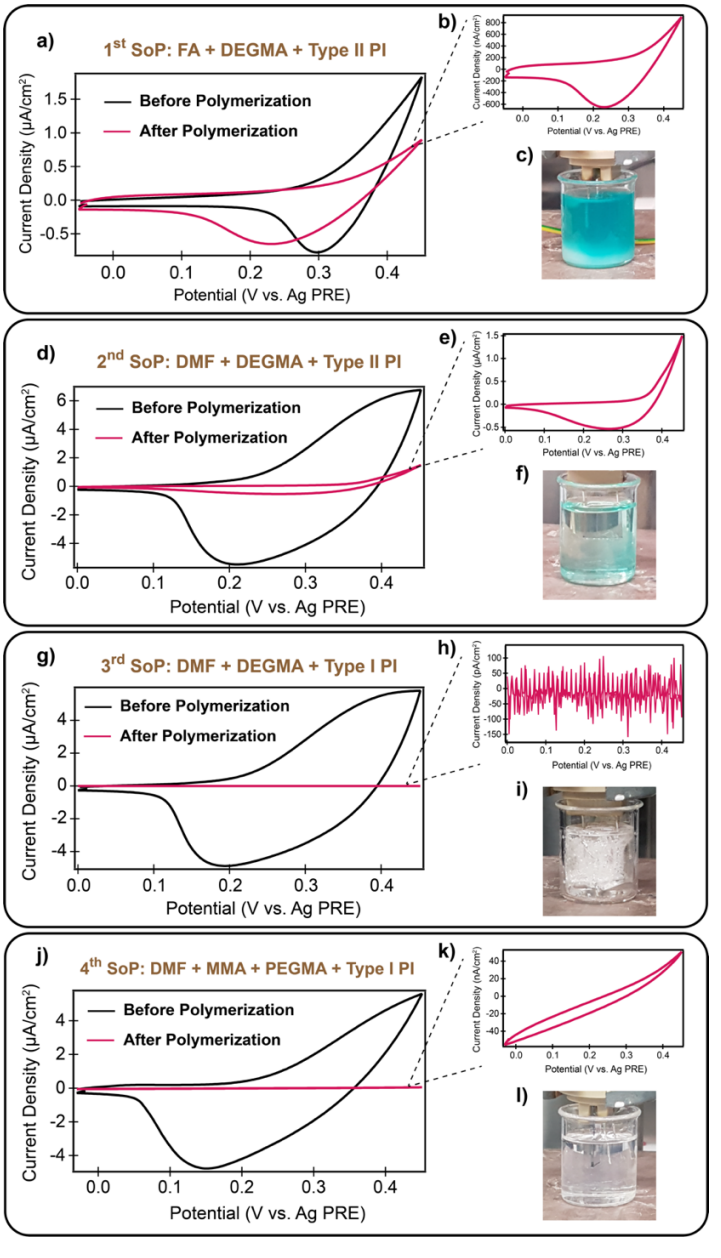

Figure 3.3 Electrochemical measurements of P3DT film before and after photopolymerization carried out in four different set of parameters (SoP). CVs of electrochemically doped P3DT film drawn on top of each other before and after photopolymerization (a), (d), (g), (j). Enlarged CVs of P3DT film after photopolymerization shown in (b), (e), (h), (k). Images taken immediately after photopolymerization reactions for four different SoP shown in (c), (f), (i), (l).

Next, we investigate the stability of the injected charges after the photopolymerization procedures. Figure 3.4a summarizes Fermi-level stability measurements on p-doped P3DT films that have undergone various photopolymerization treatments. Without photopolymerization, the potential drops to 0.29 V in ~3 hours (dashed blue line in Figure 3.4a). After photopolymerization, the potential is more stable, although the exact stability depends on the photopolymerization procedure. The potential drops to 0.29 V in 3-14 hours depending on the treatment. Here the same potential value of 0.29 V was chosen arbitrarily for a fair comparison in all stability experiments. As can be seen in Figure 3.4a, the pre-set electrochemical potential (0.45 V) of the system drops to 0.29 V in an hour with FA/DEGMA mixture (dashed red line) while it drops to the same baseline potential within 14 h (dashed yellow line) with DMF/DEGMA mixture after photopolymerization treatment on both systems.

The superior performance in photochemical fixation of dopant ions after the polymerization with Type I photoinitiator urges us to measure the stability of electrochemically injected charges after photopolymerization with this PI. Figure A3.3 in Appendix shows the Fermi-level stability measurement of DMF/DEGMA system with Type I photoinitiator. The results are however not as expected. As can be seen from Figure A3.3, the potential that we measure after p-doping at 0.45 V is never positive and shows a high degree of noise, rather than dropping slowly from the applied potential of 0.45 V back to the original open circuit potential. The Fermi-level stability experiment was repeated multiple times with the same result. This could have two explanations: (1) it could be that the radical photopolymerization interferes with the holes in the VB of the P3DT effectively dedoping the material, (2) it could be that the polymerization causes difficulties for the potential measurement itself, by electrically disconnecting the working electrode from the reference electrode. In line with the second explanation, we observe a highly aggressive polymerization reaction after 2-3 mins of UV-light irradiation causing clear micro-cracks in the polymer, as shown in Figure 3.3 (i).

To shed more light on the situation, we performed electrical conductivity measurement under the same experimental conditions to investigate the possible causes for reading out such unrealistic potential values in the measurements. Figure A3.4 in Appendix shows a set of conductivity experiments with P3DT film deposited on an interdigitated source-drain electrode for these measurements. The Figure A3.4 (a) shows the

electrical conductivity after polymerization with DMF/DEGMA and Type I photoinitiator. The measured conductivity is ~0.04 µS/cm, about 5 orders of magnitude lower than that of the p-doped film shown in Figure 3.2d, and even 40-fold lower than the conductivity of the neutral film before electrochemical doping.

To better understand this unexpected drop in the conductivity measurement, we carried out conductivity experiments during the polymerization process. Figure A3.4 (b) in the Appendix shows the source drain I-V curves during photopolymerization. The slope of these I-V curves gives the conductance of the film. As can be seen from the graph, the conductivity drops very quickly during the polymerization reaction. We carried out an additional conductivity experiment during polymerization process this time without electrochemical charge injection into the film as shown in Figure A3.4 (c) in Appendix. Unexpectedly, the conductivity of the P3DT film increased drastically about 2 mins after the start of the UV-light irradiation, which coincides with the visible observation of aggressive polymerization, followed by a drop below the intrinsic conductivity value of the P3DT film. This suggests that the radicals generated during the photopolymerization process interact with the P3DT, effectively doping the material. While the effect is clearly noticeable, we note that the observed photoinduced conductivity is <1% of the conductivity in the electrochemically p-doped P3DT film (see e.g., Figure 3.2d.). After the initial increase in conductivity, the formation of a cracked polymer probably disrupts the P3DT film, causing the final conductivity to be very low.

Both the Fermi-level and conductivity measurements discussed above clearly indicate that the polymerization reaction with DMF/DEGMA and Type I photoinitiator causes difficulties in stabilizing and measuring the doping density in the P3DT film. A possible crack formation between WE and RE might result in disruption in the internal part of the circuit during Fermi-level stability measurement. For conductivity measurements, it is likely that the crack formation in the polymer chunk might extend into the P3DT film and cause detachment of the film from the WE substrate. The crack formation is a consequence of polymerization-induced expansion and shrinkage within the polymer network during polymerization. While polymerization shrinkage cannot be eliminated completely, certain strategies can minimize the shrinkage and associated crack formation. The selection of monomer functionality and the length of monomer/cross-linking agent can influence the polymerization shrinkage stress.[40-42] In particular the shrinkage of mono-functional methacrylate-based monomers is less than that of the bi-

functional corresponding monomers. Hence, replacing the bi-functional and cross-linking DEGMA solvent by its mono-functional MMA variant may help reducing the crack formation during photopolymerizations. Further, short cross-linking molecules typically cause more shrinkage stress than longer corresponding molecules as they form a more densely packed polymer network. In that regard, the commonly used bi-functional PEGMA-550 monomer may reduce crack formation.

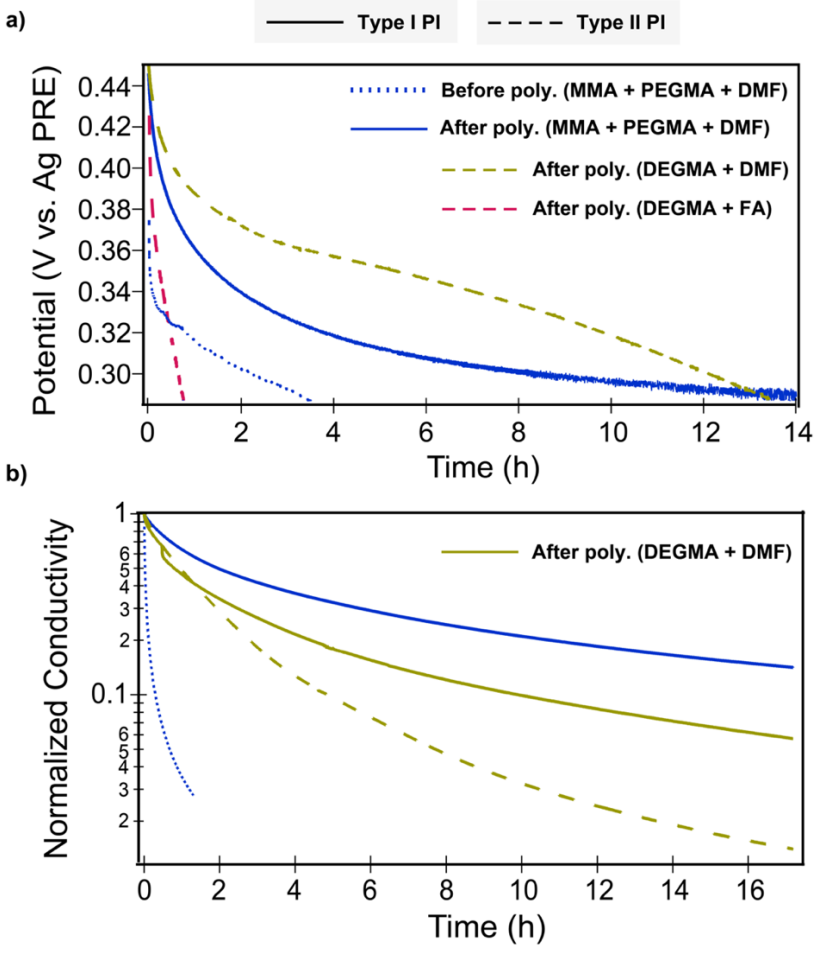

Figure 3.4 Charge stability measurements of P3DT film before and after photopolymerization carried out in different set of parameters. (a) Fermi-level stability measurements performed inside the electrochemical cell (b) conductivity measurements performed out of the cell.

As shown in Figure 3.3 (l), no crack formation is observed after polymerization with a mixture of MMA and PEGMA-550 which allows us to measure the Fermi-level stability of injected charges with type I PI after disconnecting the counter electrode, as shown as the solid blue line in Figure 3.4 (a). We note that we now observe a slow drop of the Fermi level from the potential set during charging (0.45 V) to 0.29 V in about 14 hours. This identifies the crack formation, and not the photodoping, as the problem encountered during the stability measurements of the DEGMA + type I PI procedure.

Comparing the different curves in Figure 3.4a, we observe that the charge stability of the P3DT film with DMF/DEGMA mixture and Type II photoinitiator (dashed yellow line) is slightly better than that of the film treated with MMA/PEGMA-550 mixture (solid blue line) with Type I photoinitiator. We ascribed this enhanced charge stability to the formation of a more densely packed polymer network with DEGMA, which helps hamper the diffusion of impurities into the P3DT film and thus, improving the stability of the electrochemically injected holes inside the film.

To better measure the charge stability without the formation of polymer cracks, we performed conductivity measurements outside of the electrochemical cell after electrochemical hole injection. Contrary to the Fermi-level stability experiments, the conductivity measurements are run through a Keithley SourceMeter without the need of a reference or a counter electrode after disconnecting the cell from the potentiostat. Hence both the conductivity measurement and the photopolymerization itself can be done on a film that has been taken out of the electrolyte solution. By doing so, the UV-light irradiation time for the large volume (10 ml) of bulk photopolymerization inside electrochemical cell can be shortened notably. The thin layer photopolymerization on top of the P3DT film was applied for 10 mins for all conductivity measurements. Furthermore, the amount of impurity molecules can be minimized by having the measurement outside of the cell.

The resulting measurements of the stability of the out-of-cell conductivity are shown in Figure 3.4(b). Note that Figure 3.4(b) plots the normalized conductivity on a log scale, since this is a fair comparison with the potential shown in Figure 3.4(a) ($E \propto \log(p)$, $\sigma \propto p$). The conductivity measurement from each set of parameters after polymerization without normalization can be seen in Figure A3.5 in Appendix. The out-of-cell conductivity results with Type I photoinitiator show higher charge stability compared

to the measurements with Type II photoinitiator. On the other hand, the charge stability of the MMA/PEGMA-550 mixture (solid blue line) outperforms the charge stability measured with DEGMA (solid yellow line). This enhancement of the charge stability might stem from the fact that the higher degree of polymerization might take place inside the P3DT film because of more efficient diffusion of relatively small MMA molecules compared to DEGMA molecules. Because of the long alkyl side chain, P3DT is regarded as a hydrophobic molecule. The compatibility between the hydrophobic P3DT film and hydrophobic polymer PMMA might also be a reason for improved charge stability compared to hydrophilic polymer PEG, in which the former may provide a better encapsulation towards (electro)chemical side reactions of injected holes with impurities in the system.

Overall, the results show that photopolymerization of the solvent and anions after electrochemical doping strongly enhances the stability of the injected holes in P3DT films. The best results are obtained when the photopolymerization is (1) performed on a mixture of MMA and PEGMA-550, to minimize shrinkage and crack formation during polymerization, (2) using dry DMF as additional solvent for the electrolyte ions and (3) with a type I photoinitiator. The stability of the electrical conductivity is enhanced from minutes to hours, showing a photoconductivity that is 20% of the initial value after 16 hours. While this is a strong enhancement, it is much less than the stability of several weeks that we showed for electrochemically n-doped ZnO and PbS quantum dot films,[1] showing that there is still significant room for improvement, probably through optimizing the structure of the generated polyacrylate polymer.

3.3 Conclusion

In summary, we showed that electrochemically injected holes disappear quickly from P3DT films when the working electrode is disconnected from the counter electrode due to electrochemical side reactions with water and possibly other impurities. However, photopolymerization of the solvent and electrolyte ions can stabilize the injected charges. CVs taken before and after photopolymerization indicate that the ions become immobilized to different degrees for different polymerization procedures. Electrical conductivity and Fermi-level stability experiments enabled us to measure the stability of injected charges inside the film. We demonstrated that the stability of electrochemically injected holes inside P3DT film is substantially enhanced after

photopolymerization at room temperature. With a systematic study, we also showed that the stability of injected charges and diffusion of the dopant ions are strongly dependent on the impurity levels in the solvents, the choice of monomer/cross-linking agent and the type of photoinitiator molecules used. The combination of DMF/MMA/PEGMA-550 mixture with a Type I photoinitiator demonstrated the highest charge stability, with 20% of the conductivity retained after 16 hours. On the one hand, this shows that photopolymerization can be used as a tool to enhance the stability of electrochemically doped conducting polymer films, on the other hand it is clear that there is still considerable room for improvement.

2.4 Methods

Materials. Poly(3-decylthiophene-2,5-diyl) (P3DT, Regioregular), methyl methacrylate (MMA, contains ≤ 30 ppm monomethyl ether hydroquinone as inhibitor, 99%), di(ethylene glycol) dimethacrylate (DEGMA, contains 300 ppm monomethyl ether hydroquinone as inhibitor, 95%), poly(ethylene glycol) dimethacrylate (PEGMA-550, average M_n 550, contains 80-120 ppm monomethyl ether hydroquinone and 270-330 ppm butylated hydroxytoluene as inhibitor), 2-acrylamido-2-methyl-1-propanesulfonic acid (AMPSH, 99%), formamide (FA, ≥99%), 1,2-dicholorobenzene (99%), diphenyl(2,4,6-trimethylbenzoyl)phosphine oxide (Photoinitiator, Type I PI, 99%), 4,4'-bis(diethylamino)benzophenone (Photoinitiator, Type II PI, ≥ 99%) were all purchased from Sigma Aldrich. N, N-Dimethylformamide (DMF, ≥99%, dry grade) was purchased from Biosolve and purified using a PureSolv micro solvent purification system with activated Alumina column. The dry solvent was stored over 4Å molecular sieves in glove box. MMA, DEGMA, PEGMA-550 and FA were vacuum degassed under rigorous stirring before use and were stored in glove box. All other chemicals were used as received. Figure 3.5 presents the chemical structures of all compounds employed in this work.

Preparation of P3DT Films. Film preparations were made on two different substrates, namely tin-doped indium oxide (ITO) or home-built interdigitated gold electrode (IDE), which were both used as working electrodes (WEs) in electrochemical cell experiments. The IDE is a glass substrate containing four separate gold WEs prepared by optical lithography. Various source-drain gaps of the electrodes provide different sensitivities in the conductivity measurements. An image of an IDE with more details is shown in Appendix Figure A3.6. The P3DT solution was prepared by dissolving 15 mg of P3DT in

1 ml of 1,2-dicholorobenzene. The substrates were spin-coated for 60 s at 3000 rpm with a ramp of 500 rpm/s. A Dektak profilometer was used to determine the thickness of the film, which was approximately 40 nm.

(Spectro)electrochemical Measurements. All (spectro)electrochemical measurements were performed in a nitrogen-filled glove box to ensure oxygen- and water-free conditions (≤0.1 ppm O_2 and ≤0.5 ppm H_2O). An Autolab PGSTAT128N potentiostat including an additional dual-mode bi-potentiostat BA module was used to maintain the potential of the WE at a constant level with respect to the reference electrode (RE) by adjusting the current at the counter electrode (CE). The P3DT film deposited on the WE was immersed in an electrochemical cell containing an electrolyte solution together with an Ag wire as pseudo-reference electrode (PRE) and Pt wire as CE.

The CV measurements were performed with a scan rate of 10 mV/s, starting near the open circuit potential (Voc) of the system in the positive direction until hole injection into the valence band of the P3DT film takes place. Upon electrochemical hole injection, electrolyte ions ($AMPS^-$) diffuse into the P3DT film for electrostatic charge compensation. Here, the electrolyte ions were aimed to covalently immobilize upon UV exposure, which then fixes the Fermi level of the system at the potential specified. As a function of applied potential, changes in absorption of the P3DT film were recorded simultaneously with a fiber-based UV-Vis spectrometer, Ocean Optics USB2000 with an Ocean Optics DH 2000 lamp as light source. The spectroelectrochemical measurements of P3DT films were performed on ITO substrates.

Fermi-level Stability Measurements. A change in the potential of the system will result in a change in the Fermi level of the system. The stability of electrochemically injected charges can be measured by carrying out the so-called potential *vs.* time, a.k.a. Fermi-level stability measurements after disconnecting the cell from the potentiostat. That requires removing the electrical connection between WE and CE to assure that no additional charge is injected or extracted through the external circuit while the potential between WE and PRE is being measured over time.

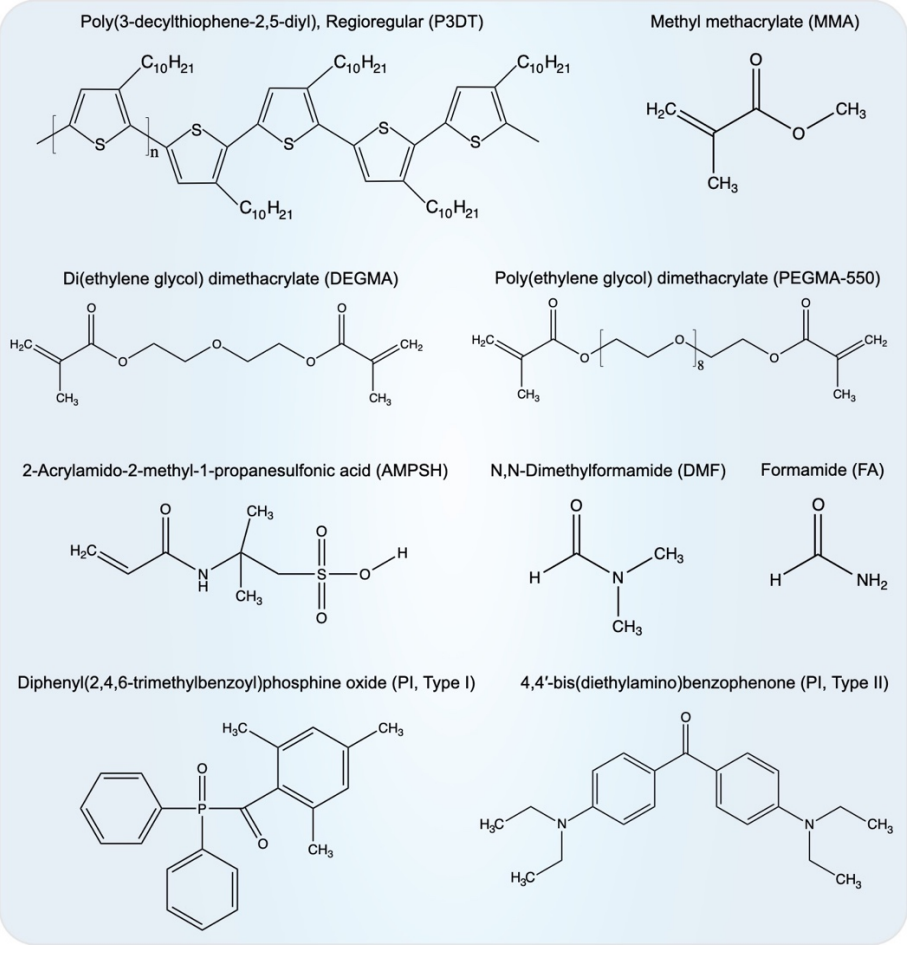

Figure 3.5 The chemical structures of all compounds used in this work.

Electrical conductivity measurements. The second method used for measuring the stability of the injected charges is to monitor the change in the electrical conductivity of the P3DT film after disconnecting the cell from the potentiostat. If electrochemically injected holes leave the valence band of the P3DT film, the conductivity of the film will drop. The conductivity measurements of P3DT films were carried out only on IDE substrates by using a Keithley 2400 SourceMeter. During the measurements, two WEs,

namely WE1 and WE2 were used in a source-drain electrode configuration and after removing the connections of the cell from the potentiostat, the source-drain current was recorded for a constant 10 mV source-drain bias applied between WE1 and WE2 with the Keithley source meter. The width of the source-drain gap was 25 μm and the total length of the interdigitated gap was 85 cm. The slope of the current vs potential gives the conductance, G, of the film. From the conductance, one can calculate the source-drain electron conductivity according to equation 1, σ:

$$\sigma = \frac{G \times w}{l \times h}$$

where *w* is the source-drain gap width, *l* is the gap length, and *h* is the height of the P3DT film.

Photopolymerization experiments. All photopolymerization experiments were carried out in the nitrogen-filled glove box. A UV-LED light source (600 mW/cm^2) with an emission wavelength of 395 nm was used to initiate the free radical chain polymerization reaction. 0.05 M of polymerizable electrolyte solution was prepared by dissolving AMPSH in 10 ml of different solution mixtures. Each solution mixture consists of different combination of solvent, monomer/ cross-linking agent, and type of photoinitiator. Water, FA and DMF were used as solvents to dissolve AMPSH. As monomer/cross-linking agents, MMA, DEGMA and PEGMA-550 were employed. Two different types of photoinitiator molecules (PIs) were exploited namely, diphenyl (2,4,6 –trimethylbenzoyl)phosphine oxide (Type I PI) and 4,4'-bis(diethylamino)benzophenone (Type II PI).

Here, for clearer illustration of the parameters used in photopolymerization experiments, we categorized each solution mixture by four sets of parameters (SoP) as tabulated in Table 1. A three-electrode electrochemical cell was immersed in a beaker filled with an electrolyte solution. The electrochemical potential of the WE was set and kept at 0.45 V *vs.* Ag PRE during the entire photopolymerization experiment in order to secure the injection of holes into the valence band of P3DT film and to give time for the photochemical fixation of the dopant ions.

Table 1. Four separate set of parameters, SoP used in photopolymerization of p-doped P3DT film.

	Salt	Solvent	Monomer	Type of	Mixing
1st SoP	AMPSH	FA	DEGMA	Type II	1:4 v/v
2nd SoP	AMPSH	DMF	DEGMA	Type II	1:4 v/v
3rd SoP	AMPSH	DMF	DEGMA	Type I	1:4 v/v
4th SoP	AMPSH	DMF	MMA/PEGMA-550	Type I	1:7:2 v/v/v

After 90 mins of UV-light irradiation, the electrochemical cell was disconnected from the potentiostat, so that there is no additional hole injection or extraction through the external circuit, and Fermi-level stability measurements were performed as a function of time to see how long the electrochemically injected holes remain in the P3DT film after disconnecting the cell. For conductivity measurements, the photopolymerization process was instead performed out of the electrochemical cell. This is carried out by disconnecting the cell immediately after the electrochemical doping and removing the electrode from the electrolyte solution and then illuminating the electrode. The main reasons for doing so will be discussed in detail in the Results and Discussion part. For out-of-cell photopolymerization experiments, the irradiation time for the UV-light was 10 mins. This shortening in time for the light irradiation arises from the fact that the volume of polymerizable solution is much less compared to the bulk polymerization in the cell.

References

1. Eren, H.; Bednarz, R. J.-R.; Alimoradi Jazi, M.; Donk, L.; Gudjonsdottir, S.; Bohländer, P.; Eelkema, R.; Houtepen, A. J., Permanent Electrochemical Doping of Quantum Dot Films through Photopolymerization of Electrolyte Ions. Chemistry of Materials 2022, 34 (9), 4019-4028.

2. Twenty-five years of conducting polymers. Chemical Communications 2003, (1), 1-4.

3. Bronstein, H.; Nielsen, C. B.;Schroeder, B. C.; McCulloch, I., The role of chemical design in the performance of organic semiconductors. Nature Reviews Chemistry 2020, 4 (2), 66-77.

4. Guo, X.; Facchetti, A., The journey of conducting polymers from discovery to application. Nature Materials 2020, 19 (9), 922-928.

5. Swager, T. M., 50th Anniversary Perspective: Conducting/Semiconducting Conjugated Polymers. A Personal Perspective on the Past and the Future. Macromolecules 2017, 50 (13), 4867-4886.

6. Gross, M.; Müller, D. C.; Nothofer, H.-G.; Scherf, U.; Neher, D.; Bräuchle, C.;Meerholz, K., Improving the performance of doped π-conjugated polymers for use in organic light-emitting diodes. Nature 2000, 405 (6787), 661-665.

7. Ragni, R.; Operamolla, A.; Farinola, G. M., 1 - Synthesis of electroluminescent conjugated polymers for OLEDs. In Organic Light-Emitting Diodes (OLEDs), Buckley, A., Ed. Woodhead Publishing: 2013; pp 3-48.

8. Pandey, M.; Kumari, N.; Nagamatsu, S.; Pandey, S. S., Recent advances in the orientation of conjugated polymers for organic field-effect transistors. Journal of Materials Chemistry C 2019, 7 (43), 13323-13351.

9. Yang, J.; Zhao, Z.; Wang, S.; Guo, Y.; Liu, Y., Insight into High-Performance Conjugated Polymers for Organic Field-Effect Transistors. Chem 2018, 4 (12), 2748-2785.

10. Sandström, A.; Dam, H. F.; Krebs, F. C.; Edman, L., Ambient fabrication of flexible and large-area organic light-emitting devices using slot-die coating. Nature Communications 2012, 3 (1), 1002.

11. Pei, Q.; Yu, G.; Zhang, C.; Yang,Y.; Heeger, A. J., Polymer Light-Emitting Electrochemical Cells. Science 1995, 269 (5227), 1086.

12. Coakley, K. M.; McGehee, M. D., Conjugated Polymer Photovoltaic Cells. Chemistry of Materials 2004, 16 (23), 4533-4542.

13. Günes, S.; Neugebauer, H.; Sariciftci, N. S., Conjugated Polymer-Based Organic Solar Cells. Chemical Reviews 2007, 107 (4), 1324-1338.

14. Shirakawa, H.; Louis, E. J.; MacDiarmid, A. G.; Chiang, C. K.; Heeger, A. J., Synthesis of electrically conducting organic polymers: halogen derivatives of polyacetylene, (CH). Journal of the Chemical Society, Chemical Communications 1977, (16), 578-580.

15. Scholes, D. T.; Yee, P. Y.; McKeown, G. R.; Li, S.; Kang, H.; Lindemuth, J. R.; Xia, X.; King, S. C.; Seferos, D. S.; Tolbert, S. H.; Schwartz, B. J., Designing Conjugated Polymers for Molecular Doping: The Roles of Crystallinity, Swelling, and Conductivity in Sequentially-Doped Selenophene-Based Copolymers. Chemistry of Materials 2019, 31 (1), 73-82.

16. Kiefer, D.; Kroon, R.; Hofmann, A. I.; Sun, H.; Liu, X.; Giovannitti, A.; Stegerer, D.; Cano, A.; Hynynen, J.; Yu, L.; Zhang, Y.; Nai, D.; Harrelson, T. F.; Sommer, M.; Moulé, A. J.; Kemerink, M.; Marder, S. R.; McCulloch, I.; Fahlman, M.; Fabiano, S.; Müller, C., Double doping of conjugated polymers with monomer molecular dopants. Nature Materials 2019, 18 (2), 149-155.

17. Hofmann, A. I.; Kroon, R.; Zokaei, S.; Järsvall, E.; Malacrida, C.; Ludwigs, S.; Biskup, T.; Müller, C., Chemical Doping of Conjugated Polymers with the Strong Oxidant Magic Blue. Advanced Electronic Materials 2020, 6 (8), 2000249.

18. Jeon, I.-R.; Noma, N.; Claridge, R. F. C.; Shirota, Y., Electrochemical Doping of Poly(3-vinylperylene) and Electrical Properties of Doped Polymers. Polymer Journal 1992, 24 (3), 273-279.

19. Yuen, J. D.; Dhoot, A. S.; Namdas, E. B.; Coates, N. E.; Heeney, M.; McCulloch, I.; Moses, D.; Heeger, A. J., Electrochemical Doping in Electrolyte-Gated Polymer Transistors. Journal of the American Chemical Society 2007, 129 (46), 14367-14371.

20. Hulea, I. N.; Brom, H. B.; Houtepen, A. J.; Vanmaekelbergh, D.; Kelly, J. J.; Meulenkamp, E. A., Wide Energy-Window View on the Density of States and Hole Mobility in Poly(Phenylene Vinylene). Physical Review Letters 2004, 93 (16), 166601.

21. Aoai, T.; Nishio, R.; Hayashi, N.; Nomura, K., Photo Doping Process of Conductive Polymer with PAG and Application for Organic Thermoelectric Materials. Journal of Photopolymer Science and Technology 2016, 29 (2), 335-341.

22. Koizumi, H. In Radiation-induced doping of conducting polymers, The conference abstract book of the 1st Asian-Pacific symposium on radiation chemistry, China, China, 2006; p 161.

23. Vanmaekelbergh, D.; Houtepen, A. J.; Kelly, J. J., Electrochemical gating: A method to tune and monitor the (opto)electronic properties of functional materials. Electrochimica Acta 2007, 53 (3), 1140-1149.

24. Tang, S.; Edman, L., Light-Emitting Electrochemical Cells: A Review on Recent Progress. Topics in Current Chemistry 2016, 374 (4), 40.

25. Pei, Q.; Yang, Y.; Yu, G.; Zhang, C.; Heeger, A. J., Polymer Light-Emitting Electrochemical Cells: In Situ Formation of a Light-Emitting p–n Junction. Journal of the American Chemical Society 1996, 118 (16), 3922-3929.

26. Edman, L.; Moses, D.; Heeger, A. J., Influence of the anion on the kinetics and stability of a light-emitting electrochemical cell. Synthetic Metals 2003, 138 (3), 441-446.

27. Alam, K.; Mehreen, T.; Basher, M. K.; Haque, M. A. S.; Ghosh, S. C.; Hossain, K. S. In Fabrication and Characterization Of A P-N Junction For Large Area Silicon Solar Cell, 2018 International Conference on Innovations in Science, Engineering and Technology (ICISET), 27-28 Oct. 2018; 2018; pp 147-150.

28. Matyba, P.; Maturova, K.; Kemerink, M.; Robinson, N. D.; Edman, L., The dynamic organic p–n junction. Nature Materials 2009, 8 (8), 672-676.

29. Gao, J.; Yu, G.; Heeger, A. J., Polymer light-emitting electrochemical cells with frozen p-i-n junction. Applied Physics Letters 1997, 71 (10), 1293-1295.

30. Gao, J.; Li, Y.; Yu, G.; Heeger, A. J., Polymer light-emitting electrochemical cells with frozen junctions. Journal of Applied Physics 1999, 86 (8), 4594-4599.

31. Gudjonsdottir, S.; van der Stam, W.; Koopman, C.; Kwakkenbos, B.; Evers, W. H.; Houtepen, A. J., On the Stability of Permanent Electrochemical Doping of Quantum Dot, Fullerene, and Conductive Polymer Films in Frozen Electrolytes for Use in Semiconductor Devices. ACS Applied Nano Materials 2019, 2 (8), 4900-4909.

32. Gudjonsdottir, S.; Houtepen, A. J., Permanent Electrochemical Doping of Quantum Dots and Semiconductor Polymers. Advanced Functional Materials 2020, 30 (49), 2004789.

33. Leger, J. M.; Rodovsky, D. B.; Bartholomew, G. P., Self-Assembled, Chemically Fixed Homojunctions in Semiconducting Polymers. Advanced Materials 2006, 18 (23), 3130-3134.

34. Leger, J. M.; Patel, D. G.; Rodovsky, D. B.; Bartholomew, G. P., Polymer Photovoltaic Devices Employing a Chemically Fixed p–i–n Junction. Advanced Functional Materials 2008, 18 (8), 1212-1219.

35. Kosilkin, I. V.; Martens, M. S.; Murphy, M. P.; Leger, J. M., Polymerizable Ionic Liquids for Fixed-Junction Polymer Light-Emitting Electrochemical Cells. Chemistry of Materials 2010, 22 (17), 4838-4840.

36. Tang, S.; Irgum, K.; Edman, L., Chemical stabilization of doping in conjugated polymers. Organic Electronics 2010, 11 (6), 1079-1087.

37. Tang, S.; Edman, L., On-demand photochemical stabilization of doping in light-emitting electrochemical cells. Electrochimica Acta 2011, 56 (28), 10473-10478.

38. Bredas, J. L.; Street, G. B., Polarons, bipolarons, and solitons in conducting polymers. Accounts of Chemical Research 1985, 18 (10), 309-315.

39. Boehme, S. C.; Wang, H.; Siebbeles, L. D. A.; Vanmaekelbergh, D.; Houtepen, A. J., Electrochemical Charging of CdSe Quantum Dot Films: Dependence on Void Size and Counterion Proximity. ACS Nano 2013, 7 (3), 2500-2508.

40. Bland, M. H.; Peppas, N. A., Photopolymerized multifunctional (meth)acrylates as model polymers for dental applications. Biomaterials 1996, 17 (11), 1109-1114.

41. Barszczewska-Rybarek, I. M., A Guide through the Dental Dimethacrylate Polymer Network Structural Characterization and Interpretation of Physico-Mechanical Properties. Materials (Basel) 2019, 12 (24), 4057.

42. Malhotra, N.; M, K.; Acharya, S., Strategies to Overcome Polymerization Shrinkage − Materials and Techniques. A Review. Dental Update 2010, 37 (2), 115-125

Appendix

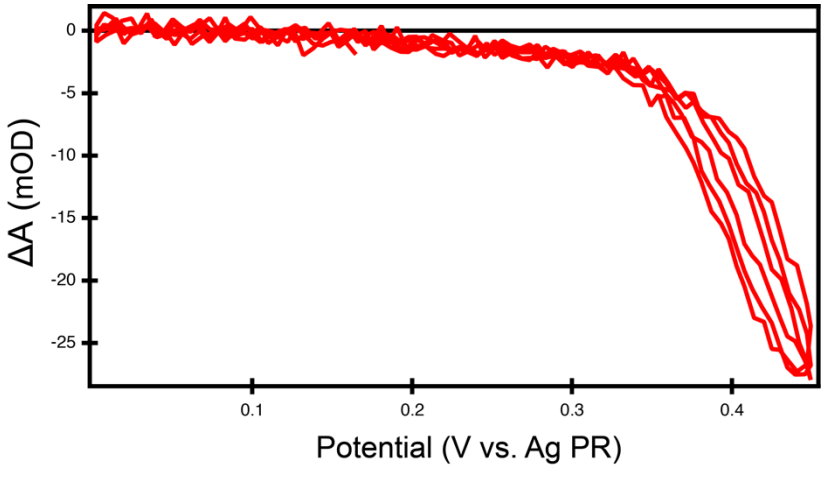

Figure A3.1 Differential absorbance (ΔA) *vs.* potential graph shows the changes in absorption of the P3DT film at 525 nm as a function of applied potential with a scan rate of 10 mV/s. Figure 3.2b displays the 2D color map of this measurement, which is performed in an electrolyte solution containing 0.05 M AMPSH in DMF:MMA:PEGMA-550 (1:7:2 v/v/v).

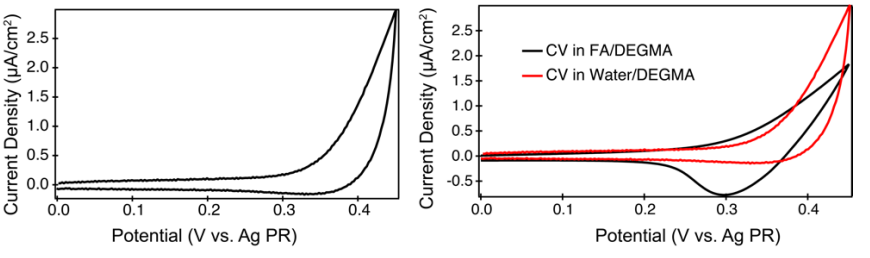

Figure A3.2 CV of P3DT film scanned outside of the glove box in an electrochemical cell containing 0.05 M AMPSH dissolved in water/DEGMA mixture (left), comparison of CVs taken inside (FA/DEGMA) and outside (water/DEGMA) of glove box for P3DT film (right).

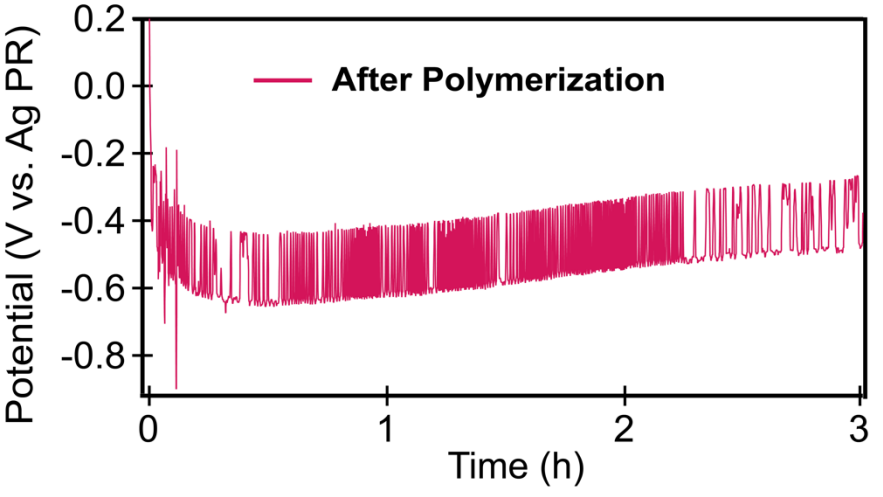

Figure A3.3 Fermi-level stability measurement of P3DT film in DMF/DEGMA mixture with Type I photoinitiator.

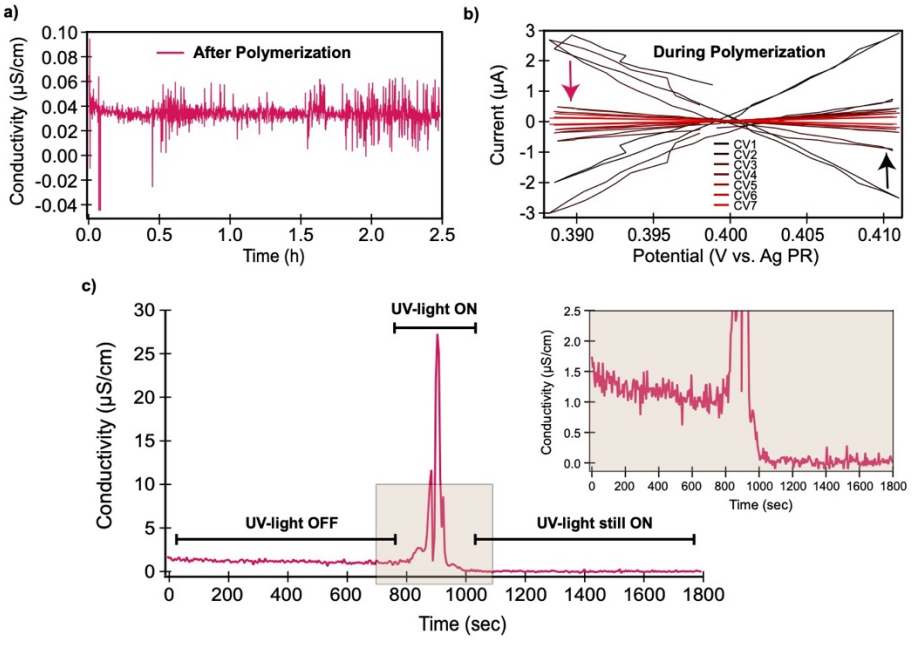

Figure A3.4 Set of conductivity experiments with P3DT film deposited on IDE substrate. (a) demonstrates the conductivity measurement after the polymerization with DMF/DEGMA and Type I photoinitiator, (b) the CVs measured in a source-drain manner with a scan rate of 1 mV/sec where the slope of I-V gives the conductance of the film, (c) shows the conductivity experiment during photopolymerization process this time without electrochemical charge injection into P3DT film.

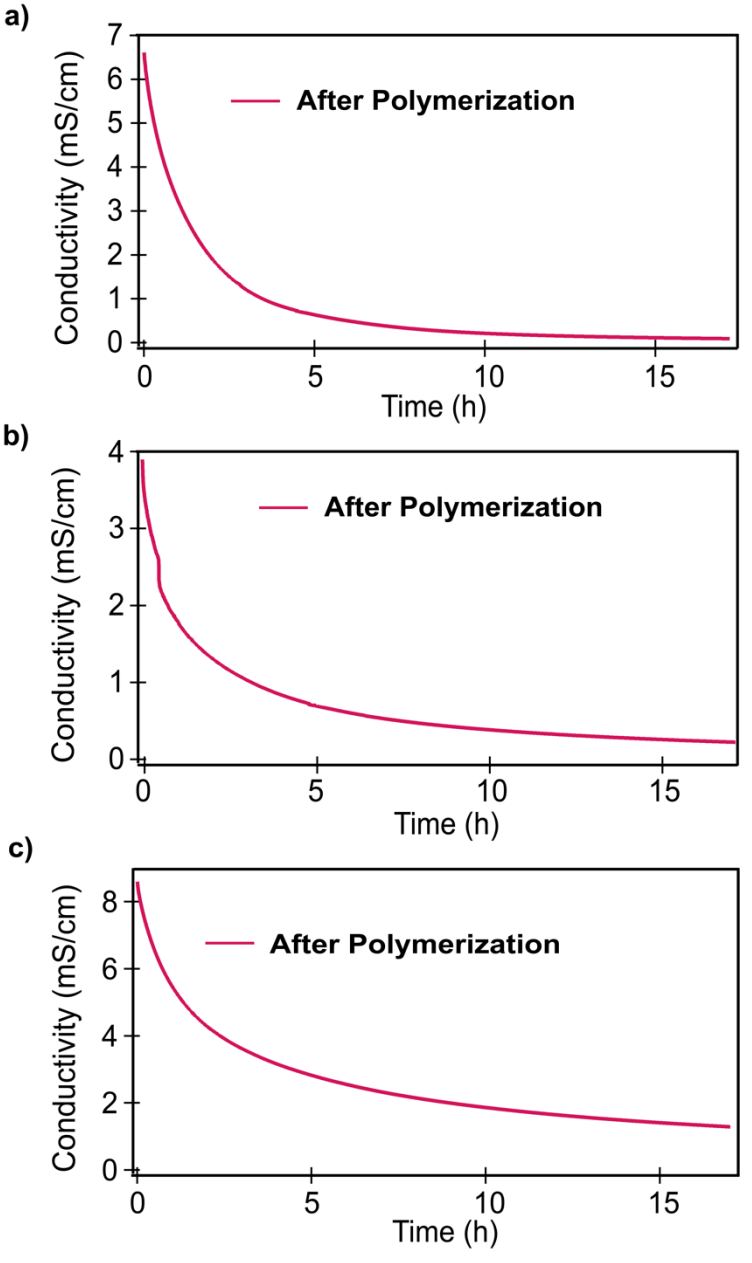

Figure A3.5 The conductivity experiments with P3DT film deposited on IDE substrate. (a) with DMF/DEGMA and Type II photoinitiator, (b) with DMF/DEGMA and Type I photoinitiator, (c) with DMF/MMA/PEGMA and Type I photoinitiator. All above experiments are measured outside of the cell.

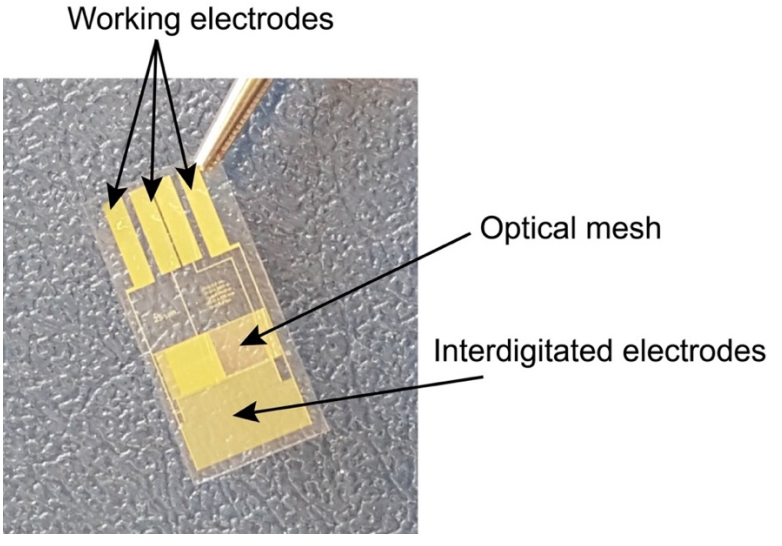

Figure A3.6 Home-built inter-digitated gold electrode. The electrode is a glass substrate coated with four separate gold WEs which provide five source-drain gaps of different sensitivities.

Chapter 4

The Influence of Photoinitiator Type and Irradiation Time on the Stabilization of Electrochemically Doped Quantum Dot Films via Photopolymerization

Abstract

In Chapter 2, we showed that photopolymerization of the solvent and dopant ions can drastically enhance the stability of electrochemically n-doped QD films. In this chapter, we systematically investigate the influence of using two types of photoinitiator molecules, namely type I and type II initiators and UV light exposure time on dopant ion fixation and charge stability in electrochemically doped ZnO QD films. Particularly, by systematically reducing the irradiation time, we compare the degree of photochemical fixation of dopant ions and how it relates to the charge stability using both types of photoinitiator systems. By conducting Fermi-level stability measurements, we demonstrate that the polymerization treatment using Type I initiator strongly outperforms the treatment with Type II initiator with decreasing irradiation time. With the help of cyclic voltammetry and FT-IR analyses, we show that a much higher degree of photochemical fixation of dopant ions can be achieved using Type I photoinitiators. The results offer promising avenues for further stabilization of electrochemically doped QD films in a quicker and more efficient manner.

This chapter is based on: Hamit Eren, Reinout Ubbink, Wolter F. Jager and Arjan J. Houtepen. In Preparation.

4.1 Introduction

Doping of bulk semiconductors to tailor their optical and electrical properties enabled widespread technological applications in microelectronics and optoelectronics industries.[1-4] This is achieved by intentional insertion of impurity atoms into the crystal lattice, which in turn changes the charge carrier concentration and affects the conductivity of the material.[5, 6] The ability to control the charge carrier density is the basis for the fabrication of many optoelectronic devices such as LEDs,[7, 8] solar cells,[9, 10] transistors,[11, 12] lasers[13, 14] and photodetectors.[15, 16]

The prospect of new technologies and the shrinkage in the device dimensions to nanoscale have stimulated similar efforts to dope semiconductor nanomaterials.[17-20] In this respect, semiconductor nanocrystals, a.k.a. quantum dots (QDs) have emerged as a novel class of building blocks with size-dependent optical and electronic properties for constructing practical electronic devices. The richly tunable chemical and physical properties of QDs in conjunction with their facile and cheap solution-based synthesis make them attractive for both fundamental and applied sciences.[21-23] However, electronic doping of QDs has proven challenging because of the nanometer size of the semiconductor crystal, therefore impeding their integration into optoelectronic devices.[20, 24]

Impurity doping,[25, 26] chemical doping,[27, 28] photodoping[29, 30] and electrochemical doping[31, 32] are the most commonly used methods for electronic doping of QDs to change chemical and physical properties of the material. Among them, electrochemical doping is arguably the most powerful and versatile method for doping QDs. It offers to precisely and controllably tune the charge carrier concentration and thus the doping levels as a function of applied potential in a reversible and non-destructive manner. In this approach, by regulating externally applied potential, electrons or holes can be injected into the QD film, which is immersed in an electrochemical cell with an electrolyte solution.

As a result of electrochemical charge injection into the system, counter ions in the electrolyte solution diffuse into the voids of QD film to maintain electroneutrality. Due to this nanoscale charge compensation, very high doping densities up to 10^{21} cm^{-3} can be reached. The electrolyte ions, which act as external dopants, are mostly not

incorporated into the QD material itself, which minimizes the structural distortion in crystal lattice and overall, the film morphology upon doping. Additionally, it does not introduce any defect states in the band gap of the material, which can act as recombination centers for electrons and holes, as is the case for impurity doping.

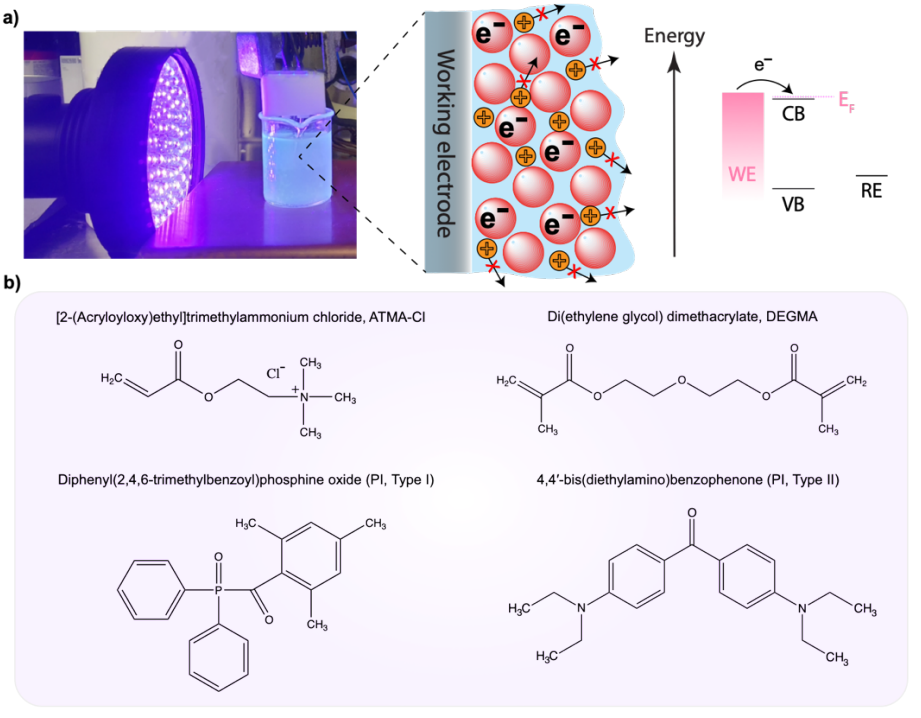

Figure 4.1 (a) shows an image of the experimental set-up and a schematic picture of electrochemical charge injection into the QD film where the Fermi level is above the conduction band of the QD (b) shows the chemical structures of both monomers and photoinitiators used in this study.

Unfortunately, it is usually observed that the injected charges are not very stable and quickly disappear after the electrochemical cell is disconnected from the external voltage source. The loss of injected charges could be because of electrochemical side reactions with impurity molecules such as dissolved O_2 or H_2O present in the cell as evidenced in our previous works[31, 33, 34] or intrinsic side reactions with the material itself. In addition, the disappearance of the injected charges results in diffusion of dopant ions out of the porous QD film. In addition, the dynamic movement of dopant

ions causes problems when an electric field is applied, particularly in an operating device.[35-37] Overall, the challenge for achieving stable electrochemical doping of QDs is twofold: enhancement of the charge stability over time and fixation of the dopant ions. We have previously shown that both of these challenges can be addressed with a photopolymerization treatment at room temperature in Chapter 2. An image of the experimental set-up and a schematic picture of electrochemical charge injection into the QD film are shown in Figure 4.1a. By photochemically fixating the polymerizable dopant ion solution, the mobility of the impurity molecules is strongly reduced and thus the stability of injected charges enhanced by many orders of magnitude, from minutes to several weeks.

The photochemical fixation process is triggered by UV light irradiation of photoinitiator (PI) molecules which then generate free radical species to initiate the polymerization. Free radical PIs can be classified into Type I and Type II initiators based on their decomposition mechanism.[38-40] Type I PIs are unimolecular free radical generators; that is, when exposed to UV light, a specific bond within the initiator's structure undergoes homolytic cleavage to generate two radical fragments. On the other hand, type II PIs absorb UV light to form excited molecules (triplet states) which then abstract a hydrogen atom from a donor molecule in the environment. This creates an active donor radical that reacts with a monomer to initiate polymerization. Overall, two highly reactive radical species are generated from one single Type I PI molecule whereas only one reactive radical species is produced from one single Type II PI molecule, as shown in detail in the decomposition mechanisms in Figure 4.2. The former situation could be favorable for faster kinetics and a higher degree of conversion in the polymerization system.[41]

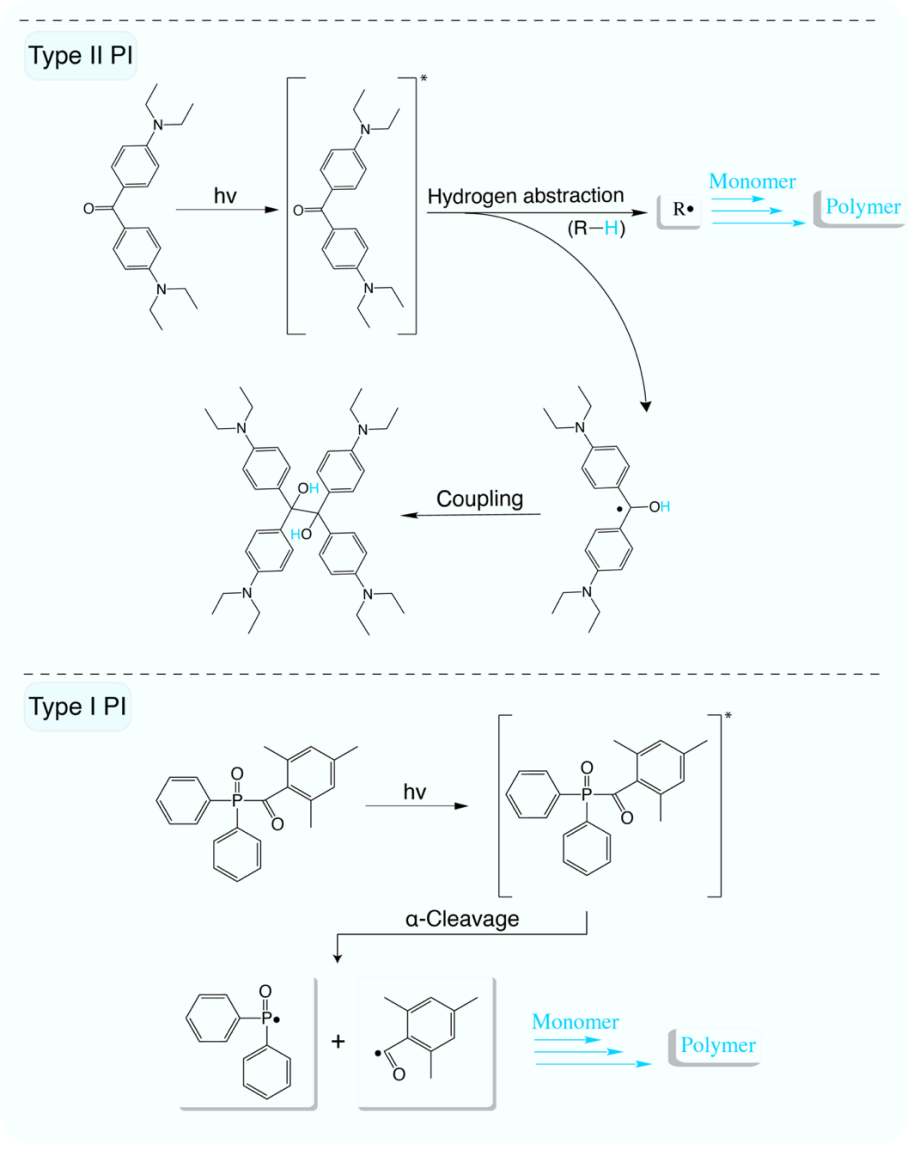

Figure 4.2 Photo-decomposition mechanisms of both type I and type II PIs.

The aim of the present study is to improve the photopolymerization procedure that enhances the stability of electrochemically doped QD films, as described in Chapter 2. Here, we systematically investigate the influence of using two types of PI molecules and UV light irradiation time on dopant ion fixation and charge stability in electrochemically doped ZnO QD films. For both types of PI system, we compare the degree of

photochemical fixation of dopant ions and the resulting charge stability by systematically reducing the irradiation time from the previously reported 90 mins (see Chapter 2) to 2 mins. By conducting Fermi-level stability measurements, we demonstrate that the Type I PI outperforms the Type II PI in charge stability with decreasing irradiation time. With the help of cyclic voltammetry and FT-IR analyses, we show that a much higher degree of photochemical fixation of dopant ions can be achieved using the Type I PI. Importantly, much faster photopolymerization achieved with type I PI allows the irradiation time to be reduced from 1.5 hour to a few minutes, while maintaining the charge stability. The results offer promising avenues for further optimization of stabilized electrochemically doped QD films by this method.

4.2 Results and Discussion

Figure 4.1a presents a schematic of the desired formation of a photochemically stabilized electrochemically doped QD film. At sufficiently negative applied potential, electrons are injected into the conduction band of the ZnO QDs, which are electrostatically compensated by diffusion of $ATMA^+$ ions from the electrolyte solution. This doping density is only stable as long as the applied voltage remains, which makes it unpractical for most device applications. Our previous studies showed that an irreversible one-electron reduction reaction of dissolved O_2 molecule with injected electrons might cause this instability with a rapid loss of charge density after disconnecting the cell from potentiostat.[31, 33, 34] We attempt to rectify these challenges by exposing the doped structure with UV light in the presence of a PI molecule, which eventually results in formation of a highly cross-linked and immobile polymer network. The type of PI molecules in free-radical photopolymerization process is crucial along with the source and dose of UV radiation and exposure time, as discussed in detail below.

4.2.1 Photochemical fixation of dopant ions

FT-IR spectroscopy is a common technique to investigate polymerization kinetics and the degree of polymerization.[42-44] Figure 4.3 presents FT-IR spectra of three samples: a spectrum of the electrolyte solution before polymerization (blue line) and spectra after 90 mins of UV illumination with type I (red line) and type II (green line) PIs. The extent of the conversion can be determined by measuring the intensity decrease of the

acrylate/methacrylate (C=C) stretching and (C–H) bending absorption bands at 1638 cm^{-1} and 810 cm^{-1}, respectively. The vibrational fingerprints of the carbon double bond from DEGMA and $ATMA^+$ ions are clearly visible in the pristine electrolyte solution before treatment, are completely absent for the Type I PI photopolymerization, and are strongly reduced, but still visible, for the Type II photopolymerization. This shows that there is efficient conversion of the DEGMA and $ATMA^+$ monomers in both cases, with a slightly higher degree of conversion with type I initiator.

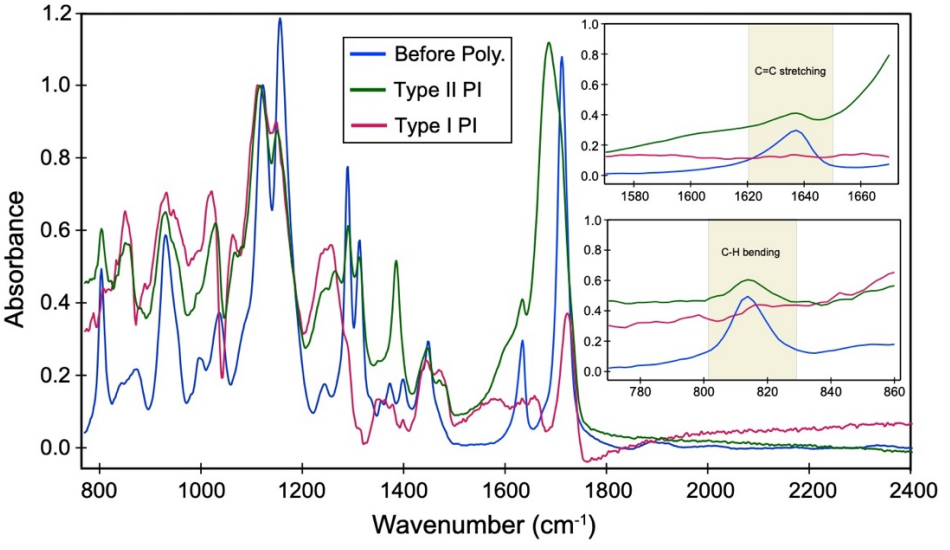

Figure 4.3 shows the FT-IR spectra of electrolyte solutions measured before (blue line) and after photopolymerization treatment with both type I (red line) and type II (green line) initiators. The FT-IR spectra of photopolymerized samples is taken after 90 mins of UV irradiation for both types of initiators. The insets show clearly the extent of the conversion with the intensity decrease of the acrylate/methacrylate (C=C) stretching and (C–H) bending absorption bands at 1638 cm^{-1} and 810 cm^{-1}, respectively. The vibrational fingerprints of the carbon double bond from DEGMA and $ATMA^+$ ions are clearly visible in the pristine electrolyte solution before treatment, are completely absent for the Type I PI photopolymerization, and are strongly reduced, but still visible, for the Type II photopolymerization.

Figure 4.4 shows cyclic voltammetry (CV) experiments on ZnO QD films before (black lines) and after (red lines) photopolymerization with either type I PI or type II PI, and

for various UV illumination times. All CVs taken before polymerization treatment exhibited quite reversible charge injection and extraction behavior with slightly asymmetric features. This asymmetry is caused by slow diffusion of relatively large $ATMA^+$ ions moving in the viscous electrolyte solvent. More symmetric CVs of doping ZnO QD films with smaller electrolyte ions such as Li^+ in less viscous solvents like acetonitrile have been demonstrated in our previous work.[45]

CVs of ZnO QD films after 90 mins of UV exposure at -0.75 V (top row, red line) show a strongly reduced and linear current density for both types of PIs. In both cases the current density is truly zero at the potential of -0.75 V applied during polymerization. This shows that the open circuit potential of the QD film has become -0.75 V. The residual small current at potentials more positive than -0.75 V is probably caused by a very small amount of ions that can still move somewhat under the applied overpotential (see detailed discussion below). This is however insufficient to lead to a change in the open circuit potential since the current density is again 0 at the potential of -0.75 V at the end of the scan. We find that after photopolymerization the current densities at 0 V differ slightly; positive current densities of ~250 nA and ~80 nA were recorded for type II and type I PIs, respectively. While the charging and discharging is effectively prevented for both type of PIs, the smaller remaining current density for the type I PI suggests that the electrolyte ions are immobilized even better.

The middle row in Figure 4.4 shows the CVs for 10 mins of UV exposure. The measurement with type I PI (Figure 4.4d) is almost identical to the CV obtained after 90 mins of UV exposure. The insert in Figure 4.4d shows that the current at 0 V is now 200 nA/cm^2, about 2.5 times higher than after 90 mins of exposure. On the other hand, the CV in Figure 4.4c shows clear signs of charging and discharging of the ZnO QD film, even after polymerization. The maximum current density is on ~25% lower than before polymerization, and maximum in the reverse scan appears at ~0.15 V more positive potential, indicating that the diffusion of ions has become slower, but has not been prevented. This shows that 10 mins of UV exposure is not enough for photochemical fixation of dopant ions using the type II PI.

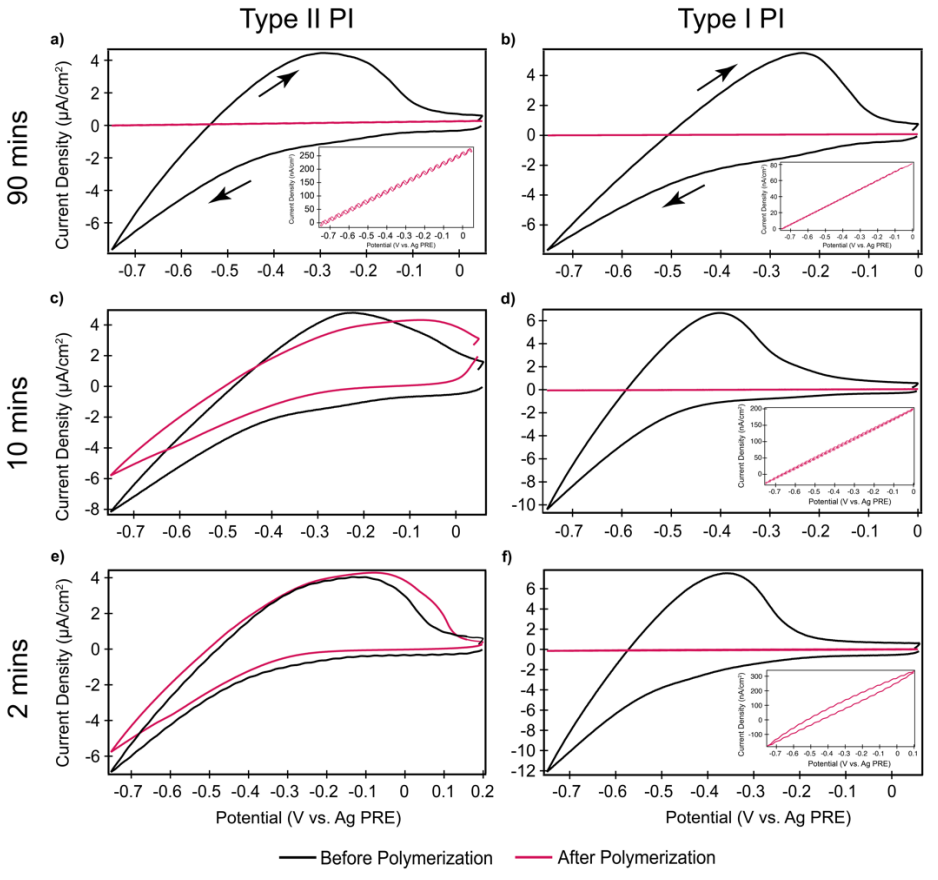

Figure 4.4 shows the CVs of ZnO QD films before (black lines) and after photopolymerization (red lines) treatment with both type I and type II initiators and different UV exposure times of 90 mins, 10 mins and 2 mins. All the CVs of the QD films were measured in an electrochemical cell containing 0.1 M of polymerizable electrolyte solution prepared by dissolving PI molecule (~1 mg) and ATMA-Cl salt in 10 mL of FA:DEGMA (2:3 v/v) solvent mixture. The arrows on the CVs indicate the scan directions with a scan rate of 30 mV/s. The top row (red lines) displays a strongly reduced and linear current density for both types of PIs after 90 mins of UV exposure. The middle row shows the CVs taken after 10 mins of light irradiation for type I and II initiators, in which CVs in (4.4c) show clear signs of charging and discharging of the ZnO QD film, even after polymerization. The bottom row demonstrates the CVs recorded after 2 mins of UV irradiation. While the shape of the CV and the current density for the system

polymerized with the type I PI in (red line, 4.4f) shows no significant difference with longer UV radiation as shown in (4.4b, d), the CV of the QD film after treatment with type II PI, (red line, 4.4e) seems to be almost identical with the CV taken before polymerization (black line, 4.4e), meaning that the dopant ions are quite mobile and able to diffuse in and out of the QD film readily.

The bottom row in Figure 4.4 shows the results for 2 minutes of UV irradiation. Remarkably, the shape of the CV and the current density for the system polymerized with the type I PI (Figure 4.4f) shows no significant difference with longer UV radiation. The insert in Figure 4.4f shows that the current at 0 V is now ~300 nA/cm^2, about ~4 times higher than after 90 mins of exposure. In contrast, the CV of the QD film after treatment with type II PI (red curve in Figure 4.4e) seems to be almost identical with the CV taken before polymerization, meaning that the dopant ions are quite mobile and able to diffuse in and out of the QD film readily.

To verify that the dramatic current density drops in the CVs might be explained by the reduced diffusion of electrolyte ions after polymerization, and that this indeed causes the observed Ohmic IV curves shown in Figures 4.4a, b, d and f, we performed numerical modelling to simulate the behavior of electrolyte ions before and after polymerization treatment. The numerical model solves the drift-diffusion equations for electrons, anions, and cations and uses Poisson's equation to determine the electrostatic potential profile of the system. The details of the model can be seen in Appendix. The CVs of QD film are simulated in electrolyte solution with different orders of magnitude for ion mobilities, which are 10^4, $3x10^4$, and 10^5 times lower than the initial ion mobility. (See Appendix, Figure A4.2) The results show that indeed straight (Ohmic) curves are obtained with a nA/cm^2 current density that is exactly zero at the potential used during polymerization, in excellent agreement with the experimental data shown in Figure 4.4. This confirms that the observed Ohmic CVs after polymerization are certainly explained by a reduction of the ionic conductivity by ~4 orders of magnitude.

The efficiency of the type I initiator can be attributed to its photo-decomposition mechanism. Absorption of light by type II PI brings the molecule to a reactive excited state. While in the excited state, type II PI molecule may interact with a donor molecule (co-initiator), such as formamide or DEGMA in our case, to abstract a hydrogen atom

resulting in free radical formation on donor molecule which then initiates polymerization. The radical formed on type II PI molecule itself is not able to start polymerization due to the delocalization of unpaired electron and steric hindrance. Based on this bimolecular reaction mechanism of type II PI, the initiation is generally slower compared to type I PI, which yields more active radicals after homolytic cleavage of carbon-phosphorus bonds. The decrease in UV irradiation time from 90 mins to 2 mins without compromising for fixation of dopant ions indicates the great potential of using type I PI over type II PI system in an electrochemically doped QD film.

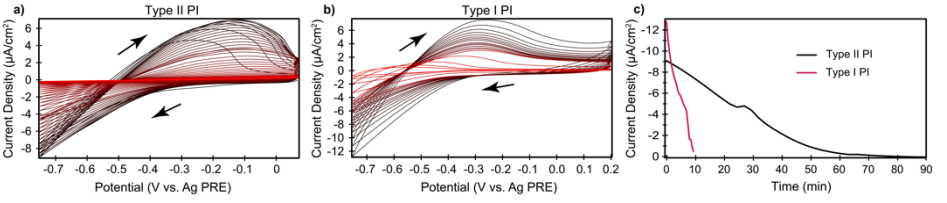

Figure 4.5 shows the continuously recorded CVs of ZnO QD films during photopolymerization treatment with both type I (a) and type II (b) initiators and the comparison of the maximum cathodic current density *vs.* time for the two types of PI molecules (c). Both (a) and (b) clearly show that as the photopolymerization continues the characteristic shape of the CVs change and become more and more flat, indicating a reduction in ionic conductivity due to polymerization. The comparison between the two PIs in (c) shows clear differences: for the type II PI (black line) it takes 90 mins of light irradiation for complete immobilization of dopant ions, while for the type I PI (red line) it takes 10 mins.

To gain more detailed information on the kinetics of polymerization with both types of PI, we continuously recorded CVs while exposing the systems to UV irradiation in order. Figure 4.5a and b present the CVs of ZnO QD film taken during photopolymerization with both types of PI molecules. Figure 4.5c compares the maximum cathodic current density *vs.* time for the two types of PI. In both cases, it is clear that immediately after UV exposure the current density starts to decrease, indicating a reduction in ionic conductivity due to polymerization. As the photopolymerization continues the characteristic shape of the CVs change and become more and more flat. However, for these experiments we do not achieve the very low current densities and Ohmic CV curves after polymerization that were shown in Figure 4.4. The comparison between

the two PIs in Figure 4.5c shows clear differences: for the type II PI (black line) it takes 90 mins of light irradiation for complete immobilization of dopant ions, while for the type I PI (red line) it takes 10 mins. The 90 minutes for type II PI is in line with the results shown in Figure 4.4, while the 10 mins for type I PI is longer than the expected 2 mins based on the results from Figure 4.4.

While the results shown in Figure 4.5 are in qualitative agreement with those in Figure 4.4, the lack of a completely flat CV curve, and the longer time required for the polymerization in the experiments shown in Figure 4.5 show that the photopolymerization was less efficient that case. The reason is not entirely clear but could be related to the different conditions during both experiments. In Figure 4.4 a constant negative potential is applied, while in Fig 4.5 the potential is continuously cycled between 0 and -0.75V. The forces ionic migration, or the on average more positive potential could be responsible for the observed changes.

4.2.2 Stability of injected charges

As explained above, electrochemically injected charges spontaneously disappear after the CE is disconnected. This loss of charge density is similar to self-discharge in batteries.[46-49] The spontaneous voltage decay in doped QD films could be because of impurity molecules such as dissolved O_2 or H_2O in the electrolyte solution that might react with the injected electrons. In our previous works, we demonstrated how detrimental such impurity molecules are for the stability of the charge density by intentionally exposing the electrochemically doped QD films to air.[31, 34] One of the beneficial effects of photopolymerization is therefore likely, that it also reduces the diffusion of such impurities.

Therefore, we compare the stability of electrochemically doped ZnO QD films after photopolymerization with both type of PIs. Figure 4.6 shows the open circuit potential vs. time after disconnection the counter electrode. The black line shows the rapid drop (in ~15 mins) of the potential before photopolymerization, while the red lines show the potential after polymerization, for both types of PI molecules and with different UV exposure times.

For 90 minutes of UV irradiation the potential remains constant at the charging potential of -0.75V over the full 10 hours of the measurement, and for both PIs, as shown in Figure 4.6a and b. This shows that for such long UV illumination times both

PIs are sufficiently effective in polymerizing the solvent and electrolyte ions, to stabilize the charge density. Based on the higher degree of polymerization observed with FT-IR (Figure 4.3), and the smaller residual current density (Figure 4.4) we expect that the stability obtained with the Type I PI is somewhat better than for the Type II PI, however this difference is likely on the timescale of several weeks (see chapter 2) and is thus well beyond the current measurements.

In the case of 10 mins irradiation, the Fermi level stability measurements present a subtle difference in between the two PIs. With type I initiator, the potential starts to decay slightly lower (-0.74 V) than the initial charging potential of QD film and falls to -0.7 V over 10 hours of measurement as shown in Figure 4.6d. On the other hand, the potential already drops starting from -0.72 V to -0.6 V in 10 hours with type II PI after polymerization treatment (Figure 4.6c). This difference in potential drop can be related to a smaller degree of polymerization with type II initiator, which then might allow the diffusion of impurity molecules inside QD film resulting in side-reactions with injected electrons.

A much faster drop in potential was observed with 2 mins of light exposure using type II initiator as shown in Figure 4.6e. Within 2.5 hours of measurement, the potential falls to the original $V_{oc,}$ indicating that all the injected electrons in the conduction band of the QD material were lost over the course of stability measurement. This result is in line with the CVs obtained in Figure 4.4e, in which the dopant ions were still mobile during charging and discharging of the QD film after treatment. On the other hand, the Fermi level stability measurement using type I initiator with 2 mins of UV exposure presents a much higher stability as shown in Figure 4.6f. Although the potential showed a sudden drop to -0.65 V instead of starting -0.75 V in the very beginning of the measurement, it only decayed to -0.58 V over 10 hours after disconnecting the counter electrode. The QD film can still be regarded in a doped state at this potential (-0.58 V) considering the fact that the charge injection into conduction band of the QD film starts around -0.5 V.

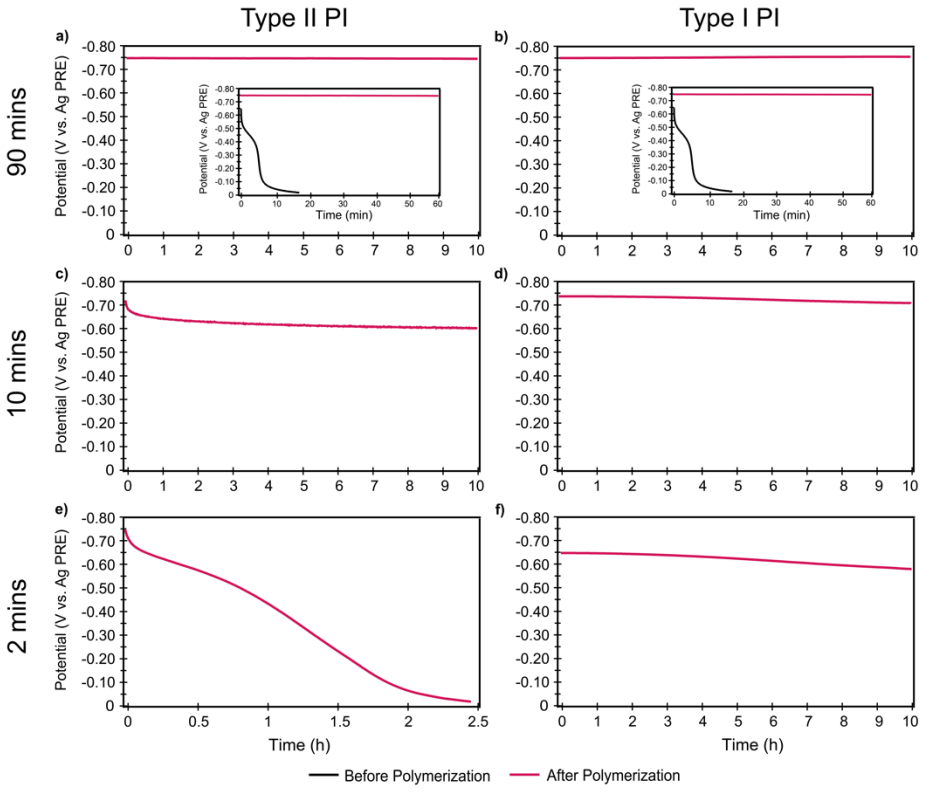

Figure 4.6 shows Fermi-level stability measurements (potential *vs.* time) of ZnO QD films when disconnecting the cell from the potentiostat. The potential drops from the charging potential of -0.75 V *vs.* Ag PRE were recorded over time. All measurements were carried out in an electrochemical cell containing 0.1 M of polymerizable electrolyte solution prepared by dissolving PI molecule (~1 mg) and ATMA-Cl salt in 10 mL of FA:DEGMA (2:3 v/v) solvent mixture. The red lines in (a)-(f) demonstrate results of after photopolymerization treatment with both type I and type II initiators and different UV exposure times of 90 mins, 10 mins and 2 mins. The black lines in insets of (a) and (b) show results of before photopolymerization treatment with both type I and type II initiators and only for 90 mins of UV exposure time.

All the results shown so far clearly demonstrate that photopolymerization with a type I initiator has a strong positive effect on both photochemical fixation of dopant ions and charge stability in electrochemically doped ZnO QD films. Due to the formation of highly cross-linked polymer matrix using type I PI, the diffusion of both impurities and

electrolyte ions is strongly reduced, enhancing the stability of injected charges significantly. Although both charge stability and photochemical anchoring of dopant ions are also achieved successfully using type II initiator with 90 mins of UV light exposure, a similar performance was not observed when reducing light irradiation times to 10 mins and 2 mins. Therefore, we conclude that the use of type I initiators is favorable for faster kinetics and a higher degree of photopolymerization, especially with short light exposure times. The results show that there is still considerable room for improvement in achieving stable doping of QDs with even shorter irradiation times (<1 min) with type I initiator without compromising for fixation of dopant ions.

4.3 Conclusion

In summary, we demonstrated that QD film can be controllably doped using electrochemistry, and that the stability of such doped QD films can be strongly enhanced using photopolymerization of the electrolyte solvent and ions. We showed that the type of photoinitiator molecules and UV light irradiation time can play a crucial role in dopant ion fixation and charge stability in electrochemically doped ZnO QDs. We presented that the polymerization treatment using Type I photoinitiator strongly outperforms photopolymerization with Type II photoinitiator, especially for short irradiation times. Results from CV and FT-IR measurements showed that a higher degree of photochemical fixation of dopant ions can be achieved using Type I photoinitiators. When using type I PI, the UV irradiation time can be decreased from 90 mins to 2 mins with only a minor decrease in the stability of injected charges. The results offer promising avenues for further optimization of stable electrochemically doped QD films.

4.4 Methods

Materials. Zinc acetate dihydrate ($Zn(CH_3COO)_2{\cdot}2H_2O$ ACS reagent, ≥ 99.8 %), potassium hydroxide (KOH, pellets EMPLURA®), methanol (anhydrous ≥ 99.8 %), ethanol (anhydrous ≥ 99.9 %), hexane (anhydrous ≥ 99.8 %), formamide (FA, ≥ 99 %), [2-(Acryloyloxy)ethyl]trimethylammonium chloride (ATMA-Cl, 80 wt. % in H_2O, contains 600 ppm monomethyl ether hydroquinone as inhibitor), di(ethylene glycol) dimethacrylate (DEGMA, 95 %, contains 300 ppm monomethyl ether hydroquinone as inhibitor), diphenyl(2,4,6-trimethylbenzoyl)phosphine oxide (Photoinitiator, Type I PI, 99%), and 4,4'-bis(diethylamino)benzophenone (Photoinitiator, Type II PI, ≥ 99%) were

all purchased from Sigma Aldrich. ATMA-Cl salt was further treated to decrease the water content by carefully heating up the salt solution to 85 °C for 30 mins until white salt crystals are observed. Next, it was connected to a vacuum line overnight at room temperature to obtain dry powder of ATMA-Cl salt, which was then placed into a nitrogen-filled glove box for storage. FA and DEGMA were vacuum degassed for 3h under rigorous stirring before use and were stored in a nitrogen-filled glove box. All other chemicals were used as received.

Synthesis & characterization of ZnO QDs. ZnO QDs were synthesized under air with slight modifications from literature.[50, 51] Zinc acetate dihydrate (3.43 mmol) was added to 50 mL of ethanol in an erlenmeyer flask equipped with a magnetic stirbar and heated up to 60 °C. Potassium hydroxide (KOH) pellets (6.25 mmol) was added to 5 mL of methanol and sonicated for 3 mins at room temperature. After complete dissolution of both reagents, KOH solution was added dropwise to zinc acetate solution under constant stirring over 10 mins. The solution was then allowed to stir for one additional minute before removing the heat source and demonstrated a pale blue-green emission when excited with UV light.

ZnO QDs were purified by adding hexane until the solution became turbid. The flocculates were isolated by centrifugation at 2000 rpm for 1 minute and the colorless supernatant decanted. ZnO QDs were then redispersed in ethanol and filtered through a syringe filter (0.2 μm). The dispersion was stored at -20 °C to avoid further growth of nanocrystals. Absorption spectrum of ZnO QDs in ethanol can be seen in Figure A4.1 in Appendix.

Preparation of ZnO QD films. Tin-doped indium oxide (ITO) substrate was used for deposition of the QD film, which served as working electrode (WE) in our electrochemical cell experiments. The films were prepared by drop-casting of ZnO QD dispersion on top of the substrate followed by annealing treatment at 60 °C for one hour in air. A Dektak profilometer was used to determine the thickness of ZnO QD film, which was approximately 2 μm.

Electrochemical measurements. All electrochemical measurements were performed in a nitrogen-filled glove box to ensure oxygen- and water-free conditions (≤0.1 ppm O_2 and ≤0.5 ppm H_2O) unless stated otherwise. An Autolab PGSTAT128N potentiostat

including an additional dual-mode bi-potentiostat BA module was used to control the potential difference between the WE and the reference electrode (RE) by adjusting the current at the counter electrode (CE). The QD film was immersed in an electrochemical cell containing an electrolyte solution together with an Ag wire as pseudoreference electrode (PRE) and Pt wire as CE.

Fermi-level stability measurements. The stability of electrochemically injected charges was measured by running the so-called potential *vs.* time or Fermi-level stability measurements after removing the electrical connection between WE and CE. That is to ensure that no additional charge is to be injected or extracted through the external circuit whilst the voltage difference between WE and PRE is being measured over time. Any change in the potential of the system after doping will result in a change in the Fermi level of the system or vice versa.

Photopolymerization experiments. All photopolymerization experiments were performed in a nitrogen-filled glove box. A UV-LED light source (600 mW/cm^2) with an emission wavelength of 395 nm was used to start the free radical polymerization after electrochemical charge injection. 0.1 M of polymerizable electrolyte solution was prepared by dissolving ATMA-Cl salt in 10 mL of FA:DEGMA (2:3 v/v) solvent mixture. FA was used to dissolve ATMA-Cl, which is an ammonium salt with a functional acrylate group at one end and DEGMA was employed as a cross-linking agent in the polymerization reaction, which has bifunctional methacrylate groups on each side. Two different types of PIs were used namely, Type I PI and Type II PI and in all experiments ~1 mg of PI was added. The chemical structures of both monomers and PIs can be seen in Figure 4.1b. A three-electrode electrochemical cell is immersed in electrolyte solution and the potential of the WE (ITO electrode with QD film deposited on it) was set and kept at -0.75 V vs. the Ag PRE during the entire photopolymerization experiment. By doing so, we assure that the QD film is in the n-doped state while the photochemical fixation of the electrolyte solution is taking place; this fixes the Fermi level of the system at exactly the potential determined. After 90 mins, 10 mins and 2 mins of UV light irradiation times, the WE was disconnected from the counter electrode so that no further electron injection or extraction could take place through the external circuit during the charge stability measurements.

Fourier Transform Infrared (FT-IR) measurements. FT-IR measurements were recorded on a Nicolet 6700 spectrometer from Thermo Electron Corporation equipped with an Attenuated Total Reflection (ATR) element. A drop from electrolyte solution mixture (before polymerization) and a piece of solid polymer (after polymerization) were used without further processing by pressing onto a diamond crystal. The samples were measured with 32 scans and a resolution of 4 cm^{-1}. The spectra were recorded in the range of 4000–400 cm^{-1}.

References

1. Méndez, H.; Heimel, G.; Opitz, A.; Sauer, K.; Barkowski, P.; Oehzelt, M.; Soeda, J.; Okamoto, T.; Takeya, J.; Arlin, J.-B.; Balandier, J.-Y.; Geerts, Y.; Koch, N.; Salzmann, I., Doping of Organic Semiconductors: Impact of Dopant Strength and Electronic Coupling. Angewandte Chemie International Edition 2013, 52 (30), 7751-7755.

2. Schubert, E. F., Doping in III-V Semiconductors. Cambridge University Press: Cambridge, 1993.

3. Electronic properties of doped semiconductors by B. I. Shklovskii and A. L. Efros. Acta Crystallographica Section A 1985, 41 (2), 208-208.

4. Thompson, S. E.; Parthasarathy, S., Moore's law: the future of Si microelectronics. Materials Today 2006, 9 (6), 20-25.

5. Jones, E. D., Control of Semiconductor Conductivity by Doping. In Electronic Materials: From Silicon to Organics, Miller, L. S.; Mullin, J. B., Eds. Springer US: Boston, MA, 1991; pp 155-171.

6. Abram, R. A.; Rees, G. J.; Wilson, B. L. H., Heavily doped semiconductors and devices. Advances in Physics 1978, 27 (6), 799-892.

7. Chen, K.; Wei, Z., High-efficiency single emissive layer color-tunable all-fluorescent white organic light-emitting diodes. Chemical Physics Letters 2022, 786, 139145.

8. Zhang, J.; Wang, L.; Zhang, X.; Xie, G.; Jia, G.; Zhang, J.; Yang, X., Blue light-emitting diodes based on halide perovskites: Recent advances and strategies. Materials Today 2021, 51, 222-246.

9. Sengupta, D.; Das, P.; Mondal, B.; Mukherjee, K., Effects of doping, morphology and film-thickness of photo-anode materials for dye sensitized solar cell application – A review. Renewable and Sustainable Energy Reviews 2016, 60, 356-376.

10. Schloemer, T. H.; Christians, J. A.; Luther, J. M.; Sellinger, A., Doping strategies for small molecule organic hole-transport materials: impacts on perovskite solar cell performance and stability. Chemical Science 2019, 10 (7), 1904-1935.

11. Casula, G.; Lai, S.; Matino, L.; Santoro, F.; Bonfiglio, A.; Cosseddu, P., Printed, Low-Voltage, All-Organic Transistors and Complementary Circuits on Paper Substrate. Advanced Electronic Materials 2020, 6 (5), 1901027.

12. Sun, Y.; Liu, Y.; Zhu, D., Advances in organic field-effect transistors. Journal of Materials Chemistry 2005, 15 (1), 53-65.

13. John, M. D., Light, Lasers, and the Nobel Prize. Advanced Photonics 2020, 2 (5), 1-3.

14. Cun-Zheng, N., Semiconductor nanolasers and the size-energy-efficiency challenge: a review. Advanced Photonics 2019, 1 (1), 1-10.

15. Tian, W.; Liu, D.; Cao, F.; Li, L., Hybrid Nanostructures for Photodetectors. Advanced Optical Materials 2017, 5 (4), 1600468.

16. Zhao, Y.; Li, C.; Shen, L., Recent research process on perovskite photodetectors: A review for photodetector—materials, physics, and applications. Chinese Physics B 2018, 27 (12), 127806.

17. Pradhan, N.; Sarma, D. D., Advances in Light-Emitting Doped Semiconductor Nanocrystals. The Journal of Physical Chemistry Letters 2011, 2 (21), 2818-2826.

18. Chen, X.; Lou, Y.; Dayal, S.; Qiu, X.; Krolicki, R.; Burda, C.; Zhao, C.; Becker, J., Doped Semiconductor Nanomaterials. Journal of Nanoscience and Nanotechnology 2005, 5 (9), 1408-1420.

19. Kovalenko, M. V.; Manna, L.; Cabot, A.; Hens, Z.; Talapin, D. V.; Kagan, C. R.; Klimov, V. I.; Rogach, A. L.; Reiss, P.; Milliron, D. J.; Guyot-Sionnnest, P.; Konstantatos, G.; Parak, W. J.; Hyeon, T.; Korgel, B. A.; Murray, C. B.; Heiss, W., Prospects of Nanoscience with Nanocrystals. ACS Nano 2015, 9 (2), 1012-1057.

20. Kagan Cherie, R.; Lifshitz, E.; Sargent Edward, H.; Talapin Dmitri, V., Building devices from colloidal quantum dots. Science 2016, 353 (6302), aac5523.

21. Baskoutas, S.; Terzis, A. F., Size-dependent band gap of colloidal quantum dots. Journal of Applied Physics 2006, 99 (1), 013708.

22. Bailey, R. E.; Smith, A. M.; Nie, S., Quantum dots in biology and medicine. Physica E: Low-dimensional Systems and Nanostructures 2004, 25 (1), 1-12.

23. Jovin, T. M., Quantum dots finally come of age. Nature Biotechnology 2003, 21 (1), 32-33.

24. Makkar, M.; Viswanatha, R., Frontier challenges in doping quantum dots: synthesis and characterization. RSC Advances 2018, 8 (39), 22103-22112.

25. Mocatta, D.; Cohen, G.; Schattner, J.; Millo, O.; Rabani, E.; Banin, U., Heavily Doped Semiconductor Nanocrystal Quantum Dots. Science 2011, 332 (6025), 77-81.

26. Zhao, F. A.; Xiao, H. Y.; Bai, X. M.; Zu, X. T., Effects of Ag doping on the electronic and optical properties of CdSe quantum dots. Physical Chemistry Chemical Physics 2019, 21 (29), 16108-16119.

27. Noor Ul, A.; Eriksson, M. O.; Schmidt, S.; Asghar, M.; Lin, P.-C.; Holtz, P. O.; Syväjärvi, M.; Yazdi, G. R., Tuning the Emission Energy of Chemically Doped Graphene Quantum Dots. Nanomaterials 2016, 6 (11).

28. Du, Y.; Guo, S., Chemically doped fluorescent carbon and graphene quantum dots for bioimaging, sensor, catalytic and photoelectronic applications. Nanoscale 2016, 8 (5), 2532-2543.

29. Araujo, J. J.; Brozek, C. K.; Kroupa, D. M.; Gamelin, D. R., Degenerately n-Doped Colloidal PbSe Quantum Dots: Band Assignments and Electrostatic Effects. Nano Letters 2018, 18 (6), 3893-3900.

30. Hartstein, K. H.; Erickson, C. S.; Tsui, E. Y.; Marchioro, A.; Gamelin, D. R., Electron Stability and Negative-Tetron Luminescence in Free-Standing Colloidal n-Type CdSe/CdS Quantum Dots. ACS Nano 2017, 11 (10), 10430-10438.

31. Gudjonsdottir, S.; Houtepen, A. J., Permanent Electrochemical Doping of Quantum Dots and Semiconductor Polymers. Advanced Functional Materials 2020, 30 (49), 2004789.

32. Guyot-Sionnest, P., Charging colloidal quantum dots by electrochemistry. Microchimica Acta 2008, 160 (3), 309-314.

33. Gudjonsdottir, S.; Koopman, C.; Houtepen, A. J., Enhancing the stability of the electron density in electrochemically doped ZnO quantum dots. The Journal of Chemical Physics 2019, 151 (14), 144708.

34. Gudjonsdottir, S.; van der Stam, W.; Koopman, C.; Kwakkenbos, B.; Evers, W. H.; Houtepen, A. J., On the Stability of Permanent Electrochemical Doping of

Quantum Dot, Fullerene, and Conductive Polymer Films in Frozen Electrolytes for Use in Semiconductor Devices. ACS Applied Nano Materials 2019, 2 (8), 4900-4909.

35. Matyba, P.; Maturova, K.; Kemerink, M.; Robinson, N. D.; Edman, L., The dynamic organic p–n junction. Nature Materials 2009, 8 (8), 672-676.

36. Tang, S.; Edman, L., On-demand photochemical stabilization of doping in light-emitting electrochemical cells. Electrochimica Acta 2011, 56 (28), 10473-10478.

37. Tang, S.; Irgum, K.; Edman, L., Chemical stabilization of doping in conjugated polymers. Organic Electronics 2010, 11 (6), 1079-1087.

38. Eibel, A.; Fast, D. E.; Gescheidt, G., Choosing the ideal photoinitiator for free radical photopolymerizations: predictions based on simulations using established data. Polymer Chemistry 2018, 9 (41), 5107-5115.

39. Vaidyanathan, T. K.; Vaidyanathan, J.; Lizymol, P. P.; Ariya, S.; Krishnan, K. V., Study of visible light activated polymerization in BisGMA-TEGDMA monomers with Type 1 and Type 2 photoinitiators using Raman spectroscopy. Dental Materials 2017, 33 (1), 1-11.

40. Ravve, A., Photosensitizers and Photoinitiators. In Light-Associated Reactions of Synthetic Polymers, Ravve, A., Ed. Springer New York: New York, NY, 2006; pp 23-122.

41. Bail, R.; Patel, A.; Yang, H.; Rogers, C. M.; Rose, F. R. A. J.; Segal, J. I.; Ratchev, S. M., The Effect of a Type I Photoinitiator on Cure Kinetics and Cell Toxicity in Projection-Microstereolithography. Procedia CIRP 2013, 5, 222-225.

42. Yang, D. B., Kinetic studies of photopolymerization using real time FT-IR spectroscopy. Journal of Polymer Science Part A: Polymer Chemistry 1993, 31 (1), 199-208.

43. Zhai, Q.; Wu, X.; Zhao, S.; Zhou, C., Curing Kinetics Study by FTIR Spectroscopy and Properties Analysis of Methyl Silicone Resin Membrane. Silicon 2020, 12 (11), 2761-2768.

44. Scherzer, T.; Decker, U., Real-time FTIR–ATR spectroscopy to study the kinetics of ultrafast photopolymerization reactions induced by monochromatic UV light. Vibrational Spectroscopy 1999, 19 (2), 385-398.

45. Gudjonsdottir, S.; van der Stam, W.; Kirkwood, N.; Evers, W. H.; Houtepen, A. J., The Role of Dopant Ions on Charge Injection and Transport in Electrochemically Doped Quantum Dot Films. Journal of the American Chemical Society 2018, 140 (21), 6582-6590.

46. Seong, W. M.; Park, K.-Y.; Lee, M. H.; Moon, S.; Oh, K.; Park, H.; Lee, S.; Kang, K., Abnormal self-discharge in lithium-ion batteries. Energy & Environmental Science 2018, 11 (4), 970-978.

47. Conway, B. E.; Pell, W. G.; Liu, T. C., Diagnostic analyses for mechanisms of self-discharge of electrochemical capacitors and batteries. Journal of Power Sources 1997, 65 (1), 53-59.

48. Liu, K.; Yu, C.; Guo, W.; Ni, L.; Yu, J.; Xie, Y.; Wang, Z.; Ren, Y.; Qiu, J., Recent research advances of self-discharge in supercapacitors: Mechanisms and suppressing strategies. Journal of Energy Chemistry 2021, 58, 94-109.

49. Niu, J.; Conway, B. E.; Pell, W. G., Comparative studies of self-discharge by potential decay and float-current measurements at C double-layer capacitor and battery electrodes. Journal of Power Sources 2004, 135 (1), 332-343.

50. Wood, A.; Giersig, M.; Hilgendorff, M.; Vilas-Campos, A.; Liz-Marzán, L. M.; Mulvaney, P., Size Effects in ZnO: The Cluster to Quantum Dot Transition. Australian Journal of Chemistry 2003, 56 (10), 1051-1057.

51. Mashford, B. S.; Stevenson, M.; Popovic, Z.; Hamilton, C.; Zhou, Z.; Breen, C.; Steckel, J.; Bulovic, V.; Bawendi, M.; Coe-Sullivan, S.; Kazlas, P. T., High-efficiency quantum-dot light-emitting devices with enhanced charge injection. Nature Photonics 2013, 7 (5), 407-412.

Appendix

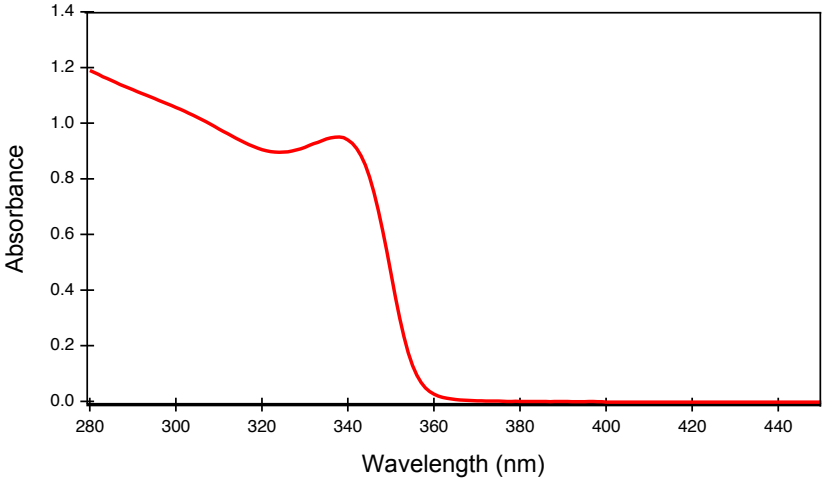

Figure A4.1 The absorption spectrum of ZnO QDs dispersed in ethanol.

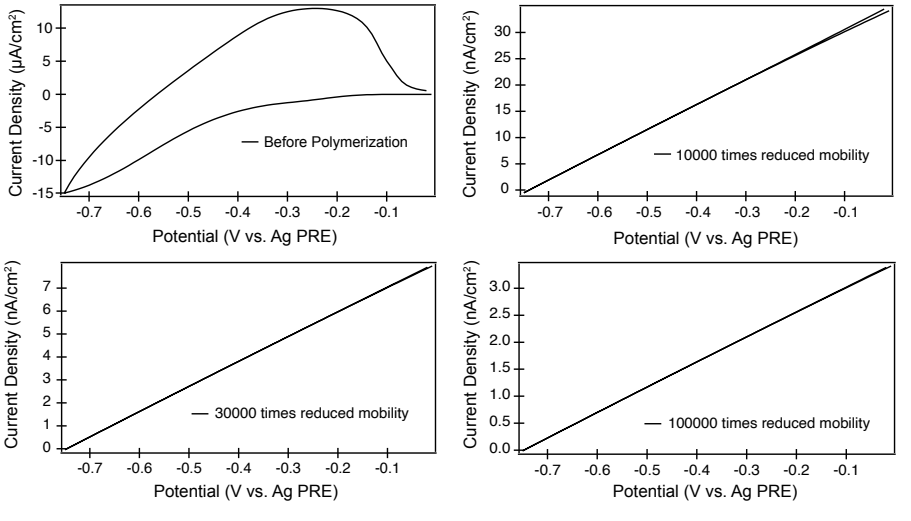

Figure A4.2 The CVs of QD film simulated in electrolyte solution with different orders of magnitude for ion mobilities, which are 10^4, $3x10^4$, and 10^5 times lower than the initial ion mobility.

One-dimensional numerical drift-diffusion simulations were adapted from a model by van Reenen and colleagues [1]. A three-electrode system was chosen were the distance between the working and counter electrodes (L = 6 µm) was divided in 89 lamellae of equal size. In each lamella, the concentration of the three charge carriers (electrons, cations, anions) was defined. The lamella up to a distance of 2 µm from the working electrode were considered to be part of the quantum dot film, while the rest was defined as the electrolyte region. The reference electrode was positioned at a distance of 4 µm away from the working electrode. During a CV simulation, the potential difference between the working and reference electrode was increased and decreased with increments of 0.01 V, while the potential at the counter electrode was allowed to float. Using the electrostatic potential at the working and reference electrode as boundary conditions, the Poisson equation (S.1) can be solved to determine the electrostatic potential profile of the system.

$$\frac{d^2V}{dx^2} = -\frac{q}{\varepsilon_r \varepsilon_0}(-n + c - a) \tag{S.1}$$

Where V is the electrostatic potential, x is the position in space and *n*, *c* and *a* correspond to the concentrations of electrons, cations and anions, respectively. Taking time steps of 0.1 µs, first the potential profile was calculated, after which the current densities of the charge carriers were determined according to the drift-diffusion equations (S.2).

$$\begin{aligned} J_n &= qn\mu_n \frac{dV}{dx} + kT\mu_n \frac{dn}{dx} \\ J_a &= qa\mu_a \frac{dV}{dx} + kT\mu_a \frac{da}{dx} \\ J_c &= qc\mu_c \frac{dV}{dx} - kT\mu_c \frac{dc}{dx} \end{aligned} \tag{S.2}$$

Here J_i is the current density corresponding to carrier *i* and μ_i is the corresponding mobility. These currents were then used to update the concentrations of the charge carriers, after which the next time step was taken. The electron current density was recorded at the end of each voltage increment step to produce the CV-curve. Electron injection was realised by assuming chemical equilibrium of electrons between the working electrode and the first lamella of the quantum dot film. The concentration of electrons in the first lamella was determined by integrating the product of the DOS

function and the Fermi-Dirac distribution, using the value of the electrostatic potential in that lamella (S.3).

$$\boldsymbol{n = \int_{Ec}^{\infty} DOS(E) * \left(\frac{e^{E-(\Phi_{WE}+\Delta V)}}{kT} + 1 \right)^{-1} dE} \quad \text{(S.3)}$$

Where n is the calculated electron concentration, DOS is the density of states function for the system, k is the Boltzmann constant and T is the temperature, which was set to 300 K by default. Φ_{WE} is the work function of the working electrode compared to the vacuum level, and ΔV is the difference in electrostatic potential between the working electrode and the first lamella.

Φ_{WE} + ΔV is equal to the Fermi level in the QDs, which increases in energy as more positive ions accumulate in the EDL at higher applied potentials. Ec corresponds to the energy level of the conduction band. The iteratively determined injection current was chosen so that the concentration of electrons in the first lamella was equal to n. The primitive double-Gaussian DOS function that was used for these simulations can be found in Figure A4.3.

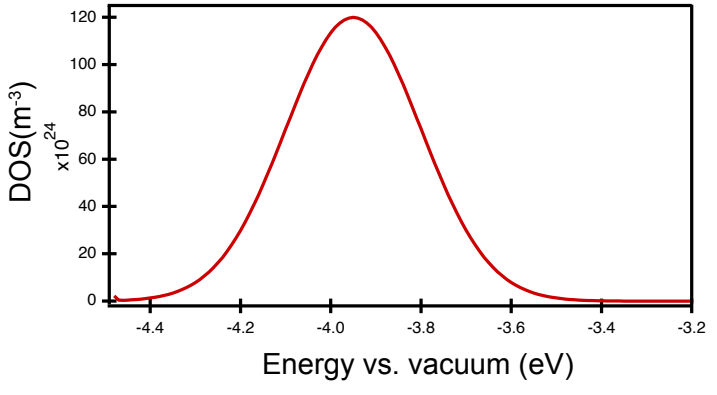

Figure A4.3 Density of states function used in the simulations. Levels more than ~1 eV above the bandgap are not considered as they will not be relevant for the applied potentials simulated here.

For the simulations after charge fixing, the initial state of the system was determined by performing a simulation at an applied potential of -0.75 V until steady state was reached, after which the mobility of ions was decreased and the CV was started as

normal. In table 1 are listed all the additional parameters that were used for simulation of the CVs before and after charge fixing.

Table 1. Parameters used in the simulation of CVs before and after charge fixing.

	Before charge fixing	**After charge fixing**
Initial ion concentration in electrolyte	50 mM	50 mM
Initial ion concentration in film	10 mM	78mM (cations)*, 1mM (anions)*
Initial electron concentration in film	0 mM	77 mM*
Electron mobility	$1.0*10^{-8}$ cm^2s^{-1}	$1.0*10^{-8}$ cm^2s^{-1}
Ion mobility	$1.5*10^{-9}$ cm^2s^{-1} (QD film) $1.0*10^{-8}$ cm^2s^{-1} (solution)	$1.5*10^{-12}$-$1.5*10^{-15}$ cm^2s^{-1}
Relative dielectric constant	4 (QD film), 37 (solution)	4 (QD film), 37 (solution)

A* indicates that this value was obtained from the steady-state simulation at -0.75 V.

Reference: [1] van Reenen, Stephan, et al. "A unifying model for the operation of light-emitting electrochemical cells." Journal of the American Chemical Society 132.39 (2010): 13776-13781.

Summary

To utilize the full potential of semiconductor materials in device applications including solar cells, LEDs, and lasers, the ability to precisely and controllably tune the charge carrier concentration and hence the doping density is crucial. The conventional methods such as impurity doping with thermal diffusion or ion implantation, have been successfully implemented for doping bulk semiconductors for decades. In spite of the maturity of doping with traditional methods, it has remained a long-standing challenge to introduce impurity doping successfully into organic and new generation of semiconductors, such as conducting polymers and quantum dots. Additionally, the prospect of new technologies and the shrinkage in the device dimensions to nanoscale have stimulated researchers to search for alternative methods for achieving doping of such semiconductor materials reliably.

Electrochemical doping is arguably the most powerful and versatile method for doping porous semiconductor materials, in which the charge carrier concentration can be precisely and controllably modulated as a function of applied potential by an external voltage source. Unfortunately, when the doped semiconductor film is disconnected from the voltage source, the electrochemically injected charges leave the film spontaneously in a matter of seconds to few minutes.

In that regard, the stability of injected charges as well as the immobilization of external dopant ions need to fixed for achieving stable electrochemical doping of such semiconductor films to be used in device applications. The research carried out in this thesis is aimed to enhance the stability of injected charges and the fixation of dopant ions with photopolymerization treatment at room temperature in electrochemically doped quantum dots and conducting polymers. This was attempted by understanding the underlying mechanism of electrochemical doping in such porous films and eliminating or minimizing possible causes for instability with the final goal of producing stable doped of semiconductor films.

Chapter 1 introduces the main concepts used in the rest of the thesis. The introduction chapter starts by describing the unique properties of the semiconductor materials in comparison to insulators and conductors. Next it is mentioned the importance of

doping semiconductor in many optoelectronic devices that we used in our daily lives such as phones and computers. Different methods of doping semiconductors are presented, namely internal (impurity) doping and external (remote) doping together with the advantages and disadvantages of both methods as well as the detailed description of the both doping techniques. It was shown that the electrochemical doping method is the most suitable and powerful technique to tune the doping densities in both quantum dots and organic semiconductors in a non-destructive and controllable manner. Finally, some main studies to stabilize the electrochemically doped structures are discussed including low temperature (freezing electrolytes), hight temperature (melting and solidifying electrolytes) and room temperature (polymerization of electrolytes).

Chapter 2 presents the realization of a fixed and stable doping densities in electrochemically doped ZnO and PbS QD films through the photopolymerization of electrolyte at room temperature. We showed that the that the stability of injected charges can be increased by many orders of magnitude from minutes to several weeks. By performing CV, we also demonstrated that the ionic mobility of dopant ions can be substantially lowered after photochemical fixation. However, the measurements with non-polymerizable electrolyte ions demonstrate only a marginal improvement of the stability after photopolymerization treatment.

Chapter 3 shows that the same methods we applied to stabilize n-doped ZnO and PbS QD films in Chapter 1 can also be used to stabilize p-doped P3DT films. Results showed that a substantial enhancement in stability can be achieved for electrochemically injected holes inside P3DT film after photopolymerization at room temperature. With a systematic study, we also demonstrated that the stability of injected charges and diffusion of the dopant ions are strongly related to the impurity levels in the solvents, the choice of monomer/cross-linking agent and the type of photoinitiator molecules employed. The combination of DMF/MMA/PEGMA-550 mixture with a Type I photoinitiator demonstrated the highest charge stability at room temperature.

Chapter 4 demonstrates that the type of photoinitiator molecules and UV light irradiation time can play a significant role in dopant ion immobilization and charge stability in electrochemically doped ZnO QD films. We showed that the polymerization treatment using Type I photoinitiator greatly outperforms photopolymerization with Type II photoinitiator, particularly for short irradiation times. Results from CV and FT-IR

measurements presented that a higher degree of photochemical immobilization of dopant ions can be achieved using Type I photoinitiators. When employing type I PI, the UV irradiation time can be shortened from 90 mins to 2 mins with only a minor decrease in the stability of injected charges.

Samenvatting

Om het volledige potentieel van halfgeleidermaterialen in apparaat toepassingen, waaronder zonnecellen, LEDs, en lasers, te benutten, is het cruciaal om de ladingsdragerconcentratie nauwkeurig en controleerbaar af te stemmen en daarmee de doteringsdichtheid. De conventionele methoden, zoals onzuiverheidsdoping met thermische diffusie of ionenimplantatie, worden al tientallen jaren met succes geïmplementeerd voor het doteren van bulkhalfgeleiders. Ondanks de volwassenheid van doping met traditionele methoden, is het een langdurige uitdaging gebleven om onzuiverheidsdoping met succes te introduceren in organische en nieuwe generatie halfgeleiders, zoals geleidende polymeren en kwantum-stippen. Bovendien hebben het vooruitzicht van nieuwe technologieën en de inkrimping van de apparaat afmetingen tot nanoschaal onderzoekers gestimuleerd om te zoeken naar alternatieve methoden om op betrouwbare wijze doping van dergelijke halfgeleidermaterialen te bereiken.

Elektrochemische dotering is misschien wel de krachtigste en meest veelzijdige methode voor het doteren van poreuze halfgeleidermaterialen, waarbij de ladingsdragerconcentratie nauwkeurig en controleerbaar kan worden gemoduleerd als een functie van aangelegd potentieel door een externe spanningsbron. Helaas, wanneer de gedoteerde halfgeleiderfilm wordt losgekoppeld van de spanningsbron, verlaten de elektrochemisch geïnjecteerde ladingen de film spontaan binnen enkele seconden tot enkele minuten.

In dat opzicht moeten de stabiliteit van geïnjecteerde ladingen en de immobilisatie van externe doteringsionen worden vastgesteld om stabiele elektrochemische dotering van dergelijke halfgeleiderfilms te bereiken die in apparaat toepassingen moeten worden gebruikt. Het onderzoek dat in dit proefschrift wordt uitgevoerd, is gericht op het verbeteren van de stabiliteit van geïnjecteerde ladingen en de fixatie van doteringsionen door fotopolymerisatie behandeling bij kamertemperatuur in elektrochemisch gedoteerde kwantum-stippen en geleidende polymeren. Dit werd geprobeerd door het onderliggende mechanisme van elektrochemische dotering in dergelijke poreuze films te begrijpen en mogelijke oorzaken voor instabiliteit te elimineren of te minimaliseren met als uiteindelijk doel het produceren van stabiele gedoteerde halfgeleiderfilms.

Hoofdstuk 1 introduceert de belangrijkste concepten die in de rest van het proefschrift worden gebruikt. Het inleidende hoofdstuk begint met het beschrijven van de unieke eigenschappen van de halfgeleidermaterialen in vergelijking met isolatoren en geleiders. Vervolgens wordt het belang genoemd van doping halfgeleiders in veel opto-elektronische apparaten die we in ons dagelijks leven gebruiken, zoals telefoons en computers. Verschillende methoden voor het doteren van halfgeleiders worden gepresenteerd, namelijk interne (onzuiverheid) doping en externe (remote) doping samen met de voor- en nadelen van beide methoden, evenals de gedetailleerde beschrijving van beide dopingtechnieken. Er werd aangetoond dat de elektrochemische doteringsmethode de meest geschikte en krachtige techniek is om de doteringsdichtheden in zowel kwantum-stippen als organische halfgeleiders op een niet-destructieve en controleerbare manier af te stemmen. Ten slotte worden enkele hoofdstudies besproken om de elektrochemisch gedoteerde structuren te stabiliseren, waaronder lage temperatuur (bevriezen van elektrolyten), hoge temperatuur (smelten en stollen van elektrolyten) en kamertemperatuur (polymerisatie van elektrolyten).

Hoofdstuk 2 presenteert de realisatie van vaste en stabiele doteringsdichtheden in elektrochemisch gedoteerde ZnO en PbS QD films door de fotopolymerisatie van elektrolyt bij kamertemperatuur. We hebben aangetoond dat de stabiliteit van geïnjecteerde ladingen met vele ordes van grootte kan worden verhoogd, van minuten tot enkele weken. Door CV uit te voeren, hebben we ook aangetoond dat de ionische mobiliteit van doteringsionen aanzienlijk kan worden verlaagd na fotochemische fixatie. De metingen met niet-polymeriseerbare elektrolyt-ionen laten echter slechts een marginale verbetering zien van de stabiliteit na fotopolymerisatie behandeling.

Hoofdstuk 3 laat zien dat dezelfde methoden die we in hoofdstuk 1 hebben toegepast om n-gedoteerde ZnO en PbS QD films te stabiliseren, ook kunnen worden gebruikt om p-gedoteerde P3DT films te stabiliseren. De resultaten toonden aan dat een substantiële verbetering van de stabiliteit kan worden bereikt voor elektrochemisch geïnjecteerde gaten in P3DT film na fotopolymerisatie bij kamertemperatuur. Met een systematische studie hebben we ook aangetoond dat de stabiliteit van geïnjecteerde ladingen en diffusie van de doteringsionen sterk gerelateerd zijn aan de onzuiverheidsniveaus in de oplosmiddelen, de keuze van het monomeer/verknopingsmiddel en het type gebruikte foto-initiatormoleculen. De

combinatie van DMF/MMA/PEGMA-550 mengsel met een Type I foto-initiator toonde de hoogste ladingsstabiliteit bij kamertemperatuur.

Hoofdstuk 4 laat zien dat het type foto-initiatormoleculen en de bestralingstijd met UV-licht een belangrijke rol kunnen spelen bij de immobilisatie van doteerionen en ladingsstabiliteit in elektrochemisch gedoteerde ZnO QD films. We hebben aangetoond dat de polymerisatiebehandeling met Type I foto-initiator veel beter presteert dan fotopolymerisatie met Type II foto-initiator, met name voor korte bestralingstijden. Resultaten van CV en FT-IR-metingen toonden aan dat een hogere mate van fotochemische immobilisatie van doteerionen kan worden bereikt met behulp van Type I foto-initiatoren. Bij gebruik van type I PI kan de UV-bestralingstijd worden verkort van 90 minuten tot 2 minuten met slechts een kleine afname van de stabiliteit van geïnjecteerde ladingen.

Acknowledgement

This PhD thesis would not have been possible without the help, support and guidance of many people, who I hope to acknowledge in this section.

To start with, I would like to thank my thesis supervisors. **Arjan**, I am very grateful for giving me such a wonderful opportunity to be part of your research group. Thank you for constantly providing your valuable guidance and support throughout my doctoral research. I have learnt a lot from you scientifically and personally. I would also like to thank my co-promotor **Rienk** for sharing his expert knowledge with me and his kind support all the time.

I am also very grateful to my PhD mentor **Wolter**. I really appreciate for teaching me, discussing with me and clearing my doubts on issues related to photopolymerization during my doctoral research. You always helped me with your great ideas and solutions for diverse problems. Thank you for your timely support and expert advice. Further, I would like to thank all the members of the defense committee, **Daniel, Bernard, Laurens and Ferdinand** for their critical evaluation of my thesis. I would like to extend my special thanks to **Tom** for all the valuable feedback in the group meetings.

I would like to express my appreciation to both of our secretaries, **Wil** and **Adinda**. Thank you for handling all those administrative works and planning all the social gatherings of the group throughout my doctoral years. I would like to extend my sincere gratitude to all the technicians in our group. Thanks **Ruben**, **Jos**, **John**, **Nick** and **Dr. Wiel** (a super post-doc) for your trainings and support regarding technical issues in particular and nice conversations in general.

I am thankful to two of brilliant students, **Laura** and **Roland** whom I supervised during my PhD. I really had a great time supervising you both and I learnt a lot from you. I wish you both all the best with your doctoral studies.

I would like to extend my special thanks to **Frank, Gianluca, Aditya, Prashant, Indy, Jence, Solrun,** and **Maryam** for being wonderful officemates. Further, I would like to equally thank my colleagues **Ryan, Jannika, Ward, Nick, Guilherme, Valentina, Nico, Zimu, Katerina, Jiashang, Abbey, Maarten, Deepika, Michele, Sourav, Dengyang,**

Silke, Davide, Rajeev, Damla, Kevin, Natalie, Magnus, Maria, Jaco, Cansel, Sudeep, Eline and Reinout. I truly have enjoyed every moment of my time here.

Of course, I would also like to thank **my lovely family**. I am so lucky to have such an inspiring, supporting and amazing family. Thanks for everything! Lastly, my heartily thanks to all the people for being around, helping me directly or indirectly throughout my doctoral stay in Delft.

Scientific Production

Patents

- A.K. Okyay, N. Biyikli, K. Topalli, A. Haider, P. Deminskyi, **H. Eren**, M. Yilmaz. "A Method for Area Selective Atomic Layer Deposition and Thereof" (January 2017), **Republic of Turkey Patent Institute**, 2016/13505.

- Arjan Houtepen, Rienk Eelkema, **Hamit Eren**, Solrun Gudjonsdottir. "Electrochemical Doping of Semiconductor Materials" (June 2020), **The Netherlands Patent Office**, 2022110.

Scientific Publications

(From post-doc)

- "Enhancing the Photo- and Thermal Stability of Natural Dyes with Metal Oxide Nanoparticles: A case study on Alizarin" **H Eren,** A Krishna, G Li, G C. H. Derksen, B Albada. *In Preparation.*

(From PhD)

- "Permanent Electrochemical Doping of Quantum Dot Films through Photopolymerization of Electrolyte Ions**"** **H Eren,** R Bednarz, L Donk, S Gudjonsdottir, P Bohlander, R Eelkema, A Houtepen. **Chemistry of Materials**, 34, (9), 4019-4028.

- "Enhancing the Charge Stability in Electrochemically p-Doped Conducting Polymers" **H Eren,** W Jager, A Houtepen. *In Preparation.*

- "The Influence of Photoinitiator Type and Irradiation Time on the Stabilization of Electrochemically Doped Quantum Dot Films via Photopolymerization" **H Eren,** R Ubbink**,** W Jager, A Houtepen. *In Preparation.*

(From MSc)

- "Facile Synthesis of Three-Dimensional Pt-TiO_2 Nano-networks: A Highly Active Catalyst for the Hydrolytic Dehydrogenation of Ammonia-Borane" MA

Khalily, **H Eren,** S Akbayrak, HH Susapto, N Biyikli, S Ozkar, MO Guler. **Angewandte Chemie**, 128, (40), 12445-12449.

- "Area-selective Atomic Layer Deposition Using an Inductively Coupled Plasma Polymerized Fluorocarbon Layer: A Case Study for Metal Oxides" A Haider, P Deminskyi, TM Khan, **H Eren**, N Biyikli. **The Journal of Physical Chemistry C**, 120, (46), 26393-26401.

- "Nano-scale Selective Area Atomic Layer Deposition of TiO_2 using E-beam Patterned Polymers" A Haider, M Yilmaz, P Deminskyi, **H Eren**, N Biyikli. **RSC Advances**, 6, (108), 106109-106119.

- "Surface Decoration of Pt nanoparticles via ALD with TiO_2 Protective Layer on Polymeric Nanofibers as Flexible and Reusable Heterogeneous Nanocatalysts" A Celebioglu, KS Ranjith, **H Eren**, N Biyikli, T Uyar. **Scientific Reports**, 7, (1), 1-10.

- "Self-assembled Peptide Nanofiber Templated ALD Growth of TiO_2 and ZnO Semiconductor Nanonetworks" R Garifullin, **H Eren**, TG Ulusoy, AK Okyay, N Biyikli, MO Guler. **Physica Status Solidi (a)**, 213, (12), 3238-3244.

- "Area-Selective Atomic Layer Deposition of Noble Metals: Polymerized Fluorocarbon Layers as Effective Growth Inhibitors" P Deminskyi, A Haider, **H Eren**, TM Khan, N Biyikli. **Journal of Vacuum Science and Technology**, in press.

- "Utilizing Embedded Ultra-small Pt Nanoparticles as Charge Trapping Layer in Flashristor Memory Cells" I Orak, **H Eren**, N Biyikli, A Dâna. **Applied Surface Science,** 467, 715-722.

- "Monodispersed, Highly Interactive Facet (111)-Oriented Pd Nanograins by ALD onto Free-Standing and Flexible Electrospun Polymeric Nanofibrous Webs for Catalytic Application" KS Ranjith, A Celebioglu, **H Eren**, N Biyikli, T Uyar. **Advanced Materials Interfaces**, 4, (24), 1700640.

- "Reusable and Flexible Heterogeneous Catalyst for Reduction of TNT by Pd Nanocube Decorated ZnO Nanolayers onto Electrospun Polymeric Nanofibers" O Arslan, **H Eren**, N Biyikli, T Uyar. **ChemistrySelect**, 2, (28), 8790-8798.

- "Pd Nanocube Decoration onto Flexible Nanofibrous Mats of Core-Shell Polymer-ZnO Nanofibers for Visible Light Photocatalysis" O Arslan, **H Eren**, N Biyikli, T Uyar. **New Journal of Chemistry**, 41, (10), 4145-4156.

About the Author

Hamit Eren was born in Istanbul, Turkey. He received a full scholarship from Fatih University to study his Bachelor of Science in Chemistry starting from 2008 till 2013. During his Bachelor years, he joined Mark Bradley's research group at the University of Edinburgh and in the following year in Seth Marder's research group at Georgia Tech as a summer research intern. After graduation with high honor from his Bachelor studies, he moved to Bilkent University to pursue his Master of Science in Materials Science and Nanotechnology. After obtaining his Master's degree with high honor, he decided to continue his career in the Netherlands. In October 2016, he started his PhD in the department of Chemical Engineer at TU Delft under the supervision of Prof. dr. Arjan J. Houtepen. Since January 2022, he has been working on a joint project as a post-doctoral researcher between Avans HBO (in Breda) and the laboratory of organic chemistry at Wageningen University & Research.

Cover designed by Freepik and modified by the author.

Printed by Ipskamp Printing, Enschede, The Netherlands.